THE UNIVERSITY OF CHICAGO

MECHANISMS OF BASEMENT MEMBRANE REMODELING AND THEIR CONTRIBUTIONS TO TISSUE MORPHOGENESIS

A DISSERTATION SUBMITTED TO
THE FACULTY OF THE DIVISION OF THE BIOLOGICAL SCIENCES
AND THE PRITZKER SCHOOL OF MEDICINE
IN CANDIDACY FOR THE DEGREE OF
DOCTOR OF PHILOSOPHY

COMMITTEE ON DEVELOPMENTAL BIOLOGY

BY

ADAM JAMES ISABELLA

CHICAGO, ILLINOIS

AUGUST 2016

DEDICATION

This dissertation is dedicated to my parents whose consistent and selfless love, encouragement, and support have made all my accomplishments possible.

TABLE OF CONTENTS

LIST OF FIGURES

LIST OF TABLES

ACKNOWLEDGEMENTS

Thank you, first and foremost, to my parents. For your enduring and unequivocal love and support. For always putting your children first, making choices that promoted my happiness and success, and for giving me the courage to do so for myself. To my sister, Christine, for her love and friendship, her enthusiasm, and for always challenging me. And to Rachael. Having you by my side – through the good, the bad, and the mundane - gave me the confidence, maturity and optimism to face any challenge, the perspective to live a fulfilling and balanced life, and the desire to constantly strive for self-improvement. I love you all.

Thank you to Sally. For always being there for me, through 5 years and countless hours. For caring about me as much as my work. For believing in me, even when I didn't. For supporting me, and challenging me, and making me feel safe to push myself, take risks, and grow. And for all the great conversations. I owe you a great deal for my growth as a scientist and a person. To my labmates, past and present. You all made the lab a stimulating and enjoyable place to be, scientifically and socially. Sharing with you the daily slog of science is what made it a pleasure. To my committee – Ed, Ben, and Rick – for their guidance and advice. And to the many other faculty and staff who made the University of Chicago a supportive and fun place to work.

Finally, thank you to all of my friends in Chicago. It was a great group, and we made a lot of great memories. You made the shared experience of graduate school manageable, you picked me up when I was down, and you constantly reminded me that there's much more to life than toiling in lab. I'll miss you all.

ABSTRACT

Basement membranes (BMs) are sheet-like extracellular matrices that provide essential support to epithelial tissues. Epithelia are common drivers of morphogenesis, the process by which complex tissue shapes are generated during development. Recent evidence suggests that regulated changes in BM architecture can direct morphogenesis; however, the mechanisms by which cells remodel their associated BMs, and how BM structure influences tissue shape change, are largely unknown. The *Drosophila* egg chamber is an organ-like structure that transforms from a spherical to an ellipsoidal shape as it matures. This elongation coincides with two changes in the BM surrounding the egg chamber: an increase in levels of Type IV Collagen (Col IV), and the formation of a polarized network of linear fibrils. I have identified the mechanisms by which the egg chamber's epithelial cells dynamically regulate the composition and structure of the BM, and elucidated the role of these remodeling events in egg chamber morphogenesis.

I first identify the Collagen-binding protein SPARC as a negative regulator of egg chamber elongation, and show that SPARC down-regulation is necessary for the increase in Col IV levels to occur. I also observe a decrease in Perlecan levels during elongation, and show that Perlecan is a negative regulator of this process. Additionally, I identify a Rab10-mediated pathway by which newly synthesized BM proteins are secreted to the pericellular spaces between epithelial cells, where they assemble into fibrils and undergo oriented insertion into the BM by directed epithelial migration. By manipulating this pathway, I show that BM fibrils influence egg chamber morphogenesis. Finally, I describe unpublished work examining how and where polarized BM secretion occurs in the egg chamber.

These data reveal that developing epithelia dynamically remodel their BMs, and that the properties of these matrices can provide crucial inputs to morphogenesis.

CHAPTER 1: BUILDING FROM THE GROUND UP: BASEMENT MEMBRANES IN *DROSOPHILA* DEVELOPMENT

1.1 PREFACE

Extracellular matrices (ECMs) are ubiquitous features of animals, occupying virtually all inter-cellular spaces. As such, ECMs play essential roles in many aspects of animal development. This dissertation will primarily focus on the structure and function of a specialized ECM, the basement membrane (BM), during morphogenesis of the *Drosophila* egg chamber. This chapter was written to provide a more comprehensive summary of the developmental roles played by BMs in *Drosophila*; thus, in addition to introducing the BM and its role in egg chamber morphogenesis, it will also discuss the role of BMs in a broader developmental context. This chapter was published in the book *Current Topics in Membranes*, Volume 76 with the following citation: Isabella, A.J., Horne-Badovinac, S., 2015. *Building from the Ground up: Basement Membranes in Drosophila Development*, in: Miner, J. (Ed.), Current Topics in Membranes. Elsevier Ltd.

1.2 ABSTRACT

Basement Membranes (BMs) are sheet-like extracellular matrices found at the basal surfaces of epithelial tissues. The structural and functional diversity of these matrices within the body endows them with the ability to affect multiple aspects of cell behavior and communication; for this reason, BMs are integral to many developmental processes. The power of *Drosophila* genetics, as applied to the BM, has yielded substantial insight into how these matrices influence development. Here, we explore three facets of BM biology to which *Drosophila* research has

made particularly important contributions. First we discuss how newly synthesized BM proteins are secreted to and assembled exclusively on basal epithelial surfaces. Next, we examine how regulation of the structural properties of the BM mechanically supports and guides tissue morphogenesis. Finally, we explore how BMs influence development through the modulation of several major signaling pathways.

1.3 INTRODUCTION TO BASEMENT MEMBRANES

Extracellular Matrices (ECMs) are proteinaceous networks that accumulate nearly ubiquitously in the spaces between cells. ECMs link and coordinate cells both within and between tissues; their existence therefore likely contributed greatly to the rise and success of multicellular life, especially in the metazoan lineage (Ozbek et al., 2010). Among the most ancient ECMs, the basement membrane (BM) is a specialized matrix that associates with the basal surfaces of epithelial tissues, as well as endothelial, fat, muscle, and Schwann cells. This chapter will focus predominantly on epithelial BMs. By electron microscopy, BMs appear as thin sheets (generally ~100nm thick). They are composed primarily of two independent web-like networks of Laminin and Type IV Collagen (Collagen IV), which are heavily interlinked by proteins such as Nidogen and the heparan sulfate proteoglycan (HSPG) Perlecan (Yurchenco, 2011) (Figure 1.1). Adhesion of the BM to cells is achieved via interactions with transmembrane receptors, such as integrins and Dystroglycan. Beyond the four core BM constituents, a large number of accessory proteins have been found to contribute to the network (Hynes and Naba, 2012). Differential incorporation of minor components, as well as varying isoforms and post-translational modifications of the core proteins, lends great structural and functional diversity to the many BMs found throughout the body.

Protein	*Drosophila* genes	Human homologs
Collagen IV 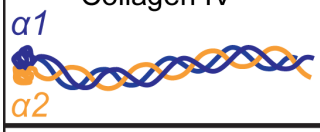	α1: *Collagen gene at 25C (Cg25C)*	*COL4A1, COL4A3, COL4A5*
	α2: *viking (vkg)*	*COL4A2, COL4A4, COL4A6*
Laminin 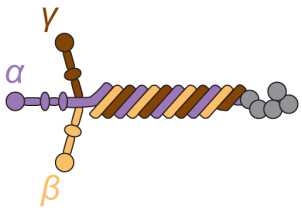	α1,2: *wing blister (wb)*	*LAMA1, LAMA2*
	α3,5: *Laminin A (LanA)*	*LAMA3, LAMA4, LAMA5*
	β: *Laminin B1 (LanB1)*	*LAMB1, LAMB2, LAMB3, LAMB4*
	γ: *Laminin B2 (LanB2)*	*LAMC1, LAMC2, LAMC3*
Perlecan 	*terribly reduced optic lobes (trol)*	*HSPG2*
Nidogen 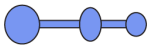	*Nidogen/entactin (Ndg)*	*NID1, NID2*

Figure 1.1: Overview of the core BM proteins in *Drosophila*

Several major roles for BMs have emerged, which will be discussed briefly here and in greater depth throughout this chapter. First, the mechanical properties of the network establish it as a physical scaffold. This property allows BMs to maintain tissue shape and integrity in the face of deformation forces and act as a substrate against which forces can be generated for cellular contraction and migration. Because of their small pore size, BMs can also provide a barrier function that helps to limit the movement of cells and large macromolecular complexes between body compartments. The ability to bind several secreted signaling molecules further allows these matrices to facilitate cell-cell communication both within and between tissues.

The functional capabilities of the BM described above make it well suited to facilitate the specification, compartmentalization, growth and morphogenesis of distinct tissue and organ

systems. Thus, it is not surprising that BMs are essential for embryonic development. The fruit fly *Drosophila melanogaster* has provided a particularly powerful system in which to dissect the specific contributions that BMs make to these processes. Nearly all developing tissue and organ systems have been well characterized and are visually and experimentally accessible. The powerful genetic techniques available, especially the ability to precisely manipulate gene expression in time and space, are also advantageous, particularly when studying a structure that plays such diverse roles in development. Moreover, the creation of functional GFP protein trap alleles of the Collagen IV α2 gene *viking* and the Perlecan gene *terribly reduced optic lobes* (*trol*) have transformed BM research in *Drosophila* by allowing unprecedented visual resolution of the native proteins in both fixed and living tissues (Buszczak et al., 2007; Morin et al., 2001).

While the core BM proteins and their receptors are well conserved between flies and humans, the fly BM can be viewed as a simplified version of its mammalian counterpart. Flies produce only 2 distinct Laminin trimers compared to 16 in humans, 1 Collagen IV trimer versus 3 in humans, and 2 β and 5 α integrin subunits versus 8 β and 18 α subunits in humans. Although this simplicity means that flies cannot recapitulate the diversity of human BMs, it increases the power to dissect protein function by limiting problems associated with redundancy.

In this chapter, we highlight important contributions that *Drosophila* research has made to our understanding of BM assembly and function during development. Because the literature on this topic is extensive, we have not attempted to provide a comprehensive summary of the data. Instead, we focus on three topic areas that exemplify the breadth and depth of BM research in this organism. First, we address the longstanding question of how BM proteins are precisely targeted to basal epithelial surfaces. We discuss how proteins produced from a variety of cellular sources achieve this goal, with a special focus on the intracellular trafficking pathway that

operates within epithelial cells to transport newly synthesized BM proteins to basal regions of the plasma membrane for secretion. Second, we address the process of morphogenesis during development. We explore mechanical contributions of BMs to this process, specifically how regulated remodeling of BM structure can help to shape a tissue. In this section, we offer an in-depth discussion of the complex contributions of the BM to egg chamber elongation. Third, we address molecular signals that mediate cell-cell communication during development. We discuss contributions that BMs make to this process through the modulation of several major signaling pathways.

1.4 SYNTHESIS, SECRETION, AND ASSEMBLY OF THE BM ON BASAL CELL SURFACES

Epithelial cells exhibit a highly polarized architecture with four distinct membrane domains – apical, junctional, lateral, and basal. To build and maintain a BM, newly synthesized components must be assembled exclusively on the basal epithelial surface. Here, we explore several ways in which BM proteins are targeted to this membrane domain, including a mechanism for the polarized secretion of BM proteins by an epithelium.

Sources of BM proteins and implications for polarized assembly

In *Drosophila,* the sources of BM proteins are complex and, in many cases, are still not clear. Some epithelia synthesize all of their own BM components, while others rely on production by other tissues. Some epithelia combine these approaches, producing a subset of their own proteins and relying on external sources for others (Figure 1.2). The major non-epithelial source of BM proteins also varies by developmental stage. In the embryo, BM proteins are primarily

produced by hemocytes - circulating immune cells that migrate throughout the body. Hemocytes display the primary signal for transcripts encoding Collagen IV and Laminin by in situ hybridization (Kusche-Gullberg et al., 1992; Le Parco et al., 1986; Mirre et al., 1988; Yasothornsrikul et al., 1997) and, when cultured, produce large volumes of BM proteins (Fessler et al., 1994). It should be noted, however, that some embryonic and larval epithelia appear to produce their own Laminin and/or Perlecan (Denef et al., 2008; Martin et al., 1999; Sorrosal et al., 2010).

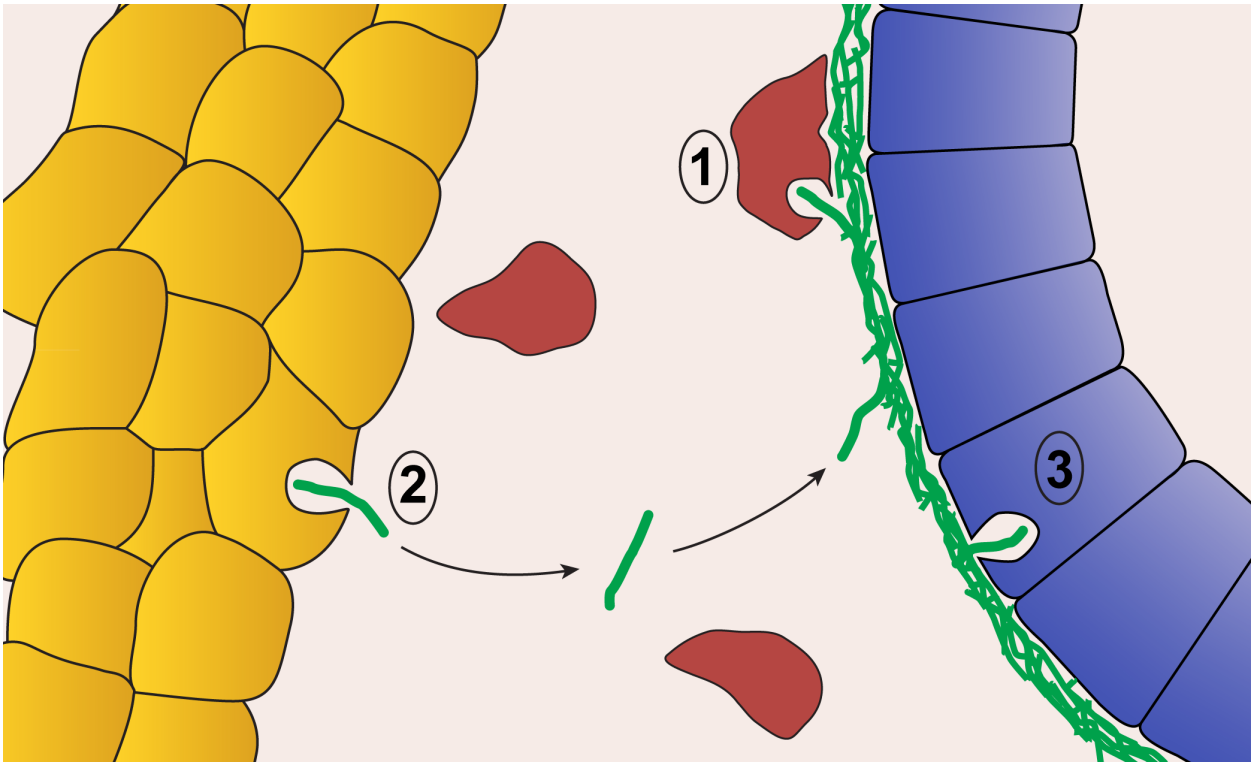

Figure 1.2. Cellular sources of BM proteins in *Drosophila*
BM proteins are synthesized and secreted by three primary cell types. 1: Synthesis and local deposition by hemocytes. 2: Synthesis by and long range diffusion from the fat body. 3: Synthesis and secretion by the epithelium itself.

How do proteins secreted by hemocytes assemble specifically on basal epithelial surfaces? This process must require establishment of the basal epithelial membrane as a competent surface to bind soluble BM proteins, likely by expression of cell surface BM

receptors. Hemocytes also tend to cluster around BM-containing tissues, probably for the purpose of BM deposition (Kusche-Gullberg et al., 1992). This phenomenon is analogous to ECM deposition by fibroblasts in vertebrates. In this case, epithelia likely recruit hemocytes to their basal surfaces.

While hemocytes continue to produce BM proteins throughout development, during late embryogenesis and larval stages Collagen IV and Laminin production is also observed strongly in the fat body – a major metabolic organ in insects (Kusche-Gullberg et al., 1992; Le Parco et al., 1986; Mirre et al., 1988; Yasothornsrikul et al., 1997). The fat body appears to take over as the major production center, at least for Collagen IV, in larvae. Blocking Collagen IV production in the fat body results in drastic loss of this protein from BMs throughout the body, including full loss from the BM surrounding the imaginal wing disc epithelium - the pouch-like precursor to the adult wing (Pastor-Pareja and Xu, 2011).

Because the fat body is fixed in place, proteins secreted from this organ must diffuse long distances through the extracellular space to their target tissues. Yet they are still incorporated efficiently into distant BMs. As was discussed with hemocytes, this is most likely achieved by ensuring that basal epithelial surfaces have the necessary adhesive properties to capture diffusing proteins. In this case, it is equally important to prevent premature protein aggregation and promiscuous adhesion to the wrong tissues. The task of escaping the fat body is particularly onerous, as this tissue is itself surrounded by a BM through which secreted proteins bound for other tissues must pass without adhering. SPARC (Secreted Protein Acidic and Rich in Cysteine) appears to promote Collagen IV diffusion away from the fat body to distant epithelia, as loss of SPARC from this tissue leads to an aberrant accumulation of Col IV between fat body cells (Pastor-Pareja and Xu, 2011; Shahab et al., 2014). Loss of SPARC from hemocytes also

prevents Collagen IV from reaching target tissues (N. Martinek et al., 2008). While the role of SPARC in hemocytes is less clear, it may also be required here to prevent inappropriate adhesion of BM proteins to secreting cells.

Although it is likely that the hemocytes and fat body continue to produce BM proteins throughout the life of the fly, there is one epithelium, found in adult females, that is known to synthesize and secrete all of its own major BM proteins – the follicular epithelium that surrounds the developing germ cells within the ovary. For the rest of this section, we will describe recent studies, primarily performed within this tissue, that have begun to elucidate how BM proteins synthesized within the epithelium itself are targeted exclusively to basal regions of the plasma membrane for secretion (Figure 1.3).

Basal localization of BM protein synthesis

In the follicular epithelium, newly synthesized BM proteins exhibit a polarized localization within the cell from the moment of translation. The mRNAs encoding both Collagen IV chains (*viking and Cg25c*) and the Laminin β chain (*LanB1*) show a 70% enrichment in the basal half of the cell (Lerner et al., 2013). Because the endoplasmic reticulum (ER) stretches throughout the cytoplasmic volume, this observation suggests that these transcripts are primarily translated into a specific sub-region of this organelle. Thus, mRNA localization may help to establish a distinct ER compartment specialized for BM protein production.

Why might such a distinct ER compartment exist? Collagen IV places a notorious burden on the ER's protein production and transport machinery. Each Collagen IV protomer is assembled from three polypeptides that wind into a triple helical structure nearly 400 nm long (Khoshnoodi et al., 2008). This complex folding reaction requires a suite of ER-resident

chaperones, several of which are Collagen-specific. For instance, Procollagen lysyl hydroxylase (Plod) and Prolyl-4-hydroxylase-alpha EFB (PH4αEFB) catalyze hydroxylation of lysines and prolines, respectively, primarily within the triple helical domain; and both enzymes are required for trimer assembly (Myllyharju and Kivirikko, 2004). Collagen IV's large size also prevents it from being packaged into standard CopII-coated vesicles for transport to the Golgi.

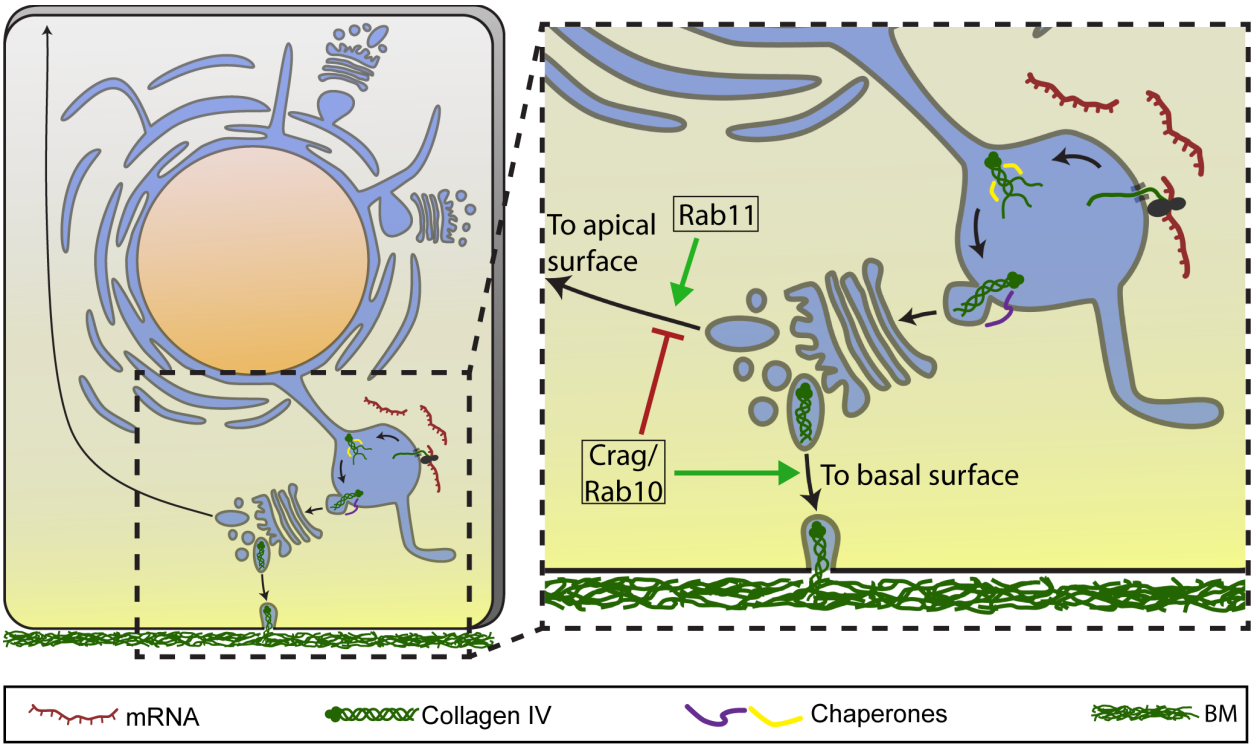

Figure 1.3. Local synthesis and polarized secretion of Collagen IV in the follicular epithelium
Within the follicular epithelium, *Collagen IV* transcripts accumulate basally and are transcribed into a basal region of the ER. ER resident proteins assist in the folding and packaging of Collagen IV for transport to the Golgi. After Collagen IV transits through the Golgi, Crag and Rab10 promote delivery of Collagen IV-containing exocytic vesicles to basal regions of the plasma membrane and prevent Rab11-dependent targeting of Collagen IV-containing vesicles to the apical surface**.** Inset: blow-up of indicated region.

The transmembrane protein Tango1 is required at ER exit sites (ERESs) to help load Collagens into enlarged Golgi-bound vesicles (Pastor-Pareja and Xu, 2011; Saito et al., 2009; Venditti et al., 2012; Wilson et al., 2011). Compartmentalization of Collagen IV production

could, therefore, increase biosynthetic efficiency while limiting any potential negative impact on other ER processes.

In support of this idea, the mRNAs encoding Plod, PH4αEFB, and Tango1 all display an enrichment in the basal cytoplasm, similar to the Collagen IV-encoding mRNAs, and the Tango1 protein primarily localizes to basal ERESs (Lerner et al., 2013). Importantly, knocking down expression of any of these 3 proteins causes Collagen IV to become trapped in a discrete region of the ER near the basal cell surface. When this happens, Collagen IV does not diffuse from this location, even over long time periods (Lerner et al., 2013). This observation suggests that a mechanism exists to prohibit diffusion of BM proteins away from their site of synthesis. Localized production of ECM proteins within sub-regions of the ER has also been observed in vertebrates, which suggests that this may be a conserved biosynthetic strategy (Vertel et al., 1989).

Because the ER compartment where BM proteins are synthesized is in the basal region of the cell, it is intriguing to speculate that this localization may also act as an initial step to bias secretion to the basal plasma membrane. While the Golgi typically takes the form of a singular organelle in mammalian cells, called the Golgi ribbon, *Drosophila* cells contain many dispersed Golgi stacks that each associate with a single ERES (Kondylis and Rabouille, 2009; Kondylis et al., 2009). This organization has led to the hypothesis that individual ERES-Golgi units could function independently of one another to facilitate polarized protein secretion. Synthesis within a basal region of the ER could, therefore, promote protein transport through basally localized ERES-Golgi units and subsequent delivery to the adjacent basal plasma membrane. However, there are several reasons to question this assertion. First, mRNA localization appears to not be absolutely required for high-fidelity polarized secretion – *Perlecan* (*trol*) mRNA does not

display a basal bias, but the protein is still faithfully secreted to the basal surface (Lerner et al., 2013). Nor is it sufficient, as disruption of post-Golgi BM protein trafficking causes aberrant secretion to the apical surface (see next subsection). Additionally, whether such a mechanism could function in mammalian cells is unclear. Trafficking through a centralized Golgi ribbon would erase the polarity induced by mRNA localization. However, not all mammalian cells have a Golgi ribbon. Golgi outposts – analogous to the independent Golgi units in *Drosophila*– have been shown to promote polarized protein secretion, possibly in conjunction with localized mRNAs, in vertebrate neurons (Bramham and Wells, 2007; Hanus and Ehlers, 2008; Horton et al., 2005; Lowenstein et al., 1994; Pierce et al., 2001; Ramírez and Couve, 2011). A distributed Golgi system has also been described in gastric parietal cells (Gunn et al., 2011)**.**

It is important to note that the two hypotheses as to why the BM proteins are preferentially produced in a basal region of the ER are not mutually exclusive and could simultaneously promote BM formation. These observations offer interesting insight into potential mechanisms regulating BM protein production and secretion, but further study is required to understand the implications of local BM protein production. Experimentally disturbing the basal bias of BM protein production in these cells will be especially useful in discerning the veracity of these hypotheses.

Post-Golgi trafficking of BM proteins to the basal surface

Apico-basal polarity depends on the polarized trafficking of newly synthesized transmembrane proteins to either the apical or combined basal and lateral (basolateral) membrane domains. Several sorting mechanisms have been identified that direct individual proteins to each of these locations (Rodriguez-Boulan et al., 2005; Stoops and Caplan, 2014). Knowledge of these

pathways, however, has failed to provide insight into the polarized trafficking pathway that transports BM proteins exclusively to the basal surface. Indeed, several classic studies performed in cultured mammalian epithelial cells have indicated that distinct pathways exist for polarized trafficking of BM versus transmembrane proteins. Treatment with NH_4Cl or colchicine, which perturbs the acidification of intracellular compartments and microtubule dynamics, respectively, disrupts the polarized secretion of BM proteins without affecting basolateral transmembrane proteins. Under these conditions, BM proteins are secreted from both the apical and basal epithelial surfaces (Boll et al., 1991; Caplan et al., 1987; De Almeida and Stow, 1991; Natori et al., 1992). Conversely, disruption of Cdc42 function disrupts polarized secretion of basolateral transmembrane proteins but has no effect on BM proteins (Cohen et al., 2001). In fact, even integrins appear to move through a different trafficking pathway than BM proteins (Boll et al., 1991). These studies revealed that a specific pathway for polarized BM secretion exists, but offered little insight into its molecular details.

Recent genetic studies in *Drosophila* have begun to identify the major molecular players that control polarized BM secretion in this system. The DENN domain-containing protein Crag (Calmodulin-binding protein related to a Rab3 GDP-GTP exchange protein) was discovered in a forward genetic screen for novel regulators of apico-basal polarity in the follicular epithelium (Denef et al., 2008). Similar to the early observations in mammalian cells, BM proteins accumulate on both the apical and basal surfaces of *Crag* mutant follicle cells, whereas apical and basolateral transmembrane proteins localize normally. Apical accumulation of Perlecan was also observed in the epidermis of *Crag* mutant embryos. Importantly, this paper confirmed that the apical deposition of BM proteins is not due to transcytosis of protein from the existing BM, but rather due to the aberrant secretion of newly synthesized proteins. Crag was initially

observed to localize to apical and lateral cell membranes and to Rab5- and Rab11-positive endosomes, although an important population near the basal surface has since been described (see below).

DENN domain-containing proteins commonly function as guanine nucleotide exchange factors (GEFs) for Rab-family GTPases (Marat et al., 2011), which are molecular switches that cycle between an active GTP-bound state and an inactive GDP-bound state. GEFs transition Rabs to the GTP-bound state, whereas GTPase activating proteins (GAPs) induce transition to the GDP-bound state. The presence of specific active Rab proteins confers identity to membrane-bound compartments within the cell, such as organelles and trafficking vesicles (Barr, 2013). Rabs are also master regulators of vesicle activity, controlling their formation, sorting, targeting, fission, and fusion (Hutagalung and Novick, 2011). It was therefore speculated that Crag might activate a Rab that plays one or more roles in the polarized secretion of BM proteins.

Crag was later found to be GEF for a known exocytic Rab, Rab10, first in mammals and then in flies (Lerner et al., 2013; Xiong et al., 2012; Yoshimura et al., 2010). Consistent with this result, Rab10 depletion also causes BM proteins to accumulate on both the apical and basal surfaces of the follicular epithelium (Lerner et al., 2013). One key function of a GEF is to recruit its cognate Rab to the correct intracellular membranes (Blümer et al., 2013). Interestingly, Rab10 and Crag co-localize on membrane-bound compartments that are tightly associated with the basal surfaces in the follicle cells, proximal to the ER compartment where BM proteins are synthesized. This basally localized population of Rab10 is lost in *Crag* mutant cells, which suggests that BM proteins likely pass through these compartments on their way to the basal surface.

Although Rab10's exact role(s) in polarized BM secretion remains to be determined, one appealing hypothesis is that this protein functions in an endosomal recycling compartment (ERC) to help sort BM cargos into a basally directed trafficking pathway. Biosynthetic cargo sorting commonly occurs in the trans-Golgi network (Anitei and Hoflack, 2011; Santiago-Tirado and Bretscher, 2011). However, in polarized epithelial cells most exocytic traffic also passes through ERCs, where additional sorting occurs (Fölsch et al., 2009; Gonzalez and Rodriguez-Boulan, 2009). Rab10 localizes to endocytic compartments in both *C. elegans* and mammalian cells (Babbey et al., 2006; Chen et al., 2006; Shi et al., 2010). Moreover, although Rab11 (another Rab that localizes to ERCs) is not normally required for BM traffic, when Rab10 or Crag are depleted, the BM proteins that travel to the apical surface do so through a Rab11-dependent mechanism (Lerner et al., 2013). This observation suggests that Crag and Rab10 promote the sorting of BM proteins away from a Rab11-dependent pathway.

Crag and Rab10 have been established as the core components of a BM-specific trafficking pathway, though how this pathway recognizes, sorts, and targets BM proteins to the basal surface remains to be discovered, as do additional components involved in this process. Two additional proteins have been identified that are required for polarized BM secretion, although the mechanisms by which they do so are less well understood. These are Phosphatidylinositol synthase (Pis), an enzyme involved in the production of phosphoinositides (Devergne et al., 2014), and Scarface, a secreted serine protease-like protein that lacks catalytic activity (Sorrosal et al., 2010).

The phosphoinositides are a family of phospholipids that regulate a stunning array of cellular processes (Balla, 2013). Various phosphoinositide isoforms are created by kinase- and phosphatase-mediated interconversion between different phosphorylation states of a common

phospholipid backbone, phosphatidylinositol. Pis synthesizes phosphatidylinositol, and is therefore required for formation of all phosphoinositides; however, the authors focused their analyses on the role of phosphatidylinositol 4,5-bisphosphate (PIP2) in polarized BM secretion (Devergne et al., 2014). PIP2 functions as an apical determinant in the regulation of epithelial polarity (Martin-Belmonte et al., 2007). It also regulates multiple steps of polarized vesicle trafficking, including cargo sorting and membrane fusion (Balla, 2013). In the follicular epithelium, PIP2 is enriched on apical and lateral membranes. Loss of Pis or other PIP2 biosynthetic enzymes decreased PIP2 levels and caused a loss of Crag from apical and lateral membranes (Devergne et al., 2014). How the lateral and apical Crag populations would feed into basal protein secretion is difficult to say. It is also unclear whether loss of these populations upon Pis depletion is specific, or is an indirect effect of a general reduction in Crag protein levels throughout the cell.

In *Scarface* mutant embryos, Laminin accumulates on the apical surface of the lateral epidermis and an adjacent extraembryonic epithelium called the amnioserosa; this phenotype is also seen in *Crag* mutant embryos (Sorrosal et al., 2010). Interestingly, expression of Scarface exclusively in the lateral epidermis is sufficient to rescue the BM secretion defect in the amnioserosa of *scarface* mutants, which suggests that this protein can act at a distance. Consistent with this finding, expression of a tagged version of Scarface in a specific region of the wing disc epithelium caused the protein to accumulate on the apical surface and within the endosomal system of non-expressing cells. Three hypotheses have been proposed for Scarface's function in polarized BM secretion (Eastburn and Mostov, 2010; Sorrosal et al., 2010). Scarface could function within an endosomal compartment to help sort BM proteins into a basally directed trafficking pathway. This possibility is appealing as it aligns well with the likely function of

Rab10. Alternatively, Scarface could function at the apical plasma membrane to prevent targeting of BM-containing vesicles to this domain, a function that has also been proposed for Crag (Denef et al., 2008; Devergne et al., 2014). Finally, Scarface could remove BM proteins from the apical surface either by stimulating a proteolytic cascade or via endocytosis. Study of Scarface in the better-understood follicular epithelium may help to build a coherent model for how Crag, Rab10 and Scarface function together to control polarized BM secretion.

Finally, while the Crag/Rab10 pathway has not yet been shown to control polarized BM trafficking in vertebrates, the utilization of distinct secretory pathways for BM and basolateral transmembrane proteins in both *Drosophila* and mammalian cells is intriguing. Such a condition could arise based on special accommodations that certain BM proteins require to move through the secretory pathway (i.e. an acidic environment, enlarged vesicles, etc.), or due to differences in recognizing transmembrane and soluble proteins by the sorting machinery. Where, precisely, these proteins leave the cell could also play a role. Basolateral transmembrane proteins appear to exit the cell though an apical region of the lateral plasma membrane, just basal to the adherens junctions (Grindstaff et al., 1998). In contrast, BM proteins are more likely to exit at or very near the basal surface; indeed, Rab10 has been found on secretory vesicles bound for a basal region of the lateral plasma membrane in mammalian cells (Cao et al., 2008). Further characterization of the proteins already known to be involved in basal targeting of BM proteins and the identification of other key players will provide a rich area for future research.

1.5 MECHANICAL CONTRIBUTIONS OF THE BM TO MORPHOGENESIS

Morphogenesis is the process by which cells and tissues change their shapes to create the complex form of adult tissues and organs. BM sheets are well designed to physically assist and

regulate morphogenetic processes - by modifying the movement of cells via adhesive interactions, by resisting the contractile forces exerted by cells, or by restricting the expansion of growing tissues. Furthermore, a large number of studies, primarily in *in vitro* cell culture systems, have found that changing the physical properties of ECMs can modulate the dynamic activities of cells. For instance, changes in matrix stiffness or cell-matrix adhesion affect cellular contractile dynamics and downstream signals within the cell (Charras and Sahai, 2014). Matrix stiffness also appears to regulate cell migration, as many cells tend to migrate from softer to stiffer ECM substrates, or towards ECM that is under deformation forces (Lo et al., 2000; Reinhart-King et al., 2008; Roca-Cusachs et al., 2013). A softer matrix, meanwhile, can promote cellular invasion through the network (Gu et al., 2014). The organization of the matrix also influences migration dynamics (D-H. Kim, Provenzano, Smith, & Levchenko, 2012); directionally aligned matrices have been found to orient cellular migration in the direction of alignment and to increase migration speed (Diehl et al., 2005; Provenzano et al., 2008, 2006; Tan and Saltzman, 2002). Confirmation of these observations *in vivo* remains an important task; *Drosophila* offers an enticing opportunity to explore these concepts within a developing animal.

In vivo, the BMs of developing tissues undergo heavy remodeling (Bernfield et al., 1984; Daley et al., 2008). Moreover, it is clear that different BMs, and even the same BMs over time, exhibit vastly different compositions and, therefore, physical properties. It is likely that the characteristics of these matrices are tuned to appropriately contribute to morphogenesis, although the changes in physical properties, their mechanisms, and their effects on morphogenesis are largely unclear.

Contributions of the BM to egg chamber elongation

The development of the egg chamber is perhaps the best understood example of how a coordinated progression of changes to BM structure and cellular activity interact to drive tissue morphogenesis (Horne-Badovinac, 2014). Egg chambers, which number in the hundreds within the adult ovary, are each responsible for the maturation of a single oocyte. They are composed of a central cluster of germ cells – one posteriorly localized oocyte and 15 supporting nurse cells – that is surrounded by the follicular epithelium that was discussed in the last section. This somatic tissue is made up of roughly 800-1000 cells, and the BM it produces ensheathes the entire organ-like structure (Figure 1.4 A). Initially small and spherical, egg chambers proceed through 14 distinct morphological stages, during which they grow to nearly 1000 times their initial volume (Cummings and King, 1969). Between stages 5 and 10, growth is channeled anisotropically to induce elongation along the anterior-posterior (A-P) axis, a process that creates the elliptical shape of the egg (Figure 1.4 C).

BM structure has been examined across egg chamber development and found to shift dramatically with the onset of elongation. The BM surrounding early egg chambers does not show any obvious structure by light microscopy. However, concurrent with the onset of elongation at stage 5, dense, linear fibril-like aggregates of Collagen IV, Laminin, and Perlecan begin to be incorporated into the existing planar matrix (Cetera et al., 2014; Gutzeit et al., 1991; Haigo and Bilder, 2011a; Schneider et al., 2006) (Figure 1.4 C). These structures all align perpendicular to the A-P axis, effectively polarizing the BM. Arrays of linear actin bundles in the adjacent basal cortex of each follicle cell, which are physically coupled to the BM via integrin-based focal adhesions, align in the same direction as the BM fibrils (Bateman et al.,

2001; Delon and Brown, 2009; Gutzeit, 1990). Together, the BM fibrils and basal actin bundles are thought to act as a "molecular corset" that directionally constrains egg chamber growth,

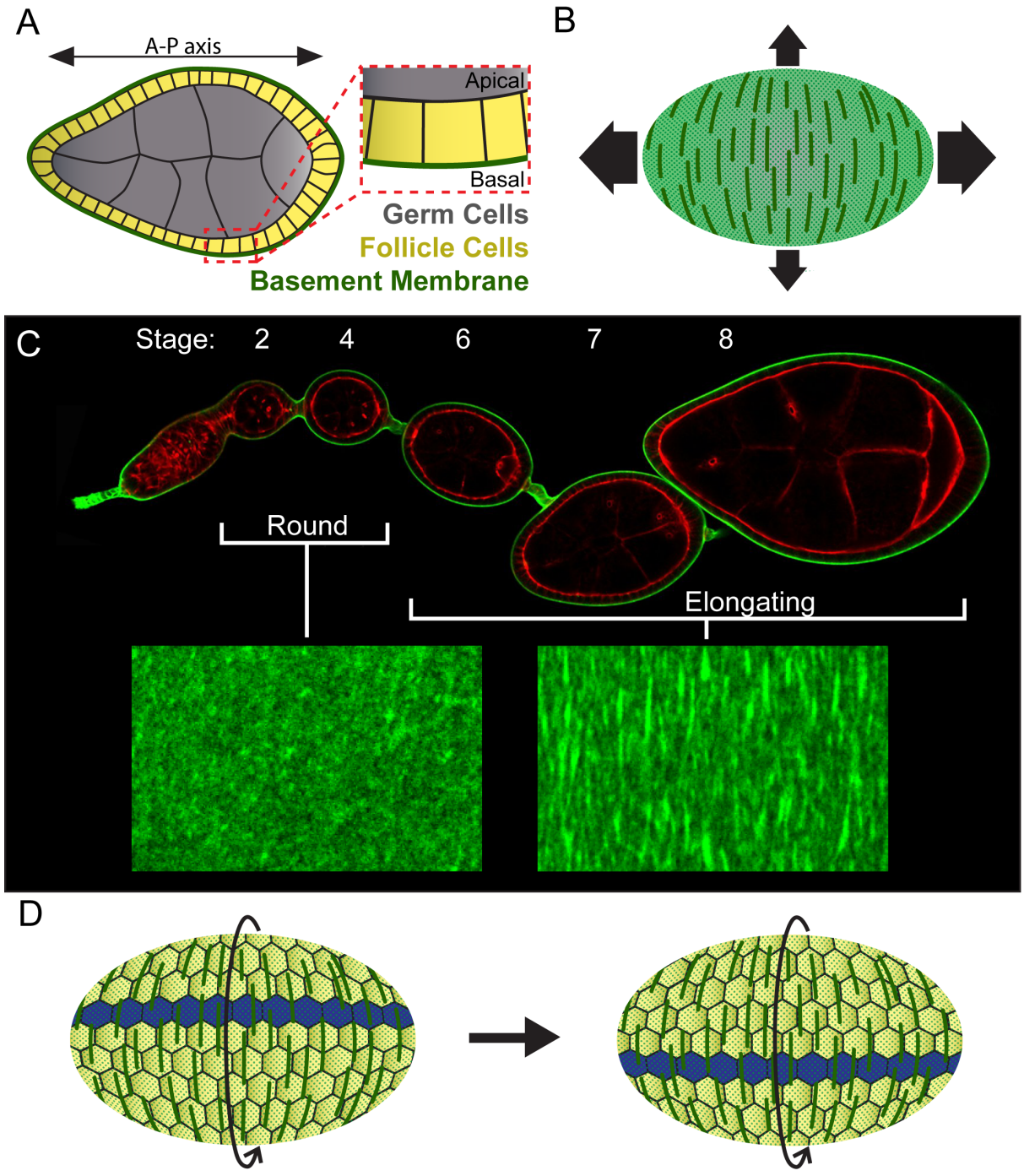

Figure 1.4. BM function in egg chamber elongation
(A) Illustration of a transverse section through an egg chamber. Central germ cells are surrounded by a somatic epithelium of follicle cells, which assemble a BM on their basal surfaces. (B) Model of the molecular corset. Polarized linear fibril-like structures in the BM are

Figure 1.4. Continued, BM function in egg chamber elongation
hypothesized to constrain egg chamber growth in the direction of polarization, biasing growth to occur along the A-P axis. Arrows indicate direction and magnitude of growth. (C) BM structural dynamics during elongation. Top: a developmental array of egg chambers showing cell outlines (actin) and the BM (Viking-GFP). Bottom: fluorescent micrographs of Collagen IV (Viking-GFP) in the BM. Young, round egg chambers exhibit no obvious BM structure, while older, elongating egg chambers display polarized fibrils within the BM. (D) Overview of egg chamber rotation. In this illustration, the BM is partially transparent to reveal the cells underneath. The dark row of cells in each image represents the same cells at two different time points. The egg chamber rotates within a stationary BM, in the direction of BM fibrils. Curved arrows indicate direction of egg chamber rotation.

thereby providing the anisotropic force that drives elongation (Gutzeit et al., 1991) (Figure 1.4 B). This hypothesis is supported by the observation that disruption of the tissue-level organization of these structures leads to the production of rounded eggs (Bateman et al., 2001; Cetera et al., 2014; Conder et al., 2007; Frydman and Spradling, 2001; Gutzeit et al., 1991; Haigo and Bilder, 2011a; Horne-Badovinac et al., 2012; Lewellyn et al., 2013; Viktorinová et al., 2009).

Formation of the molecular corset depends on a dramatic rotational motion of the egg chamber. Between stages 1 and 8, the basal surfaces of the follicle cells migrate along the BM, orthogonal to the A-P axis (Cetera et al., 2014; Haigo and Bilder, 2011a). Because the apical surfaces of the follicle cells are attached to the germ cell cluster through cadherin-based adhesions, this collective motion causes the entire egg chamber to rotate within the surrounding BM, which remains largely stationary throughout the process (Figure 1.4 D). Failure of the follicle cells to migrate disrupts the polarity of the actin and BM networks and prevents egg chamber elongation (Cetera et al., 2014; Haigo and Bilder, 2011a; Lerner et al., 2013; Viktorinová and Dahmann, 2013).

The presence of linear, fibril-like aggregates in the follicular BM is surprising, as a BM architecture of this type has not been described in other systems. Because flies do not produce

fibril-forming Collagens or fibronectin, it is intriguing to speculate as to whether these unusual BM structures might perform some of the same functions as the true fibrillar matrices found in other organisms. Future work will be required to understand the molecular organization of the BM fibrils, as well as the mechanism by which they form. Although egg chamber rotation is required for their formation (Haigo and Bilder, 2011a), it is clearly not sufficient, as rotation begins at stage 1 and BM fibrils do not begin to form until stage 5 (Cetera et al., 2014). Fibril formation does, however, happen at a time when Collagen IV levels are increasing in the matrix (Haigo and Bilder, 2011a), which could indicate a role for new protein secretion in this process. Further, because fibrils appear to play an important functional role in this BM, it will be intriguing to explore to what extent BM superstructural elements are used in other systems to regulate tissue dynamics.

In addition to polarized fibril formation, other structural changes in the BM likely also contribute to its proposed corset function. As mentioned in the previous paragraph, Collagen IV levels drastically increase in the BM between stages 5 and 8 (Haigo and Bilder, 2011a). Precise control of Collagen IV crosslinking also appears to influence elongation, as increasing Peroxidasin-dependent Collagen IV crosslinking enhances elongation while decreasing Peroxidasin activity inhibits elongation without grossly affecting BM superstructure (McCall et al., 2014). In the future, it will be important to determine whether the levels or properties of other BM components are also dynamically regulated as part of the elongation program. It will also be interesting to explore whether the complex interplay that occurs between different BM components in other tissues similarly affect the physical properties of the follicular BM (Pastor-Pareja and Xu, 2011). Finally, methods will need to be developed to directly measure how each of these changes in matrix architecture alter BM strength and stiffness.

The BM also appears to influence the tissue-level alignment and activity of the basal actin bundles during elongation. Global actin bundle alignment depends on the rotational motion of the egg chamber at early developmental stages, but this organization becomes rotation-independent concurrent with the establishment of matrix polarity (Cetera et al., 2014). Although rotation ceases at stage 8, maintenance of basal actin bundle alignment is likely to be important for the final phase of elongation, which begins at stage 9. At this stage, periodic myosin-based contraction of the basal actin bundles contributes to elongation (He et al., 2010). Proper basal actin alignment is likely required for directionality of this force. Interaction with the BM also directly influences contractile activity of the cells. Decreasing expression of the focal adhesion protein Talin shortens the period of myosin contraction, while over-expressing Paxillin, another focal adhesion protein, prolongs the period (He et al., 2010). Surprisingly, treatment of egg chambers with collagenase, which might be expected to mimic a decrease in cell-BM adhesion, has also been observed to prolong the period of myosin contraction (Koride et al., 2014). Myosin-based contractions, therefore, are likely regulated by complex inputs from BM structure and cell-BM adhesion.

Once growth has stopped and the elongation program is complete, the BM now plays an important role in maintaining the egg chamber's elliptical shape. When stage 13 egg chambers are treated with collagenase to disrupt the BM, they rapidly become rounder, shortening along the A-P axis and expanding along the orthogonal axis (Haigo and Bilder, 2011a). Thus the BM is required, in varying capacities, to support morphogenesis of the egg chamber for the entirety of its development.

As a final note, studies of egg chamber elongation have also revealed interesting potential effects of BM architecture and cell-BM adhesion on cell migration speed. Although the

collective migration of the follicle cells that causes the egg chamber to rotate begins at stage one, the speed of this migration increases sharply at stage 6, just after the BM fibrils begin to form and Collagen IV levels begin to rise (Cetera et al., 2014). However, further investigation will be required to determine whether changes in BM architecture play a causal role in this acceleration. Altering integrin levels in the follicle cells also modifies their migration speed, such that decreasing integrins increases speed and increasing integrins decreases speed (Lewellyn et al., 2013).

Contributions of the BM to the morphogenesis of other tissues

Loss of function studies have revealed that, in addition to the egg chamber, BMs also appear to play critical roles in the morphogenesis of many other fly tissues and organs. To date, however, few of these initial observations have been followed up with mechanistic studies. Two tissues that have been examined more intensely in this regard are the wing imaginal disc epithelium and migrating glial cells in the imaginal eye disc. These studies are detailed below.

In the wing disc epithelium, local matrix degradation is required for two developmental processes. During larval development, adjacent tracheal tissue must invade through the wing disc BM and contact the underlying epithelium to form the air sac primordium. This process requires local BM degradation by Matrix Metalloprotease 2 (Mmp2) (Guha et al., 2009). In the pupa, the internal wing disc protrudes through the body wall to form the external wing in a process known as disc eversion. This morphogenesis also requires Mmp2-mediated BM degradation (Srivastava et al., 2007). A unique pattern of Collagen IV cleavage is seen during disc eversion, suggesting precise, context-specific modifications of BM structure during morphogenesis (Fessler et al., 1993).

Maintenance of proper cell shape in the larval wing disc epithelium also depends on interaction with an appropriately structured BM. Integrin-based adhesion to the BM is crucial for maintaining proper cell shape (Domínguez-Giménez et al., 2007). Maintenance of cell shape also depends on balanced and opposing forces contributed by Collagen IV and Perlecan. Loss of Collagen IV causes flattening of wing disc epithelial cells and the entire tissue, while loss of Perlecan causes disc compaction and elongation of cells along their apico-basal axes (Pastor-Pareja and Xu, 2011). A similar antagonistic role for Collagen IV and Perlecan has been observed in the *C. elegans* neuromuscular junction, where the two molecules differentially regulate growth of presynaptic boutons (Qin et al., 2014).

Finally, regulation of BM structure, specifically its stiffness, impacts the migration of glial cells within the eye disc. A stiffer matrix is known to promote cell migration *in vitro* (Lo et al., 2000; Roca-Cusachs et al., 2013). It was recently demonstrated that increasing the activity of the Collagen crosslinking enzyme Lysyl Oxidase (Lox) or integrins increases BM stiffness *in vivo* in this system (Kim et al., 2014). This study further found that migrating glial cells upregulate Lox and integrin expression to promote their own migration. This is superficially similar to the observation, discussed above, that altering integrin levels affects cell migration in the egg chamber. However, during glial migration upregulation of integrins promotes migration, while in the egg chamber integrin upregulation slows migration or, when severe enough, inhibits it completely (Lewellyn et al., 2013). Integrin levels therefore appear to play a complex and context-specific role in migration dynamics.

1.6 CONTRIBUTIONS OF THE BM TO CELL-CELL SIGNALING DURING DEVELOPMENT

Cell-to-cell signaling, primarily through several major secreted molecules and their receptors, is crucial to regulate and coordinate tissue development. Although the predominant view of the BM tends to be structure-centric, it also serves as a major extracellular signaling platform. By interacting directly with secreted signaling proteins, the BM can act to limit their diffusion or modify their interactions with cell surface receptors. Genetic and biochemical evidence from flies and vertebrates indicates that the BM regulates most, if not all, major developmental signaling pathways, including TGF-β/BMP (Paralkar et al., 1991; Wang et al., 2008), FGF (Folkman et al., 1988; Klagsbrun, 1990; Lin et al., 1999; Park et al., 2003), Wingless/Wnt (Binari et al., 1997; Perrimon and Bernfield, 2000), and Hedgehog (Datta et al., 2006; Park et al., 2003; Rubin et al., 2002; The et al., 1999). An advantage of the developmental focus of *Drosophila* research is that the early studies performed in this system offered not only evidence for these interactions, but immediate indications of their developmental relevance. Since the connection was made between the BM and signaling, a diverse set of examples have emerged in *Drosophila* of the roles these interactions play in guiding specific developmental processes. Three such processes will be discussed here: axonal pathfinding, Malpighian tubule morphogenesis, and regulation of stem cell activity.

Modulation of Slit/Robo and Semaphorin/Plexin signaling during axonal pathfinding

As the nervous system develops, growth of axons away from neuronal cell bodies is required to appropriately innervate the body and promote connections with other neurons or tissues. As discussed above, the BM is an important permissive substrate for migration of many cell types,

including neurons (Takagi et al., 1996), but it also acts to regulate the response of extending axons to multiple environmental signals that provide attractive or repulsive cues to guide their growth. Slit and Robo are a highly conserved signaling duo that were first discovered in forward genetic screens for developmental defects in *Drosophila* embryos (Nüsslein-Volhard et al., 1984; Seeger et al., 1993). Subsequent work showed that Slit is an extracellular protein that primarily functions as a repellent cue for axons that express the Robo receptor (Brose et al., 1999; Dickson and Gilestro, 2006). There is evidence that Slit may bind Laminin in vertebrates (Brose et al., 1999), and Laminin misexpression causes axon guidance defects in *Drosophila* (García-Alonso et al., 1996; Kraut et al., 2001). Further, decreasing Laminin or integrin expression enhances the axon pathfinding defects in a *Slit* hypomorphic allele, suggesting that the BM modulates axonal responsiveness to Slit signals (Stevens and Jacobs, 2002). Slit binding to Heparin also enhances the Slit-Robo interaction (Hussain et al., 2006), and the transmembrane HSPG Syndecan, which can function as a BM receptor (Carey, 1997), acts with Robo as a Slit co-receptor (Johnson et al., 2004; Smart et al., 2011; Steigemann et al., 2004). Whether this interaction occurs cooperatively with or independently of the BM is unclear, although Perlecan, the BM HSPG, does not appear to exhibit similar activity (Steigemann et al., 2004).

Semaphorin-based axon guidance also relies on interactions with the BM. Semaphorin-1A is a transmembrane protein expressed at axon guidance decision points that signals to the axonal receptor Plexin A, which mediates repulsion at sites of Semaphorin contact (He et al., 2002). Similar to Slit, vertebrate Semaphorin activity is enhanced by Heparin (De Wit et al., 2005). In this case, however, the HSPG utilized appears to be Perlecan, which is heavily deposited at axon branch points and is required to augment a *Semaphorin-1A* gain-of-function mutation in *Drosophila* (Cho et al., 2012). *Syndecan* showed no genetic interaction with

Semaphorin-1A in this study. It is intriguing that two signaling pathways, Slit/Robo and Semaphorin-1A/Plexin A, which regulate similar axonal guidance events by different molecular means, exhibit non-overlapping reliance on two HSPG proteins. The coincidence of HSPG utilization among these pathways is mysterious, although utilization of different HSPG co-factors may enhance signaling diversity while maintaining signal distinction and resolution in the crowded neuronal milieu.

Modulation of BMP signaling during Malpighian tubule morphogenesis

Epithelial tubes are organized with their apical surfaces surrounding an internal lumen and their basal surfaces covered by a BM. Tubular outgrowth and branching are important in the development of several organs, including lungs, kidney, and salivary and mammary glands (Andrew and Ewald, 2010). Work in several vertebrate systems has identified mechanical roles for the BM and other ECMs in branching morphogenesis (Varner and Nelson, 2014). In *Drosophila,* the BM has been implicated in signaling during tubule morphogenesis as well. The *Drosophila* kidney ortholog, the Malpighian tubules, exhibits stereotyped outgrowth guided by a leading group of "kink cells" at the tissue's anterior (Denholm, 2013). Local expression of the BMP homolog Decapentaplegic (Dpp) in tissues along the tubule outgrowth route is necessary and sufficient to guide this morphogenesis (Bunt et al., 2010). Further, local deposition of Collagen IV by hemocytes on the outgrowing tubules is required to transduce the Dpp signal in kink cells (Figure 1.5 A). Supporting this observation, Dpp directly binds the C-terminus of Collagen IV, which enhances interaction of Dpp with its receptors (Wang et al., 2008). This interaction appears to be conserved in mammals (Paralkar et al., 1991).

In the case of the Malpighian tubules, Collagen IV helps to localize and concentrate the Dpp signal for its reception by target cells. Two other examples where Dpp and Collagen IV interact in a similar manner will be discussed in the next section. Interestingly Dpp is also known to regulate several developmental processes in *Drosophila* by formation of precise morphogen gradients. Because Collagen IV appears to restrict diffusion of Dpp, it has been proposed that the BM may play an important role in these instances of Dpp signaling as well. (Sawala et al., 2012; Umulis et al., 2010; Wang et al., 2008). It will therefore be intriguing to examine the role of the BM during Dpp signaling in other contexts.

Regulation of stem cell maintenance, differentiation, and division

Stem cells are multipotent progenitors that provide a key source of new cells during development. They also play important roles in tissue maintenance and repair in adults. The defining feature of stem cells is that they divide asymmetrically to produce two distinct cells: one stem cell to replace the mother, and one cell that will differentiate. In *Drosophila*, the capacity to identify and observe stem cells *in vivo* under different genetic conditions has revealed distinct roles for the BM in several tissues, three of which are discussed here.

In *Drosophila,* the female germline stem cells (GSCs) sit at the anterior end of the ovary in a specialized signaling environment deemed the niche (Losick et al., 2011; Xie and Spradling, 1998). The primary cells that make up the niche, the cap cells, bind GSCs through cadherin-based adhesions (Song et al., 2002). When GSCs divide, one daughter remains attached to the cap cells, while the other is expelled from this environment and, lacking the niche signals, differentiates. One key niche signal, secreted by the cap cells, is Dpp (López-Onieva et al., 2008; Wang et al., 2008). Collagen IV in the BM surrounding the niche binds Dpp and restricts

its diffusion (Figure 1.5 B); in the absence of Collagen IV, the Dpp signaling field expands to reach GSC daughter cells outside of the niche, which prevents them from differentiating and leads to an overabundance of stem cells (Wang et al., 2008). The HSPG Dally is also enriched around the niche and appears to concentrate Dpp and promote its reception by GSCs (Guo and Wang, 2009; Hayashi et al., 2009).

A mechanism similar to that seen with the GSCs also regulates adult intestinal stem cells (ISCs). While the ISC niche is not clearly understood, these cells are scattered throughout the intestinal epithelium and adhere directly to the BM (Micchelli and Perrimon, 2006; Ohlstein and Spradling, 2006). The BM appears to play a role in defining the niche, as it was recently discovered that Dpp maintains stem cell identity and that this protein is confined to the basal surface by Collagen IV. This localization allows higher signal reception by the ISCs than by the differentiating ISC daughter cells, the enteroblasts, whose cell bodies are located more apically within the epithelium (Tian and Jiang, 2014) (Figure 1.5 C). Dpp has also been proposed to regulate ISC proliferation, although the role of the BM in this case has not been elucidated (Guo et al., 2013; Li et al., 2013). The BM may therefore play a common role in regulating signals within stem cell niches.

Asymmetric division of *Drosophila* neuroblasts, the stem cells that give rise to the nervous system, occurs via an intrinsic mechanism that can, at least in part, occur independently of the cells' external environment (Broadus and Doe, 1997). This is achieved by uneven segregation of fate-determining factors into one of the two daughter cells (Knoblich, 2008). While the importance of the environment in neuroblast fate is not well understood, the BM does play a role in determining when and to what extent neuroblasts divide. *Drosophila* Perlecan was first identified as a factor that promoted activation of quiescent neuroblasts in larvae by

counteracting the anti-proliferative activity of the secreted glycoprotein Anachronism – hence its name, *terribly reduced optic lobes* (Datta, 1995; Voigt et al., 2002). Perlecan was also found to promote neuroblast proliferation by binding to and enhancing the signaling of Hedgehog and the FGF homolog Branchless (Park et al., 2003). The BM, therefore, appears to modulate several signaling pathways to ensure proper stem cell function in many contexts.

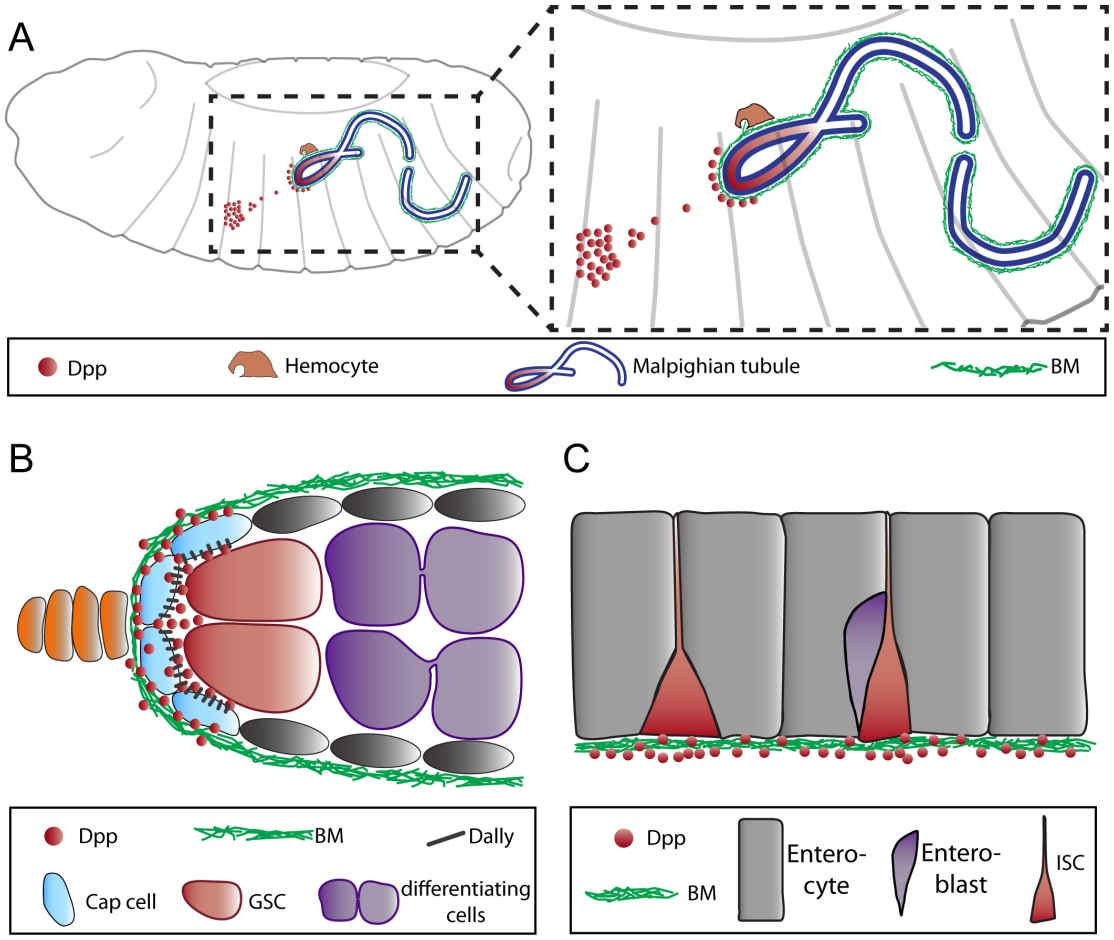

Figure 1.5. BM regulation of Dpp signaling in three developmental contexts
(A) Embryonic Malpighian tubule morphogenesis. Diffusible Dpp protein attracts the growing Malpighian tubule. Hemocyte-deposited Collagen IV around the Malpighian tubule promotes reception of the Dpp signal by tubule cells. (B) Ovarian germline stem cell (GSC) maintenance. GSCs are maintained within the stem cell niche via interaction with cap cells. Collagen IV in the BM and the HSPG Dally concentrate cap cell-derived Dpp to promote signal reception by GSCs but not differentiating daughter cells. (C) Intestinal stem cell (ISC) maintenance. ISCs exhibit basally positioned cell bodies that adhere to the BM. Dpp is concentrated by Collagen IV within the BM to promote a high level of signal reception by ISCs but not the more apically-localized, differentiating enteroblasts.

1.7 CONCLUSION

Developing tissues require precise control of their size, shape, activity and signaling environment to robustly create the adult organism. The BM has been found to integrally regulate all of these processes, thereby contributing an important external input to guide coordinated cellular activity. While studies of the BM to this point have been informative, they have also revealed how much we still have to learn. Regarding the polarized deposition and assembly of BM proteins, it will be crucial to continue to identify new factors that regulate this process. Proteins that are already known to function with Rab10 in *C. elegans* and mammalian cells are excellent candidates in this regard, and forward genetic screening strategies in *Drosophila* are likely to identify even more. In terms of understanding the functional properties of BMs once they are built, it will be important to better map their structural diversity. Although evidence from *Drosophila* and vertebrates suggests that BM architecture can vary from one tissue to the next, the precise structures of individual matrices are still largely unexplored. It will therefore be interesting to examine the composition (both of core and accessory proteins) and architecture of a diverse set of BMs, establish the levels of heterogeneity between them, and connect the physical characteristics of individual BMs to their functional properties. Expanding the library of fluorescently tagged BM proteins using modern genome editing techniques will greatly assist this endeavor. Additionally, recent evidence suggests that a BM may be more than the sum of its parts - that individual elements modify and collaborate with other proteins in the BM, on the cell surface, and within the local environment to create a complex interactive network. Understanding the nature of such interactions, in synergy with an enhanced understanding of BM structure, will further reveal the dynamic inputs of these matrices to cellular activity.

CHAPTER 2: DYNAMIC REGULATION OF BASEMENT MEMBRANE PROTEIN LEVELS PROMOTES EGG CHAMBER ELONGATION IN *DROSOPHILA*

2.1 PREFACE

The initial goal of my thesis work was to identify the mechanism of BM fibril formation in the egg chamber. To this end, I examined several proteins known to associate with the BM. This study was motivated by the observation that one such factor - the collagen-binding protein SPARC - is conspicuously down-regulated at the onset of BM remodeling and egg chamber elongation. I initially hypothesized that SPARC down-regulation promoted BM fibril formation. Although this idea was quickly ruled out, during these experiments I found that SPARC instead alters BM Col IV levels, which led me to recognize the importance of BM composition on egg chamber elongation. This chapter was published in *Developmental Biology* with the following citation: Isabella, A.J., Horne-Badovinac, S., 2015. *Dynamic regulation of basement membrane protein levels promotes egg chamber elongation in Drosophila*. Dev Biol. 406, 212-221.

2.2 ABSTRACT

Basement membranes (BMs) are sheet-like extracellular matrices that provide essential support to epithelial tissues. Recent evidence suggests that regulated changes in BM architecture can direct tissue morphogenesis, but the mechanisms by which cells remodel BMs are largely unknown. The *Drosophila* egg chamber is an organ-like structure that transforms from a spherical to an ellipsoidal shape as it matures. This elongation coincides with a stage-specific increase in Type IV Collagen (Col IV) levels in the BM surrounding the egg chamber; however, the mechanisms and morphogenetic relevance of this remodeling event have not been

established. Here, we identify the Collagen-binding protein SPARC as a negative regulator of egg chamber elongation, and show that SPARC down-regulation is necessary for the increase in Col IV levels to occur. We find that SPARC interacts with Col IV prior to secretion and propose that, through this interaction, SPARC blocks the incorporation of newly synthesized Col IV into the BM. We additionally observe a decrease in Perlecan levels during elongation, and show that Perlecan is a negative regulator of this process. These data provide mechanistic insight into SPARC's conserved role in matrix dynamics and demonstrate that regulated changes in BM composition influence organ morphogenesis.

2.3 INTRODUCTION

Basement membranes (BMs) are sheet-like extracellular matrices that adhere to the basal surfaces of epithelial tissues and play critical roles in cellular structure, specification, organization, and communication (Yurchenco, 2011). Composed primarily of Type IV Collagen (Col IV), Laminin, and the heparin sulfate proteoglycan Perlecan, BMs are often assumed to be static support structures. However, recent evidence suggests that BM structure is dynamic during development, and that regulated changes in BM architecture can direct tissue morphogenesis (Daley and Yamada, 2013; Fata et al., 2004; Miner and Yurchenco, 2004; Morrissey and Sherwood, 2015). Despite these findings, we know little about how cells remodel these matrices, or how such changes influence morphogenetic outcomes.

The *Drosophila* egg chamber provides a tractable system to study the influence of BM remodeling on morphogenesis (Isabella and Horne-Badovinac, 2015a). Egg chambers are multicellular structures within the ovary that will each give rise to one egg. They are composed of an interior germ cell cluster and a surrounding somatic epithelium of follicle cells (Figure 2.1

A). The follicle cells produce a BM that adheres to the outer surface of the egg chamber. Egg chamber development proceeds through 14 morphological stages. Between stages 5 and 10, this initially spherical structure elongates along its anterior-posterior (A-P) axis. This process depends on a precise organization of the basal epithelial surface, in which parallel arrays of actin bundles in the follicle cells and linear, fibril-like aggregates in the BM align perpendicular to the elongation axis (Cetera and Horne-Badovinac, 2015; Horne-Badovinac, 2014). The circumferential arrangement of these structural molecules is thought to act as a "molecular corset" that constrains egg chamber growth in the direction of alignment, thereby driving elongation (Figure 2.1 B) (Gutzeit et al., 1991). Elongation is also coupled to a collective migration of the follicle cells along the BM, which causes the egg chamber to rotate within the matrix and is required for alignment of basal actin bundles and BM fibrils (Cetera et al., 2014; Haigo and Bilder, 2011b).

Two changes in BM architecture coincide with egg chamber elongation. In addition to the formation of aligned BM fibrils, the amount of Col IV in the BM doubles between stages 5 and 8 (Haigo and Bilder, 2011b). These stage-specific remodeling events have been proposed to promote elongation, as defects in BM integrity or cell-matrix adhesion inhibit this process (Bateman et al., 2001; Haigo and Bilder, 2011b; Lerner et al., 2013; Lewellyn et al., 2013). However, previous experimental manipulations of the BM have also disrupted other factors required for elongation, such as rotational motion and tissue-level alignment of the basal actin bundles. Because it has so far not been possible to solely manipulate BM structure, a causal relationship between stage-specific BM remodeling and egg chamber elongation remains to be established.

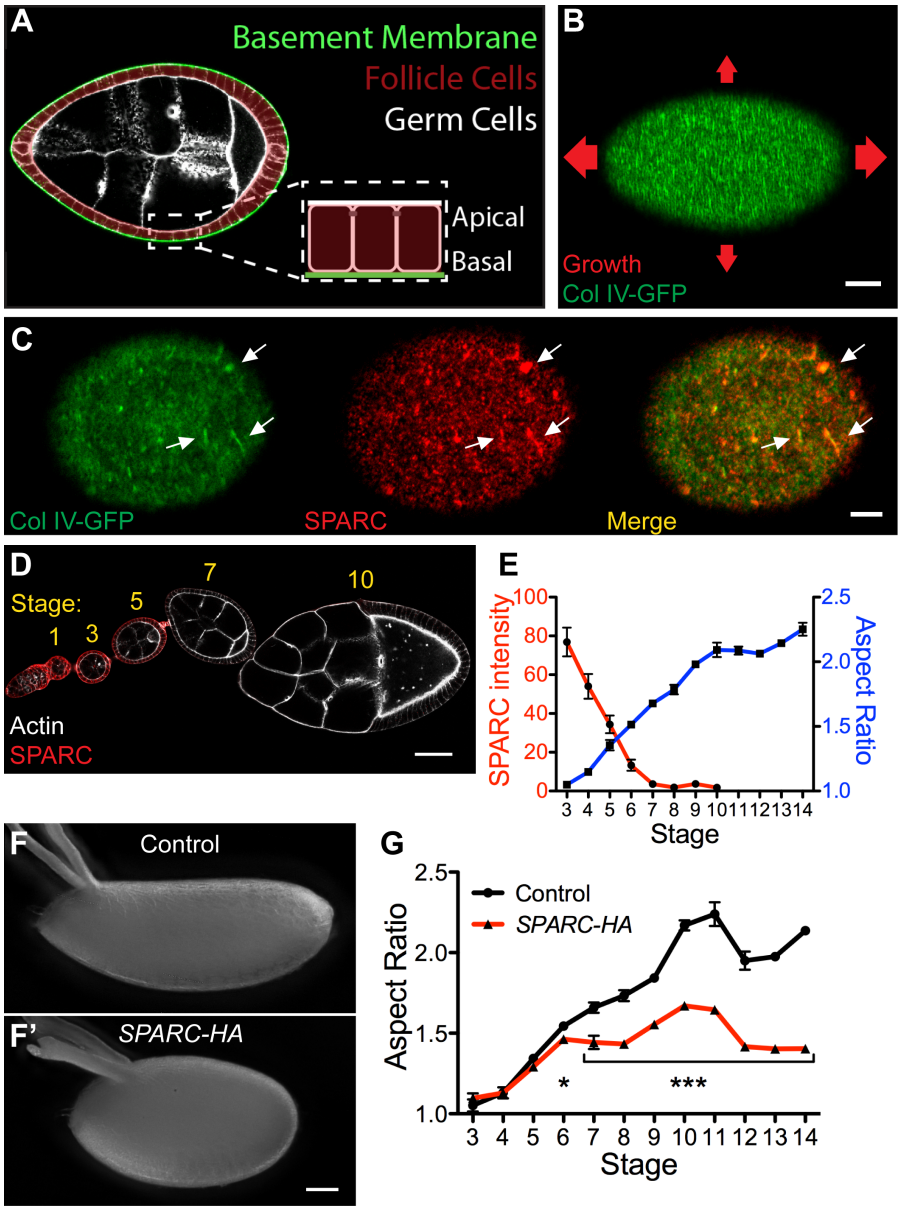

Figure 2.1. SPARC down-regulation is necessary for egg chamber elongation.
(A) Egg chamber structure. (B) In the molecular corset model, circumferentially aligned fibrils in the BM constrain egg chamber growth in the direction of alignment. Arrows indicate direction and relative magnitude of growth. Stage 8. (C) Col IV and SPARC co-localize in the egg chamber BM (arrows). Stage 5, maximum intensity projection. (D-E) Loss of SPARC immunofluorescence coincides with egg chamber elongation. (D) SPARC immunostained egg chambers. Image represents two stitched micrographs. (E) Quantification of SPARC intensity and aspect ratio. n = 6-12 (SPARC intensity), 10-11 (aspect ratio) egg chambers per data point. Aspect ratio = length/width. (F-G) Persistent *SPARC-HA* expression with *traffic jam-Gal4* inhibits egg chamber elongation. (F-F') Representative control and *SPARC-HA* eggs. (G) Persistent *SPARC-HA* expression disrupts egg chamber elongation after stage 5. n = 6-30 egg chambers per data point. (E,G) Data represent mean with s.e.m. Some error bars are too small to be seen. t-test * = P<0.05, *** = P<0.0005. Scale bars: 10 µm (B), 5 µm (C), 50 µm (D,F).

To determine the relationship between structural changes in the BM and egg chamber elongation, we sought to identify BM-associated proteins that regulate these processes. Secreted Protein Acidic and Rich in Cysteine (SPARC) is a conserved Collagen-binding protein (Bradshaw, 2009). SPARC mis-regulation perturbs the function of many extracellular matrices and associated tissues, and correlates with cancer progression (Clark and Sage, 2008; Nagaraju et al., 2014). Despite its importance in development and disease, the mechanism by which SPARC affects BM structure is uncertain. It has been proposed to regulate Collagen deposition, degradation, and adhesion to cells, but a coherent view of SPARC function is lacking (Chlenski et al., 2011; Harris et al., 2011; Nathalie Martinek et al., 2008; Pastor-Pareja and Xu, 2011; Sage et al., 1989; Shahab et al., 2015). SPARC is expressed in early stage follicle cells and accumulates with Col IV in the BM (Figure 2.1 C) (Martinek et al., 2002). Intriguingly, *SPARC* mRNA disappears from the follicle cells between stages 5 and 6, coincident with the onset of BM remodeling and egg chamber elongation (Martinek et al., 2002).

Here, we show that prolonging the expression of SPARC into later stages of development inhibits the stage-specific rise in Col IV levels within the BM and blocks egg chamber elongation. We observe that SPARC and Col IV can interact within the secretory pathway of the follicle cells, and propose a mechanism by which this interaction inhibits incorporation of newly synthesized Col IV into the BM. We then directly examine the role of BM protein levels in egg chamber elongation and find that increased Col IV and decreased Perlecan levels both promote elongation, revealing opposing effects of these two BM proteins in this system. These findings provide new insight into SPARC's effect on BM structure and show that regulated changes in BM composition can play critical roles in organ morphogenesis.

2.4 RESULTS

SPARC down-regulation is necessary for egg chamber elongation

The conspicuous timing of *SPARC* mRNA down-regulation at the onset of egg chamber elongation led us to investigate whether this event is required for morphogenesis. We first confirmed that, like the mRNA, SPARC protein disappears from the follicle cells between stages 5 and 7 (Figure 2.1 D-E). We then used the *traffic jam-Gal4* driver, which is expressed in the follicle cells at all stages, to prolong *SPARC* expression. Importantly, expression of either a HA-tagged *UAS-SPARC* transgene (*SPARC-HA*) or an untagged *UAS-SPARC* transgene (*SPARC-WT*) with *traffic jam-Gal4* inhibits egg chamber elongation (Figures 2.1 F-G, 2.2 A). This defect is first seen at stage 6, consistent with when SPARC is normally lost (Figure 2.1 G). The levels of persistent SPARC expression into later stages of development are equivalent to those of the endogenous protein at stage 5 (Figure 2.2 B-C). Moreover, failure to elongate is caused specifically by expression of *SPARC* beyond stage 5, as *SPARC-HA* expression using a *SPARC-Gal4* driver has no effect (Figure 2.2 D). Collectively, these results indicate that down-regulation of *SPARC* expression is necessary for egg chamber elongation.

SPARC negatively regulates Col IV levels in the BM

We next explored why egg chamber elongation is incompatible with SPARC expression. Because SPARC down-regulation correlates with BM remodeling, we hypothesized that SPARC might disrupt this process. Using a GFP protein trap in the Col IV-α2 gene *viking* (Col IV-GFP), we noticed a consistently dimmer Col IV-GFP signal in the BMs of *SPARC-HA* egg chambers compared to controls. Quantification of Col IV-GFP levels revealed that the increased

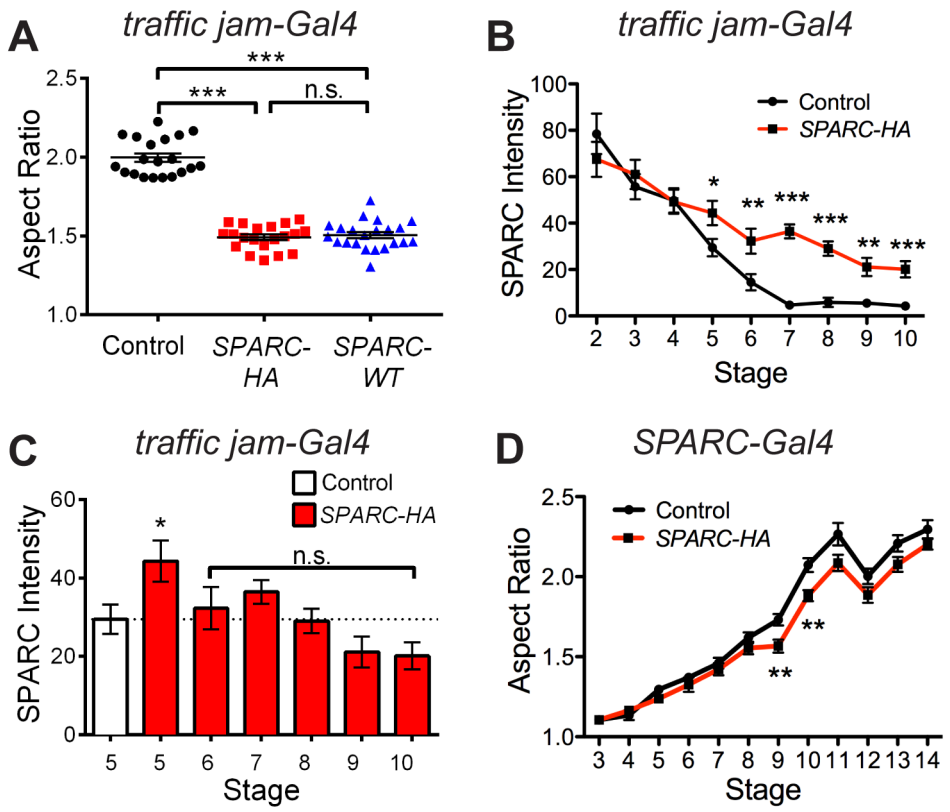

Figure 2.2. SPARC down-regulation promotes egg chamber elongation.
(A) Expression of a *SPARC-HA* or an untagged *SPARC-WT* transgene with *traffic jam-Gal4* similarly inhibit egg chamber elongation. Stage 14. (B-C) Mean SPARC immunofluorescence intensity in Control and *traffic jam-Gal4; UAS-SPARC-HA* egg chambers across stages. n=12-18 egg chambers per data point. (B) *SPARC-HA* expression with *traffic jam-Gal4* increases total SPARC levels after stage 4. (C) The level of persistent *SPARC-HA* expression is not significantly different from the endogenous expression level at stage 5. (D) *SPARC-Gal4*-driven *SPARC-HA* expression does not affect egg chamber elongation. n = 9-12 egg chambers per data point. (A-D) Data represent mean with s.e.m. Some error bars are too small to be seen. t-test * = P<0.05, ** = P<0.005, *** = P<0.0005.

accumulation of Col IV in the BM that normally begins at stage 5 is largely eliminated by prolonged *SPARC-HA* expression (Figure 2.3 A). This drop in Col IV levels is not due to a loss of Laminin, as Laminin levels are unchanged by persistent *SPARC* expression (Figure 2.4 A). In contrast, *SPARC-HA* expression does not block formation or alignment of BM fibrils (Figures 2.3 B-C, 2.4 B-C). Although the decrease in Col IV levels likely does affect fibril structure to some extent, their overall persistence in the SPARC-HA condition suggests that a mechanism

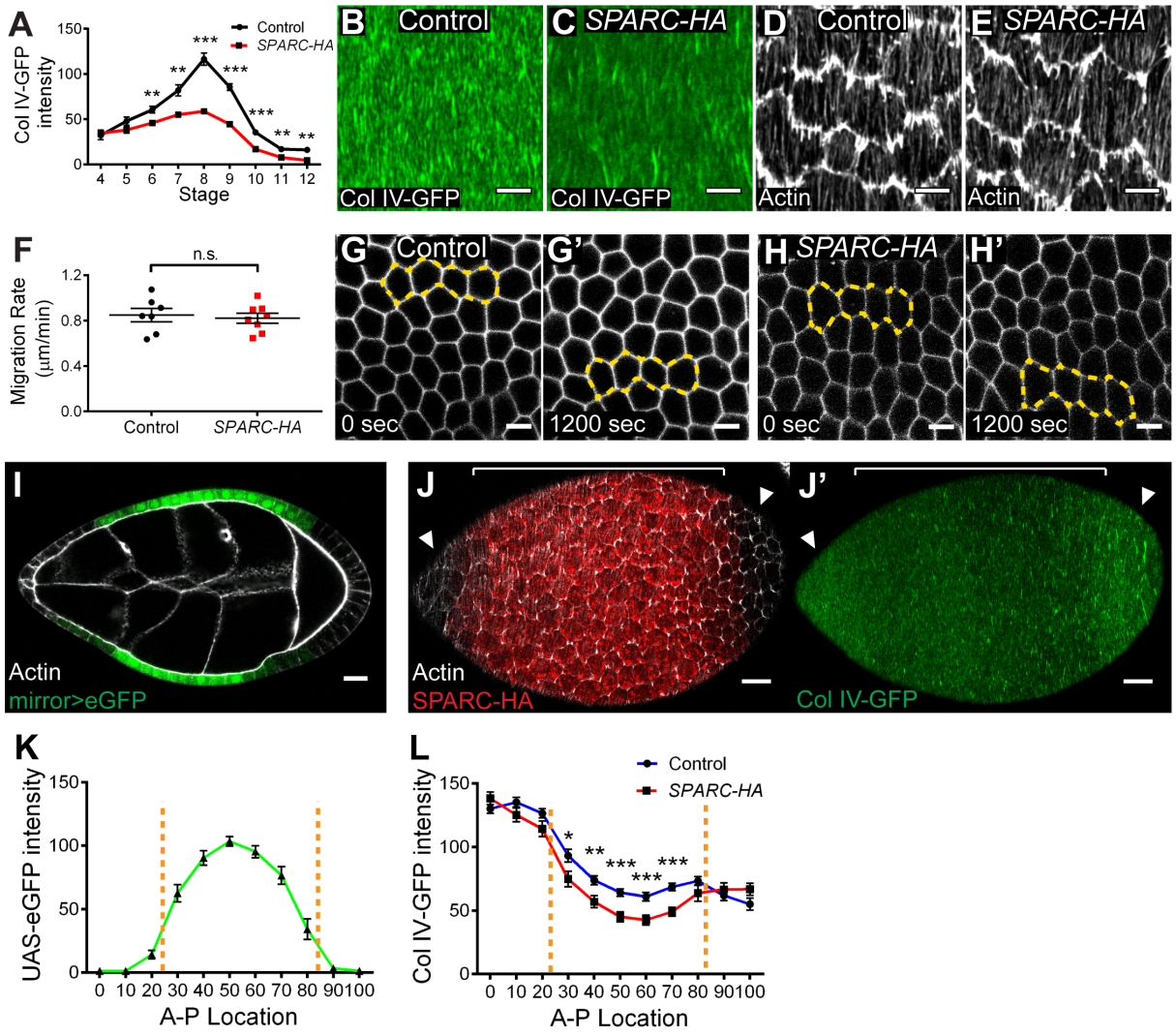

Figure 2.3. SPARC negatively regulates BM Col IV levels.
(A) SPARC-HA expression with *traffic jam-Gal4* decreases Col IV-GFP intensity in the BM, largely blocking the increase in Col IV levels normally seen during elongation stages. n = 4-20 egg chambers per data point. (B-C) *SPARC-HA* expression does not block BM fibril formation or alignment. (D-E) *SPARC-HA* expression does not alter tissue-level alignment of basal actin bundles. (F-H) SPARC-HA expression does not alter follicle cell migration rates. (F) Quantification of cell migration rates. (G-H) Still images of follicle cell migration. Yellow outlines highlight movement of the same group of cells over time. (I) The *mirror-Gal4* driver expresses *UAS-eGFP* in a central region of the follicular epithelium. (J-L) *SPARC-HA* expression locally decreases Col IV-GFP levels. (J-J') *mirror-Gal4*, *SPARC-HA* egg chamber showing *SPARC-HA* expression pattern and adjacent BM. Col IV-GFP intensity is decreased adjacent to *SPARC-HA*-expressing cells (bracketed region) relative to non-expressing cells at the poles (arrowheads). (K) Quantification of UAS-eGFP levels along the A-P axis in *mirror-Gal4* indicates *mirror* expression domain. n = 14 egg chambers per condition. (L) Col IV-GFP intensity in the BM along the A-P axis in control and *mirror-Gal4, UAS-SPARC-HA*. SPARC-HA decreases Col IV levels specifically in the *mirror*

Figure 2.3. Continued, SPARC negatively regulates BM Col IV levels.
expression domain. n = 16-21 egg chambers per condition. (K-L) 0 represents anterior pole, 100 represents posterior pole. Dotted lines delineate the *mirror* expression domain. (B-L) Stage 8. (A, F, K, L) Data represent mean with s.e.m. Some error bars are too small to be seen. t-test * = P<0.05, ** = P<0.005, *** = P<0.0005. Scale bars: 5 μm (B-E, G-H), 15 μm (I-J).

independent of the increase in Col IV levels governs their formation. Two other factors required for elongation - tissue-level alignment of basal actin bundles and egg chamber rotation - are also normal (Figures 2.3 D-H, 2.4 D). These data indicate that *SPARC* down-regulation is necessary for the increase in BM Col IV levels that coincides with egg chamber elongation.

Interestingly, by expressing *SPARC-HA* with the *mirror-Gal4* driver, which is restricted to the central region of the follicular epithelium (Figure 2.3 I), we found that the BM associated with *SPARC-HA*-expressing cells exhibits decreased Col IV levels, whereas the BM at the poles is unaffected (Figures 2.3 J-L, 2.4 E). Therefore, the effect of SPARC activity appears to be restricted to the BM immediately adjacent to *SPARC-HA*-expressing cells.

We have observed no defects resulting from the loss of SPARC function in the egg chamber. The populations of SPARC protein within the follicle cells and in the BM are both effectively depleted by RNAi (Figure 2.5 A-C). Yet, the loss of SPARC has no effect on either the intracellular or extracellular populations of Col IV, or on the shape of the egg (Figure 2.5 D-G). These data suggest that SPARC may have a Col IV-independent function during the early stages of egg chamber development, as has been seen in other *Drosophila* tissues (Portela et al., 2010).

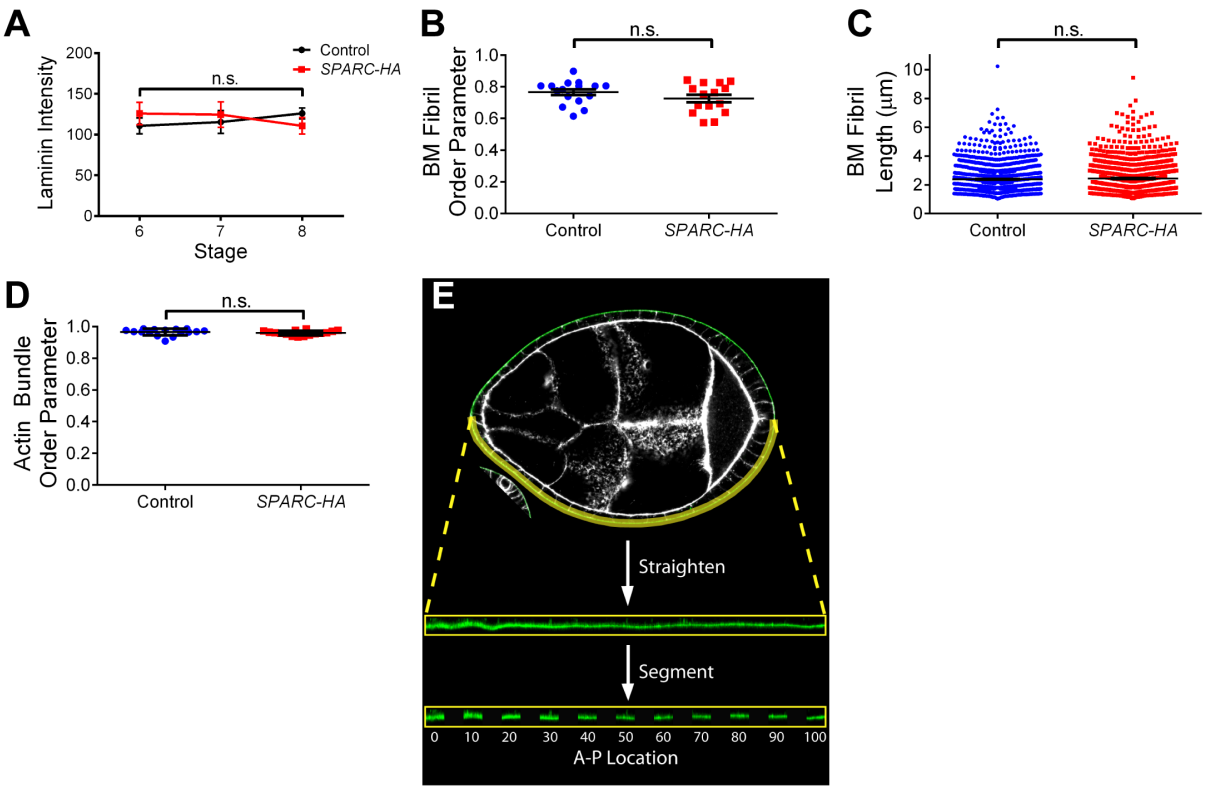

Figure 2.4. Persistent SPARC expression specifically lowers BM Col IV levels.
(A) Persistent *SPARC-HA* expression does not alter BM Laminin levels. n = 10-20 egg chambers per data point. (B-C) Persistent *SPARC* expression does not alter the global alignment (B) or mean length (C) of Col IV fibrils in the BM. (D) Persistent *SPARC* expression does not alter global alignment of actin bundles at the basal epithelial surface. (B, D) The order parameter describes the degree to which linear objects are aligned with one another; 1 = perfect alignment, 0 = random orientation. (E) Method for measuring Col IV-GFP intensity in the *mirror-Gal4* experiments shown in Figure 2I-L. BMs in transverse sections were outlined from anterior to posterior tip, straightened, segmented, and labeled according to location along the A-P axis. 0 represents anterior tip, 100 represents posterior tip of egg chamber. Mean GFP intensity of each region was then measured. (A-D) Data represent mean with s.e.m. t-test n.s. = P>0.05.

SPARC and Col IV interact within the secretory pathway

We next sought to clarify how persistent *SPARC-HA* expression reduces Col IV levels in the follicular BM. One possibility is that SPARC inhibits Col IV production or secretion. However, we observe no obvious defects in Col IV transcription, translation or exocytosis under persistent SPARC expression (Figure 2.6 A-C). Alternatively, recent work has suggested that SPARC may

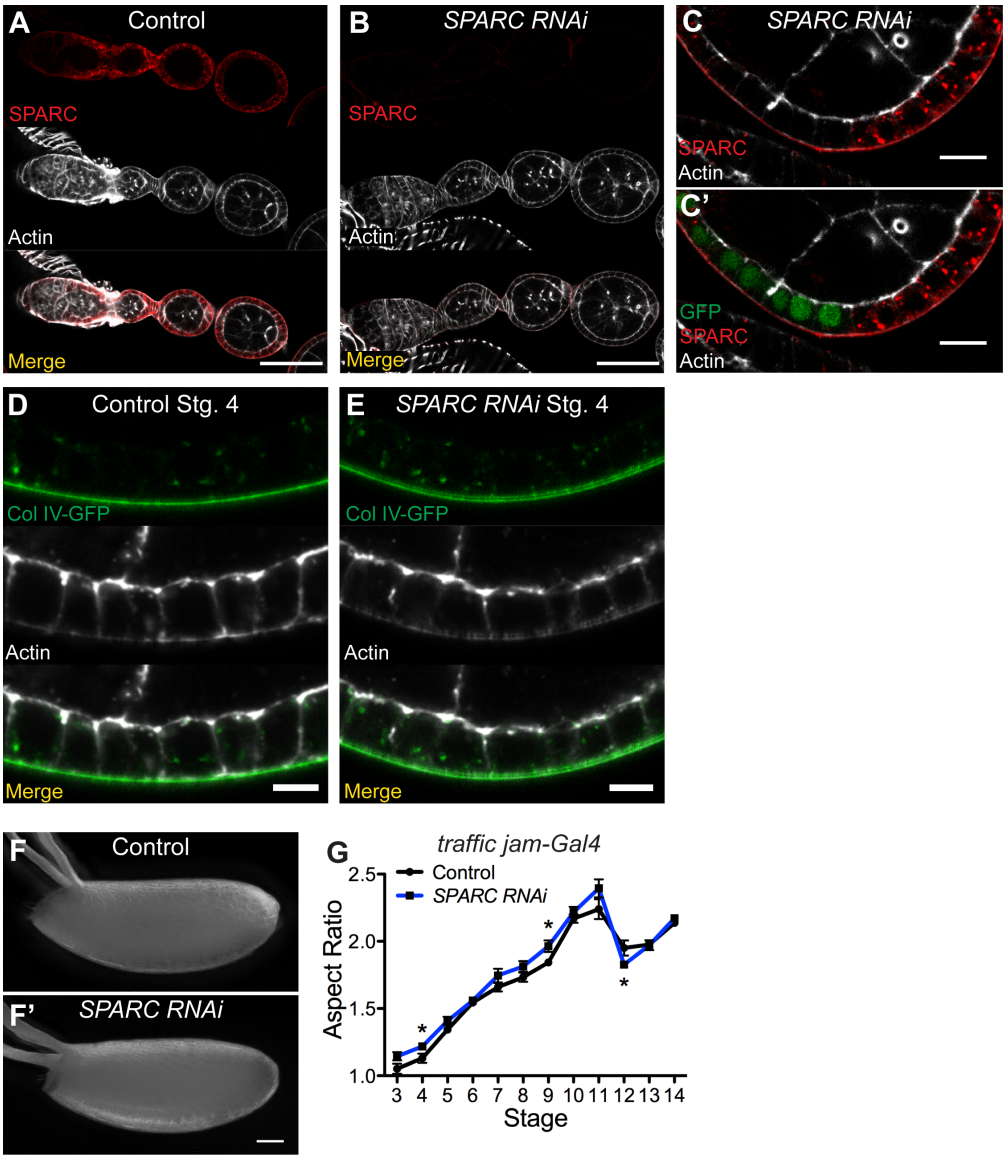

Figure 2.5. SPARC knockdown does not affect egg chamber elongation.
(A-C) *SPARC RNAi* effectively depletes SPARC protein from follicle cells. (A-B) *SPARC RNAi* expression with *traffic jam-Gal4* removes SPARC immunofluorescence signal from the BM and follicle cells. (C-C') *SPARC RNAi* expression strongly reduces intracellular SPARC signal in a follicle cell clone. GFP marks *SPARC RNAi*-expressing cells. Persistent SPARC signal adjacent to the basal side of the *SPARC RNAi* clone is extracellular SPARC deposited non-autonomously into the BM by wild-type cells during egg chamber rotation. Stage 3. (D-E) *SPARC RNAi* does not alter the amount or distribution of intracellular or extracellular Col IV-GFP in the follicle cells. Stage 4. (F-G) *SPARC RNAi* expression with *traffic jam-Gal4* does not affect egg chamber elongation. (F-F') Representative Control and *SPARC RNAi* eggs. (G) Quantification of elongation in *SPARC RNAi*-expressing egg chambers. n=6-30 egg chambers per data point. Data represent mean with s.e.m. Some error bars are too small to be seen. t-test * = P<0.05, ** = P<0.005, *** = P<0.0005. Scale bars: 50 µm (A-B, F), 10 µm (C), 5 µm (D-E).

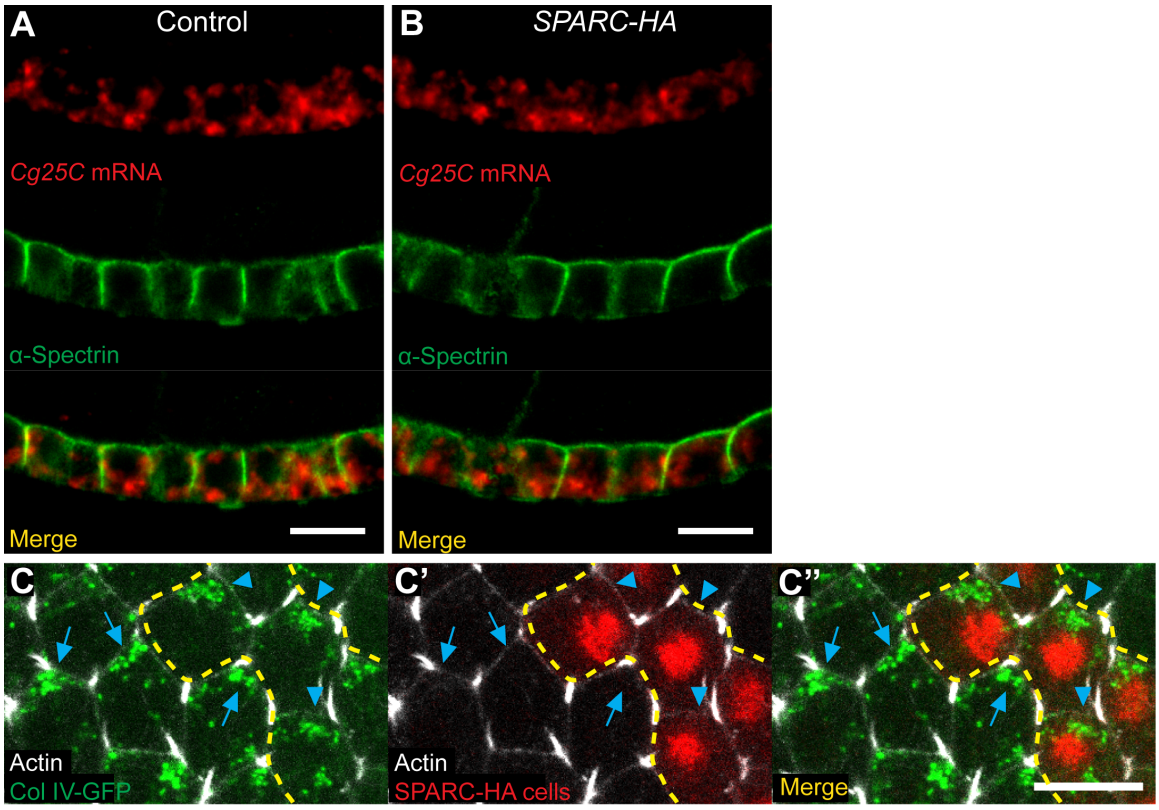

Figure 2.6. Persistent *SPARC* expression does not affect Col IV production or exocytosis. (A-B) *In situ* hybridization against the mRNA encoding the Col IV α1 chain Collagen gene at 25C (Cg25C). *SPARC-HA* expression does not alter the amount or distribution of *Cg25C* mRNA. (C) Intracellular Col IV-GFP in a *SPARC-HA* mosaic epithelium. The amount and distribution of intracellular Col IV-GFP is indistinguishable between wild-type cells (arrow) and *SPARC-HA* cells (arrowheads), indicating no effect of SPARC-HA on Col IV protein production or exocytosis. RFP indicates *SPARC-HA* expressing cells. Yellow line outlines *SPARC-HA* clone. (A-C) Stage 8. Scale bars: 10 μm.

promote solubility of Col IV in the extracellular space (Pastor-Pareja and Xu, 2011; Shahab et al., 2015). In *Drosophila* larvae, Col IV is produced by the fat body and then distributed, via the hemolymph, to organs throughout the body. The fat body itself is surrounded by a BM; thus, the Col IV produced by this organ must remain soluble in order to pass through this BM and diffuse to distant sites. Loss of SPARC in this system causes Col IV to accumulate around fat body cells in a cell-autonomous manner (Pastor-Pareja and Xu, 2011; Shahab et al., 2015). In contrast, Col IV produced by the follicle cells is meant to integrate into the adjacent BM immediately upon

secretion. We therefore reasoned that persistent SPARC-HA expression in the follicle cells might aberrantly solubilize Col IV, causing it to diffuse through the existing matrix rather than adhere.

For SPARC to efficiently perform this solubilizing function, it would likely have to bind to Col IV either before or very shortly after it exits the cell and encounters the BM. Such an interaction would also explain the observed local effect of persistent *SPARC* expression (Figure 2.3 J-L). We therefore investigated whether these two proteins form a complex within the secretory pathway. We first examined whether SPARC and Col IV co-localize within the follicle cells. To distinguish between exocytic and endocytic populations, we performed this analysis in epithelia mosaic for Col IV-GFP expression. SPARC and Col IV-GFP strongly co-localize only within Col IV-GFP-expressing cells, indicating co-localization within the secretory pathway (Figure 2.7 A).

To further explore SPARC's intracellular association with Col IV, we examined SPARC localization under two conditions that alter Col IV secretion. First, we manipulated the guanine nucleotide exchange factor *Crag (Calmodulin-binding protein related to a Rab3 GDP/GTP exchange protein),* which directs Col IV secretion to the basal epithelial surface (Denef et al., 2008; Lerner et al., 2013). RNAi knockdown of *Crag* causes both Col IV and SPARC to be aberrantly trafficked to the apical surface, where they co-localize (Figure 2.7 B-C). Second, we manipulated *prolyl-4-hydroxylase-alpha EFB* (*PH4*), an enzyme necessary for Col IV folding in the ER (Lerner et al., 2013; Myllyharju and Kivirikko, 2004; Pastor-Pareja and Xu, 2011). RNAi knockdown of *PH4* causes SPARC to accumulate with Col IV in large punctae within the ER (Figure 2.7 B,D). Significantly, although SPARC is normally lost from follicle cells by stage 8, the SPARC that is trapped in the ER under *PH4* depletion persists into this stage (Figure 2.7

E,F). This signal likely represents a SPARC population that has been aberrantly retained in the ER due to physical association with trapped Col IV.

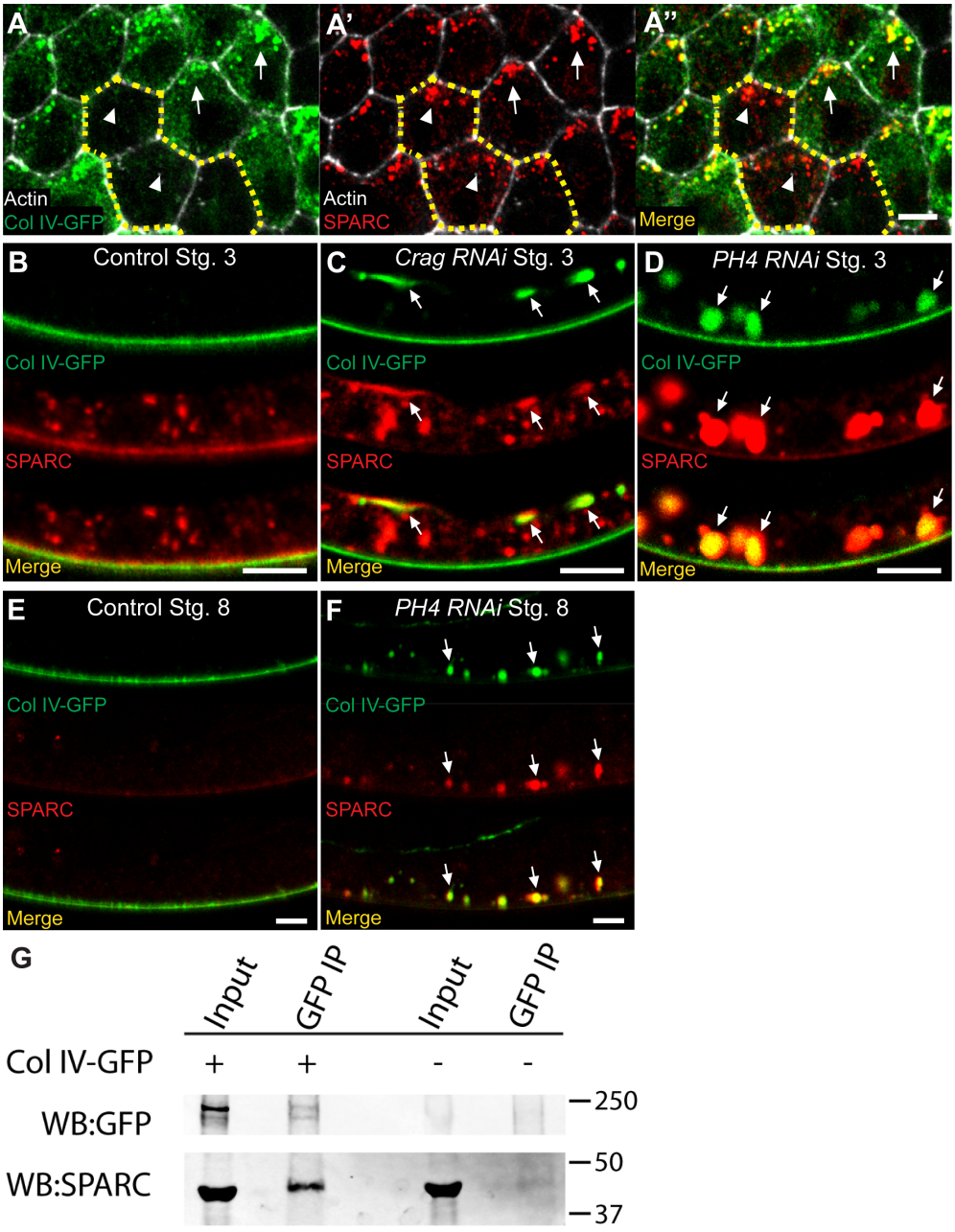

Figure 2.7. SPARC associates with Col IV in the secretory pathway.
(A-A'') In a Col IV-GFP mosaic epithelium, SPARC co-localizes with Col IV-GFP in expressing cells (arrows) but not in non-expressing cells (arrowheads), indicating co-localization within the secretory pathway. Dashed lines outline 3 cells not expressing Col IV-GFP. Stage 8. (B) Wild-type Col IV and SPARC localization at stage 3. SPARC is in the BM and intracellular punctae. (C) In *Crag RNAi* epithelia, Col IV and SPARC are mis-trafficked to the apical surface (arrows). (D) In *PH4 RNAi* epithelia, SPARC accumulates with Col IV in distended ER

Figure 2.7. Continued, SPARC associates with Col IV in the secretory pathway. cisternae (arrows). (E) Wild-type Col IV and SPARC localization at stage 8. SPARC is no longer observed within cells and its BM localization is strongly reduced. (F) In *PH4 RNAi* epithelia, SPARC that is trapped in the ER persists beyond the stage when it is normally cleared from follicle cells (arrows). (G) GFP pulldown from ovaries can co-immunoprecipitate SPARC in the presence, but not in the absence, of Col IV-GFP. IP: GFP, Blot: GFP & SPARC. Scale bars: 5 μm (A-F).

Finally, we observed, via co-immunoprecipitation from whole ovary extract, that Col IV and SPARC physically interact in the follicle cells (Figure 2.7 G). The protein observed in this experiment likely represents the intracellular population, as extracellular Col IV in the BM is insoluble and cannot be pulled down in this assay. Together, these data suggest that SPARC binds to and transits the secretory pathway with Col IV, and we propose that this interaction inhibits incorporation of newly secreted Col IV into the BM.

Col IV and Perlecan have opposing effects on egg chamber elongation

We have found that prolonged SPARC expression in the follicular epithelium causes two phenotypes: a decrease in BM Col IV levels and a defect in egg chamber elongation. It is known that complete loss of Col IV from the BM inhibits elongation (Haigo and Bilder, 2011b); however, the observations above led us to ask whether a reduction in Col IV levels is also sufficient to cause this defect. To this end, we directly manipulated Col IV levels by expressing an RNAi transgene against *viking* (*vkg RNAi)* in the follicle cells. Because Gal4 activity is temperature-sensitive, maintaining the experimental crosses at 18°C allowed us to modulate *vkg RNAi* activity to produce BM Col IV levels similar to those observed upon *SPARC-HA* expression (Figure 2.8 A-D). We found that this *vkg RNAi* condition blocks elongation similarly to *SPARC-HA* (Figure 2.8 E). Notably, reduced temperature alone does not alter elongation

(Figure 2.9 A). Thus, a reduction in BM Col IV levels is sufficient to disrupt egg chamber elongation, and likely explains why persistent SPARC expression causes this defect.

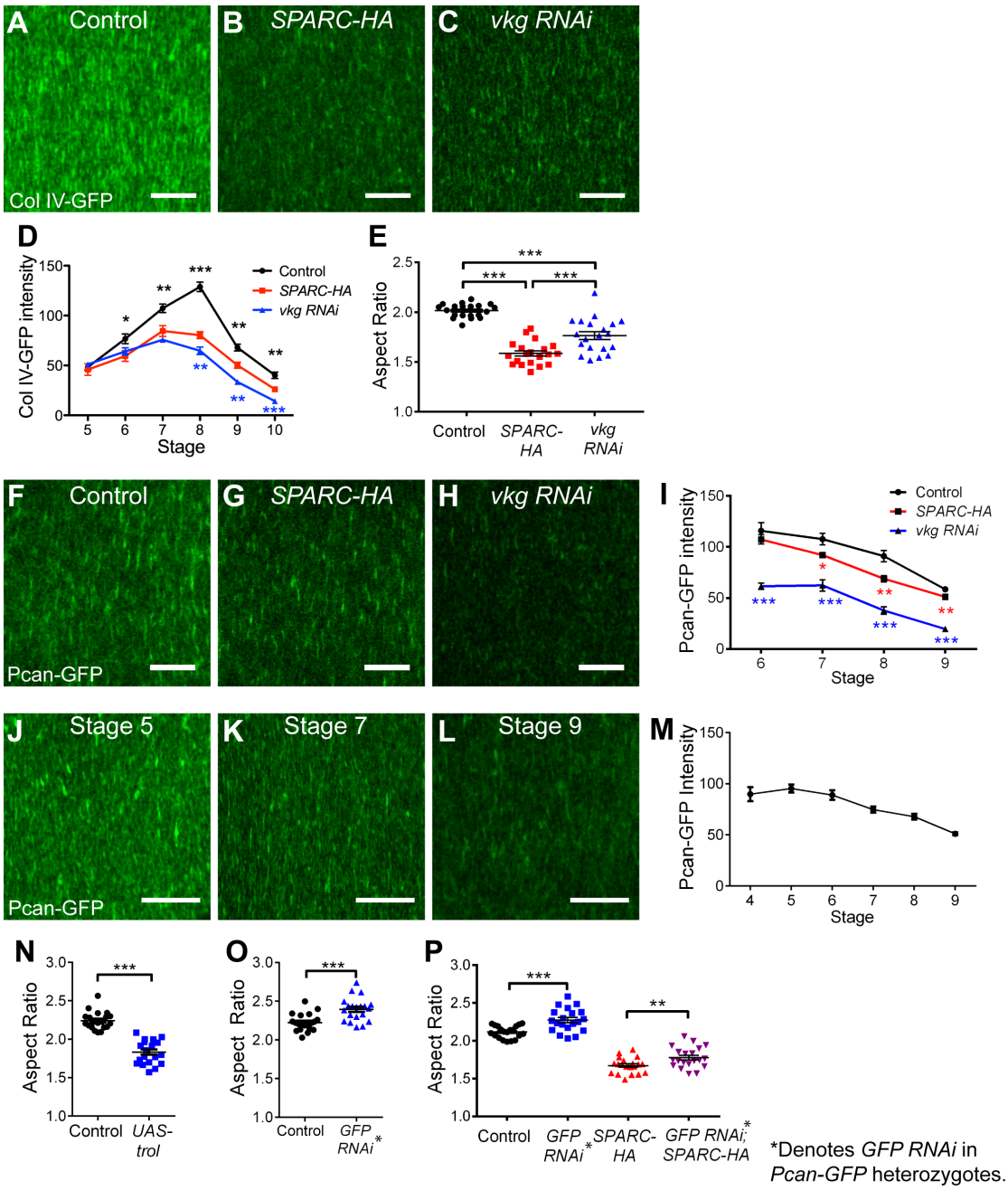

Figure 2.8. Importance of Col IV and Perlecan levels for egg chamber elongation. (A-D) 18°C *vkg RNAi* expression reduces Col IV-GFP levels in the BM similarly to *SPARC-HA* expression. (A-C) Representative images of Col IV-GFP in the BM at stage 8. (D) Quantification of BM Col IV-GFP intensity. Asterisks indicate significance relative to *SPARC-HA*. n = 4-10 egg chambers per data point. (E) 18°C *vkg RNAi* expression mostly recapitulates the effect of *SPARC-HA* expression on egg chamber elongation. (F-I) *SPARC-HA* expression

Figure 2.8. Continued, Importance of Col IV and Perlecan levels for egg chamber elongation.
modestly decreases Pcan-GFP intensity in the BM, while 18°C *vkg RNAi* strongly decreases Pcan-GFP intensity. (F-H) Representative images of Pcan-GFP in the BM at stage 8. (I) Quantification of BM Pcan-GFP intensity. n = 14-15 egg chambers per data point. Asterisks indicate significance relative to control. (J-M) Pcan-GFP levels in the BM decrease during elongation in wild-type egg chambers. (J-L) Representative images of Pcan-GFP in the BM. (M) Quantification of BM Pcan-GFP intensity. n = 10 egg chambers per stage. (N) Perlecan overexpression with *UAS-trol* inhibits egg chamber elongation. (O) 50% Perlecan knockdown via *GFP RNAi* expression in Pcan-GFP heterozygotes enhances egg chamber elongation. (P) 50% Perlecan knockdown via *GFP RNAi* in Pcan-GFP heterozygotes increases elongation in a control background and partially rescues the *SPARC-HA* elongation defect. (E, N-P) Stage 14. (D-E, I, M-P) Data represent mean with s.e.m. Some error bars are too small to be seen. t-test * = P<0.05, ** = P<0.005, *** = P<0.0005. Scale bars: 10 μm (A-C, F-H, J-L).

Intriguingly, closer examination of these data revealed an unexpected result. Although our *vkg RNAi* condition leads to slightly lower levels of Col IV than *SPARC-HA,* the elongation defect is less severe than in *SPARC-HA* (Figure 2.8 D,E). This observation suggests that some other elongation factor is differentially affected by these two conditions. Perlecan is a likely candidate, as its presence in the BM is partially dependent on Col IV (Haigo and Bilder, 2011b; Pastor-Pareja and Xu, 2011). In *Drosophila*, the gene encoding Perlecan is called *terribly reduced optic lobes* (*trol*). Using a GFP protein trap in this gene (Pcan-GFP), we observed a strong decrease in Perlecan levels in the *vkg RNAi* condition; in contrast, *SPARC-HA* expression only weakly affects Perlecan levels (Figure 2.8 F-I). These data raise the possibility that the level of Perlecan in the BM is also an important factor regulating egg chamber elongation.

The role of Perlecan in egg chamber elongation has not been previously examined. In the *Drosophila* wing disc, however, Col IV and Perlecan have been shown to confer opposing physical characteristics to the BM – Col IV promotes BM constriction, whereas Perlecan counters this force (Pastor-Pareja and Xu, 2011). We therefore hypothesized that decreasing

Perlecan levels would have an effect equivalent to increasing Col IV levels, promoting egg chamber elongation by enhancing the constrictive force of the molecular corset.

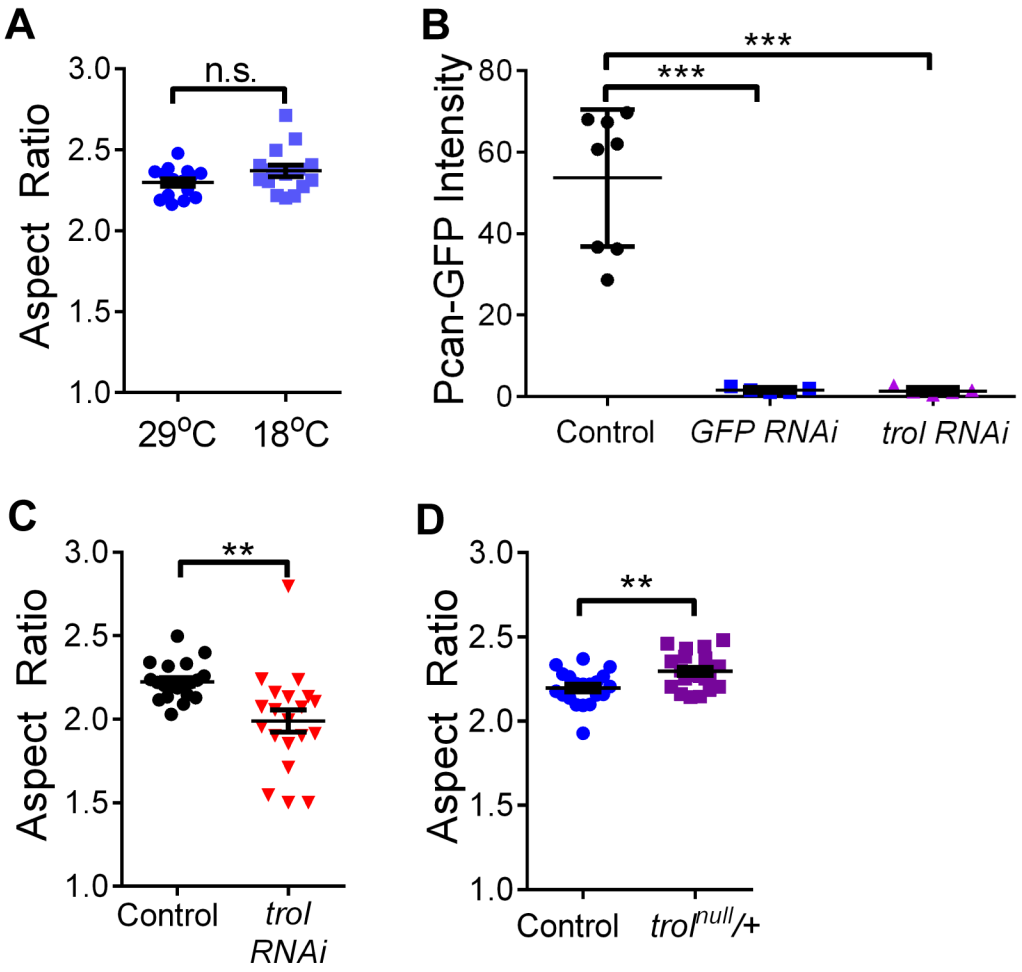

Figure 2.9. BM protein levels regulate egg chamber elongation.
(A) Aspect ratio does not differ between wild-type flies aged at 29°C vs. 18°C. (B) Quantification of BM Pcan-GFP intensity. *GFP RNAi* and *trol RNAi* effectively remove Pcan-GFP signal. Stage 8. n = 5-8 egg chambers per condition. (C) Depletion of Perlecan via expression of *trol RNAi* inhibits egg chamber elongation. (D) Egg chambers heterozygous for a *trol* null mutation exhibit slight hyper-elongation. (A, C-D) Stage 14. (A-D) Data represent mean with s.e.m. Some error bars are too small to be seen. t-test ** = P<0.005, *** = P<0.0005.

Consistent with our hypothesis, we found that Perlecan levels decrease during elongation stages in wild-type egg chambers (Figure 2.8 J-M). Moreover, over-expression of Perlecan with

a *UAS-trol* transgene significantly inhibits elongation (Figure 2.8 N). This result suggests that the natural decrease in Perlecan may be required for egg chamber elongation.

To further test how Perlecan affects elongation, we depleted this protein with RNAi. Monitoring BM levels of the Pcan-GFP protein trap confirmed efficient knockdown in all cases (Figure 2.9 B). Strong depletion of Perlecan with *trol RNAi* inhibits elongation (Figure 2.9 C). We also examined partial knockdown of Perlecan and found that this condition increases elongation (Figure 2.8 O). We first saw this phenotype by expressing RNAi against GFP (*GFP RNAi)* in Pcan-GFP heterozygotes (Figure 2.8 O), and confirmed this effect in egg chambers heterozygous for a null mutation in *trol* (Figure 2.9 D). Altogether, these data show that differences in the levels of Perlecan can result in different outcomes with respect to egg chamber elongation.

Finally, the results of the over-expression and partial knockdown experiments above suggest that a stronger decrease in Perlecan levels may explain why the elongation defect in our *vkg RNAi* condition is less severe than that of *SPARC-HA*. In this case, further reducing Perlecan levels under *SPARC-HA* should mitigate the elongation defect seen in this background. To test this idea directly, we expressed both *SPARC-HA* and *GFP RNAi* in Pcan-GFP heterozygotes. As expected, decreasing Perlecan levels partially rescues the elongation defect caused by *SPARC-HA* alone (Figure 2.8 P). Altogether, these data reveal that Col IV promotes egg chamber elongation, while Perlecan inhibits this process.

2.5 DISCUSSION

Here we show that dynamic regulation of two BM proteins is necessary for *Drosophila* egg chamber elongation. We observe that a stage-specific increase in Col IV levels promotes

elongation, and that SPARC must be down-regulated for this increase to occur. We further show that SPARC can associate with Col IV within the secretory pathway, and propose that this interaction blocks its incorporation into the BM. Finally, we observe that Perlecan levels decrease in the BM during egg chamber elongation, and find that lower Perlecan levels promote this process. Collectively, these data reveal a precise regulatory program to modulate egg chamber elongation through the control of BM protein levels (Figure 2.10).

Our work offers new insight into the relationship between SPARC and Col IV. SPARC is expressed in the follicle cells during early stages of egg chamber development. Although the function of SPARC during these stages is not yet clear, we have found that it must be down-regulated for Col IV levels to increase in the BM during egg chamber elongation. Our data do not exclude the possibility that SPARC promotes the removal of Col IV from the existing BM scaffold. However, given the previous evidence in *Drosophila* that SPARC enhances Col IV solubility (Pastor-Pareja and Xu, 2011; Shahab et al., 2015), we favor a model in which persistent SPARC expression aberrantly solubilizes Col IV and blocks its incorporation into the follicular BM.

It is likely that Col IV rapidly becomes insoluble upon secretion due to immediate access to cellular receptors and other BM molecules. We have now shown that SPARC can associate with Col IV while the two proteins are still within the secretory pathway. This intracellular interaction may be important in tissues like the fat body where Col IV must maintain solubility to diffuse to distant tissues. In the follicle cells, however, Col IV is meant to adhere to the BM immediately upon secretion. We therefore propose that the association between SPARC and Col IV in this tissue is detrimental, necessitating the observed down-regulation of SPARC.

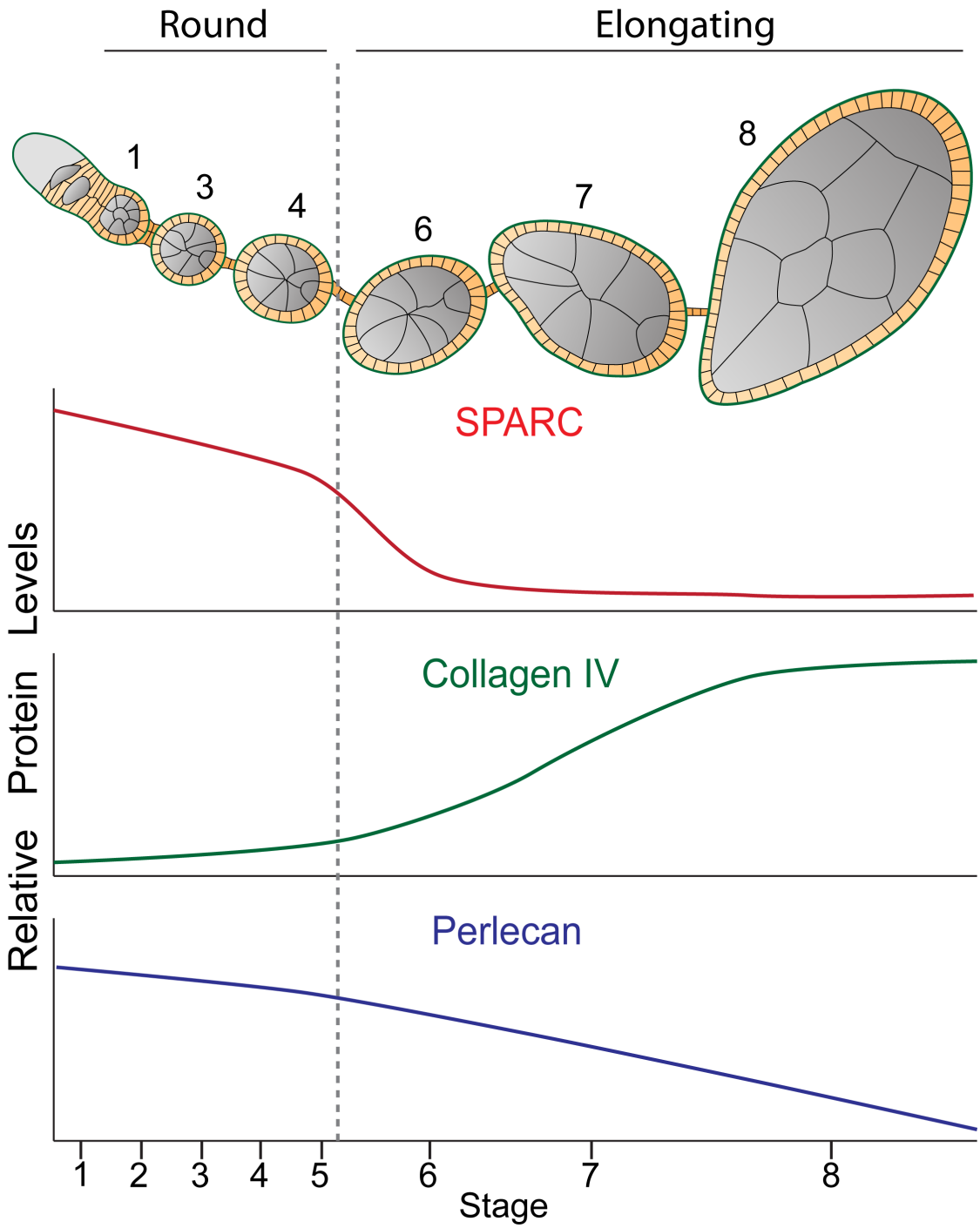

Figure 2.10. Model for the regulation of BM protein levels during egg chamber elongation. Summary of BM protein dynamics during egg chamber development. Top: schematic of egg chamber development representing round (stg. 1-4) and elongating (stg. 6-8) egg chambers. Numbers indicate stage. Bottom: SPARC and Perlecan levels decrease, and Collagen IV levels increase, in a stage-specific manner to promote egg chamber elongation. Grey dotted line indicates onset of elongation.

This work also demonstrates the need for precise BM remodeling during egg chamber elongation. Two BM remodeling events – formation of aligned fibrils and increased Col IV levels – have been shown to correlate with the onset of egg chamber elongation (Haigo and Bilder, 2011b). We have now found that the stage-specific increase in Col IV levels is required for this process. Importantly, persistent *SPARC* expression is the first condition that changes the structure of the follicular BM without also affecting the cellular processes known to be required for elongation, such as egg chamber rotation and tissue-level alignment of the basal actin bundles. This work therefore provides direct evidence that stage-specific remodeling of the BM promotes egg chamber elongation. Given that Col IV provides tensile strength to BMs, its increase is likely necessary for the molecular corset to properly constrain the growing tissue. We expect that the aligned BM fibrils contribute anisotropy to this constraining force, although future work is needed to confirm their role.

We additionally identify a role for Perlecan in controlling egg chamber elongation. Our data indicate that a low level of Perlecan in the BM maximally promotes elongation, whereas either higher levels or a complete loss inhibit this process. Although it is not yet clear why a complete loss of Perlecan blocks elongation, the phenotypes induced by moderate changes in Perlecan levels could be explained by this protein's effect on the physical properties of the BM. Perlecan has been proposed to promote BM elasticity and counter the constrictive force exerted by Col IV (Pastor-Pareja and Xu, 2011). Hyper-elasticity of a BM containing high levels of Perlecan may weaken the constraining force of the corset. In support of this notion, we have found a stage-specific decrease of Perlecan levels in the follicular BM that appears to contribute to elongation. An additional mechanism, therefore, may exist to control Perlecan levels during this process.

We and others have observed that Perlecan levels in the BM often depend on Col IV (Haigo and Bilder, 2011b; Pastor-Pareja and Xu, 2011). While co-regulation of these opposing factors may help to buffer the physical properties of the BM against variations in Col IV expression, it creates a challenge in situations requiring independent regulation of Col IV levels. Therefore, it is intriguing that *SPARC-HA* expression, unlike *vkg RNAi*, decreases Col IV levels with only a minimal effect on Perlecan. This suggests that, in some cases, SPARC may provide a valuable mechanism to uncouple these proteins and allow for specific regulation of Col IV levels. The difference between these conditions also offers insight into the relationship between Col IV and Perlecan. In *vkg RNAi*, Col IV protein is not produced. In contrast, under *SPARC-HA* expression Col IV appears to be both produced and secreted, but fails to be incorporated into the BM. Thus, our data suggest that Col IV may facilitate Perlecan secretion, but not its subsequent incorporation into the BM once outside the cell.

Altogether, this study highlights how regulated changes in BM protein levels can play a central role in organ morphogenesis.

2.6 METHODS

Drosophila Genetics

Detailed experimental genotypes are in Table S1. Most crosses were raised at 25°C and adult females aged 3 days on yeast at 29°C; exceptions are in Table S2. *Gal4* lines used for *UAS* transgene expression are in Table S3. FLP-out expression was induced by 37°C heat shocks for 1 hour, twice daily for 3 days on yeast. *vkg-GFP* clones were generated on *FRT40A* chromosomes using *T155-Gal4* to drive *UAS-FLP* expression. Most lines were obtained from the Bloomington *Drosophila* Stock Center (Bloomington, IN) with exceptions listed here. *vkg-*

GFP (CC00791), *Indy-GFP* (CC00377), *Nrg-GFP* (G00305) and *trol-GFP* (CA06698) are from Flytrap (Buszczak et al., 2007; Morin et al., 2001). *UAS-SPARC-HA* and *UAS-SPARC-WT* are from Portela et al. (2010). *UAS-SPARC RNAi* (v16678) and *UAS-vkg RNAi* (v16986) are from Vienna *Drosophila* Resource center (Vienna, Austria). *SPARC-Gal4* is from Venken et al. (2011). *traffic jam-Gal4* is from the *Drosophila* Genetic Resource Center (Kyoto Institute of Technology, Kyoto, Japan). *ubi-nls-mRFP,vkg-GFP, FRT40A* and *FRT40A; T155-Gal4, UAS-FLP* are from Haigo and Bilder (2011). *trol*^{null} is a gift from S. Haigo, originally from Voigt et al. (2002). *UAS-trol* is from Cho et al. (2012).

Table 2.1. Experimental Genotypes

Figure	Panel	Genotype
2.1	B	*w; tj-Gal4, vkg-GFP/+*
	C D	*w; vkg-GFP/vkg-GFP*
	E	*w*^{1118}
	F G	*w; tj-Gal4/+*
		w; tj-Gal4/+; UAS-SPARC-HA/+
2.3	A	*w; tj-Gal4, vkg-GFP/vkg-GFP*
		w; tj-Gal4, vkg-GFP/vkg-GFP; UAS-SPARC-HA/+
	B D	*w; tj-Gal4, vkg-GFP/vkg-GFP*
	C E	*w; tj-Gal4, vkg-GFP/vkg-GFP; UAS-SPARC-HA/+*
	F	*w, Nrg-GFP/+; tj-Gal4/+; Indy-GFP/+*
		w, Nrg-GFP/+; tj-Gal4/+; Indy-GFP/UAS-SPARC-HA
	G	*w, Nrg-GFP/+; tj-Gal4/+; Indy-GFP/+*
	H	*w, Nrg-GFP/+; tj-Gal4/+; Indy-GFP/UAS-SPARC-HA*
	I K	*w; UAS-eGFP/+; mirror-Gal4/+*
	J	*w; vkg-GFP/+; mirror-Gal4/UAS-SPARC-HA*
	L	*w; vkg-GFP/+; mirror-Gal4/+*
		w; vkg-GFP/+; mirror-Gal4/UAS-SPARC-HA
2.7	A	*w; ubi-nls-mRFP, vkg-GFP, FRT40A/FRT40A; T155-Gal4, UAS-FLP/UAS-SPARC-HA*
	B E	*w; tj-Gal4, vkg-GFP/+*
	C	*w; tj-Gal4, vkg-GFP/+; UAS-Crag RNAi*$^{TRiP.HMS00241}$*/+*
	D F	*w; tj-Gal4, vkg-GFP/+; UAS-PH4αEFB RNAi*$^{TRiP.HMS00835}$*/+*
	G	*w; tj-Gal4, vkg-GFP/vkg-GFP*
		w; tj-Gal4/+
2.8	A	*w; tj-Gal4, vkg-GFP/+*

Table 2.1. Experimental Genotypes, Continued

Figure	Panel	Genotype
2.8	B	*w; tj-Gal4, vkg-GFP/+; UAS-SPARC-HA/+*
	C	*w; tj-Gal4, vkg-GFP/UAS-vkg RNAi^{V16986}*
	D	*w; tj-Gal4, vkg-GFP/+*
		w; tj-Gal4, vkg-GFP/+; UAS-SPARC-HA/+
		w; tj-Gal4, vkg-GFP/UAS-vkg RNAi^{V16986}
	E	*w; tj-Gal4/+*
		w; tj-Gal4/+; UAS-SPARC-HA/+
		w; tj-Gal4/UAS-vkg RNAi^{V16986}
	F	*trol-GFP/+; tj-Gal4/+*
	G	*trol-GFP/+; tj-Gal4/+; UAS-SPARC-HA/+*
	H	*trol-GFP/+; tj-Gal4/UAS-vkg RNAi^{V16986}*
	I	*trol-GFP/+; tj-Gal4/+*
		trol-GFP/+; tj-Gal4/+; UAS-SPARC-HA/+
		trol-GFP/+; tj-Gal4/UAS-vkg RNAi^{V16986}
	J K L M	*trol-GFP/trol-GFP*
	N	*w; tj-Gal4/+*
		w; tj-Gal4/+; UAS-trol-RG/+
	O	*trol-GFP/+; tj-Gal4/+*
		trol-GFP/+; tj-Gal4/UAS-GFP.dsRNA^{BL9330}
	P	*trol-GFP/+; tj-Gal4/+*
		trol-GFP/+; tj-Gal4/UAS-GFP.dsRNA^{BL9330}
		trol-GFP/+; tj-Gal4/+; UAS-SPARC-HA/UAS-mcd8-RFP^{BL32218}
		trol-GFP/+; tj-Gal4/UAS-GFP.dsRNA^{BL9330}; UAS-SPARC-HA/+
2.2	A	*w; tj-Gal4, vkg-GFP/vkg-GFP*
		w; tj-Gal4, vkg-GFP/vkg-GFP; UAS-SPARC-HA/+
		w; tj-Gal4, vkg-GFP/vkg-GFP; UAS-SPARC-2/+
	B C	*w; tj-Gal4, vkg-GFP/+*
		w; tj-Gal4, vkg-GFP/+; UAS-SPARC-HA/+
	D	*w; ; SPARC-Gal4/+*
		w; ; SPARC-Gal4/UAS-SPARC-HA
2.4	A	*w; tj-Gal4/+*
		w; tj-Gal4/+; UAS-SPARC-HA/+
	B C D	*w; tj-Gal4, vkg-GFP/+*
		w; tj-Gal4, vkg-GFP/+; UAS-SPARC-HA/+
2.5	A	*w; tj-Gal4/+*
	B	*w; tj-Gal4/+; UAS-SPARC RNAi^{V16678}/+*
	C	*w; hs-FLP/+; ; act5c>>Gal4, UAS-GFP/UAS-SPARC RNAi^{V16678}*
	D	*w; tj-Gal4, vkg-GFP/+*
	E	*w; tj-Gal4, vkg-GFP/+; UAS-SPARC RNAi^{V16678}/+*
	F G	*w; tj-Gal4/+*
		w; tj-Gal4/+; UAS-SPARC RNAi^{V16678}/+
2.6	A	*w; tj-Gal4/+*
	B	*w; tj-Gal4/+; UAS-SPARC-HA/+*

Table 2.1. Experimental Genotypes, Continued

Figure	Panel	Genotype
2.6	C	*w; hs-FLP/+;vkg-GFP/vkg-GFP; act5c>>Gal4, UAS-GFP/UAS-SPARC-HA*
2.9	A	*w;tj-Gal4/+*
	B	*trol-GFP/+; tj-Gal4/+* *trol-GFP/+; tj-Gal4/UAS-GFP.dsRNA^{BL9330}* *trol-GFP/+; tj-Gal4/+; UAS-trol RNAi$^{TRiP.JF03376}$/+*
	C	*trol-GFP/+; tj-Gal4/+* *trol-GFP/+; tj-Gal4/+; UAS-trol RNAi$^{TRiP.JF03376}$/+*
	D	*w^{1118}* *$trol^{null}/w^{1118}$*

Table 2.2. Experimental conditions

Most crosses were raised at 25°C and females aged on yeast for 3 days at 29°C. Experiments using different conditions are detailed here.

Figure	Panels	Temp at which cross was raised	Females on yeast	
			Temp	No. days
2.1	C	25	RT	4
	D	25	25	2
	E (Red)	25	25	4
	E (Blue)	25	25	3
2.3	I	25	25	3
	J	25	25	2
2.7	C	25	29	2
	D E F G	25	25	3
2.8	A B F G	18	29	3
	C H	18	18	3
	D E I (Control, *SPARC-HA*)	18	29	3
	D E I (*vkg RNAi*)	18	18	3
	O	22	25	3
2.4	A	25	29	4
2.5	C	25	HS	3

Table 2.2. Experimental conditions, Continued

Figure	Panels	Temp at which cross was raised	Females on yeast	
			Temp	No. days
2.6	C	25	HS	3
2.9	A (29°C)	18	29	3
	A (18°C)	18	18	3
	B C	22	25	3
	D	25	25	3

Staining and microscopy

Ovaries were dissected in S2 medium and fixed for 15 minutes in PBS + 0.1% Triton (PBT) + 4% EM-grade formaldehyde (Polysciences), then separated from the muscle sheath by gentle pipetting. TRITC-Phalloidin (1:200, Sigma) stains were performed during fixation. Antibody stains were performed in PBT and detected with Alexa Fluor-conjugated secondary antibodies (1:200, Invitrogen). With antibody stains, Alexa Fluor 647 Phalloidin (1:50, Invitrogen) was used to mark actin. Egg chambers were mounted in SlowFade Antifade (Invitrogen). Antibodies used: rabbit α-HA (1:200, Rockland), rabbit α-SPARC (1:400) (Martinek et al., 2002), guinea pig α-laminin (1:400) (Harpaz and Volk, 2012). All images were obtained using a Zeiss LSM 510 or LSM 880 confocal microscope, except 1F and S1F, which were obtained with a Leica FluoIII microscope with Canon rebel camera and 4E, N-P, S1A, and S5A,C-D, which were obtained using a Leica DM550B microscope with a Leica DFC425C camera**.** Image processing and custom image analysis were performed in ImageJ (see detailed descriptions below). Graphing & statistical analyses were performed in Prism (Graphpad).

Measurements of fluorescence intensity

For SPARC intensity measurements, a representative group of 5-10 follicle cells from central transverse sections of SPARC immunostained egg chambers was outlined, and mean intensity measured. All images were obtained at the same settings.

To measure egg chamber BM Col IV-GFP and Pcan-GFP intensity, a confocal section through the plane of the BM was acquired. Mean intensity of the brightest region was measured. All images were obtained at the same settings.

For the anterior-posterior Col IV-GFP and eGFP intensity measurements in *mirror-Gal4* egg chambers, 5 pixel wide (Col IV-GFP) or 10 pixel wide (eGFP) lines were drawn over the BM (Col IV-GFP) or follicle cells (eGFP) in central transverse sections from the anterior to posterior tip, straightened, and segmented into 21 equal regions (Figure 2.4 E). The 11 odd-numbered regions were labeled from 0 (anterior tip) to 100 (posterior tip) in increments of 10, and mean GFP intensity of each region was measured. All images were obtained at the same settings.

For Laminin immunofluorescence intensity measurements, control and *SPARC-HA*-expressing egg chambers were stained in the same tube with α-Laminin and α-SPARC to differentiate between conditions. Laminin intensity was measured as described above for Col IV-GFP and Pcan-GFP.

Measurement of follicle cell migration rates

For follicle cell migration rates, 20-30 minute time-lapse movies were acquired from *Neuroglian-GFP* and *Indy-GFP*-expressing egg chambers. Live imaging of follicle cell migration was performed as previously described (Lerner et al., 2013). The leading edge of a

single follicle cell was marked at the start and end of the movie and distance traveled was measured and divided by movie length (minutes). Two distant cells were measured and their rates averaged for each egg chamber.

Measurement of egg chamber aspect ratios

For aspect ratio measurements, in central transverse sections egg chamber length (anterior to posterior tip) and width (widest region perpendicular to anterior-posterior axis) were measured, and ratio of length:width was calculated.

Measurement of tissue-level alignment of actin bundles

Images of basal actin bundles were acquired in fixed, phalloidin-stained egg chambers. To determine the average orientation of the actin bundles within each cell, a circular region of interest (ROI) was manually drawn over each cell to include basal actin bundles but exclude cell boundaries and orientation of each ROI was determined using the "Measure" feature of the OrientationJ plugin in ImageJ (Rezakhaniha et al., 2012). The tissue-level alignment ("order parameter") was calculated as previously described (Cetera et al., 2014) using a custom Python script.

Measurement of the length and tissue-level alignment of BM fibrils

Confocal sections through the plane of the BM were acquired in fixed, Col IV-GFP egg chambers. BM fibrils were isolated via two sequential thresholding steps: first an intensity threshold to remove the dimmest 95% of pixels, followed by a step to remove objects with an area of $<0.38\ \mu m^2$ and circularity >0.35 using the "Analyze Particles" tool in ImageJ. Length

(feret's diameter) and orientation (feret's angle) were calculated for each fibril using the "Analyze Particles" tool. The fibril order parameter was calculated as described above for basal actin bundles using the orientation of each fibril rather than the average orientation of each cell.

Co-immunoprecipitation and western blotting

Adult females were aged 3 days on yeast at 25°C and dissected in S2 media. Ovaries from 25 females per genotype were collected and lysed in cold modified RIPA buffer (50mM Tris pH 7.8, 100 mM NaCl, 2 mM $CaCl_2$, 0.1% SDS, 0.5% Sodium Deoxycholate, 1% triton) + complete protease inhibitor cocktail (Roche) by manual grinding and passage through a 27-gauge needle. Lysate was centrifuged at 13000 RPM and supernatant collected. GFP immunoprecipitation reactions were performed using GFP-Trap beads (Chromotek) at 4°C overnight. Input lysate and immunoprecipitate were analyzed via Western Blot on a 4-15% Mini-PROTEAN TGX Gel (Bio-Rad) using the following antibodies: rabbit α-SPARC (1:1500) (Martinek et al., 2002), chicken α-GFP (1:10,000, abcam). IRDye (LI-COR) secondary antibodies were used at 1:5000. Blots were imaged with Odyssey software version 2.1 (LI-COR Biosciences).

***In Situ* hybridization**

In situ hybridization for the *Cg25C* transcript was performed as previously described (Lerner et al., 2013) with the following modification: a *gurken* probe was included in addition to the *Cg25C* probe to ensure probe penetrance into germ cells. Primers used for *gurken* probe production (blue text indicates position of T7 promoter sequence): F: CAGCAGCAGATCCAGGAGAC, R: TAATACGACTCACTATAGGGCGCTCTCCATCGTAGTCGTT.

CHAPTER 3: RAB10-MEDIATED SECRETION SYNERGIZES WITH TISSUE MOVEMENT TO BUILD A POLARIZED BASEMENT MEMBRANE ARCHITECTURE FOR ORGAN MORPHOGENESIS

3.1 PREFACE

My work on SPARC provided valuable insight into mechanisms of BM remodeling in the egg chamber, but failed to identify the mechanism of BM fibril formation. This study, rather than taking a candidate-based approach, was driven by my observations from live imaging of fibril formation in wild-type egg chambers, which provided a clear model on which I could expound. This chapter was published in *Developmental Cell* with the following citation: Isabella, A.J., Horne-Badovinac, S., 2016. Rab10-mediated secretion synergizes with tissue movement to build a polarized basement membrane architecture for organ morphogenesis. Dev. Cell, 38, 47-60.

3.2 ABSTRACT

Basement membranes (BMs) are planar protein networks that support epithelial function. Regulated changes to BM architecture can also contribute to tissue morphogenesis, but how epithelia dynamically remodel their BMs is unknown. In *Drosophila*, elongation of the initially spherical egg chamber correlates with the generation of a polarized network of fibrils in its surrounding BM. Here, we use live imaging and genetic manipulations to determine how these fibrils form. BM fibrils are assembled from newly synthesized proteins in the pericellular spaces between the egg chamber's epithelial cells, and undergo oriented insertion into the BM by directed epithelial migration. We find that a Rab10-based secretion pathway promotes pericellular BM protein accumulation and fibril formation. Finally, by manipulating this

pathway, we show that BM fibrillar structure influences egg chamber morphogenesis. This work highlights how regulated protein secretion can synergize with tissue movement to build a polarized BM architecture that controls tissue shape.

3.3 INTRODUCTION

BMs are specialized extracellular matrices (ECMs) at the basal sides of epithelia. They are composed of a conserved set of core proteins, including Type IV Collagen (Col IV), Laminin, and the heparin sulfate proteoglycan Perlecan, that self-assemble into a planar network (Yurchenco, 2011). Beyond these shared features, BMs show compositional and structural diversity necessary to support the homeostatic needs of their associated tissues (Hynes and Naba, 2012). They can also be remodeled during development to facilitate tissue morphogenesis (Daley and Yamada, 2013; Morrissey and Sherwood, 2015). However, the mechanisms by which tissues modify BM structure, and how BM structure in turn modulates tissue dynamics, are poorly understood.

The *Drosophila* egg chamber offers a powerful system to study the interplay between BM structure and morphogenesis (Isabella and Horne-Badovinac, 2015a). Egg chambers are organ-like structures in the ovary that each generates one egg. They contain an interior germ cell cluster and an enveloping layer of somatic epithelial cells, called follicle cells (Figure 3.1 A). The follicle cells are polarized with their apical membranes contacting the germ cells and their basal membranes facing outward. This epithelium produces a BM that surrounds the egg chamber. Egg chamber development is categorized into 14 morphological stages. Between stages 5 and 10, egg chambers elongate along their anterior-posterior (A-P) axes to produce the ellipsoidal shape of the egg (Figure 3.2 A).

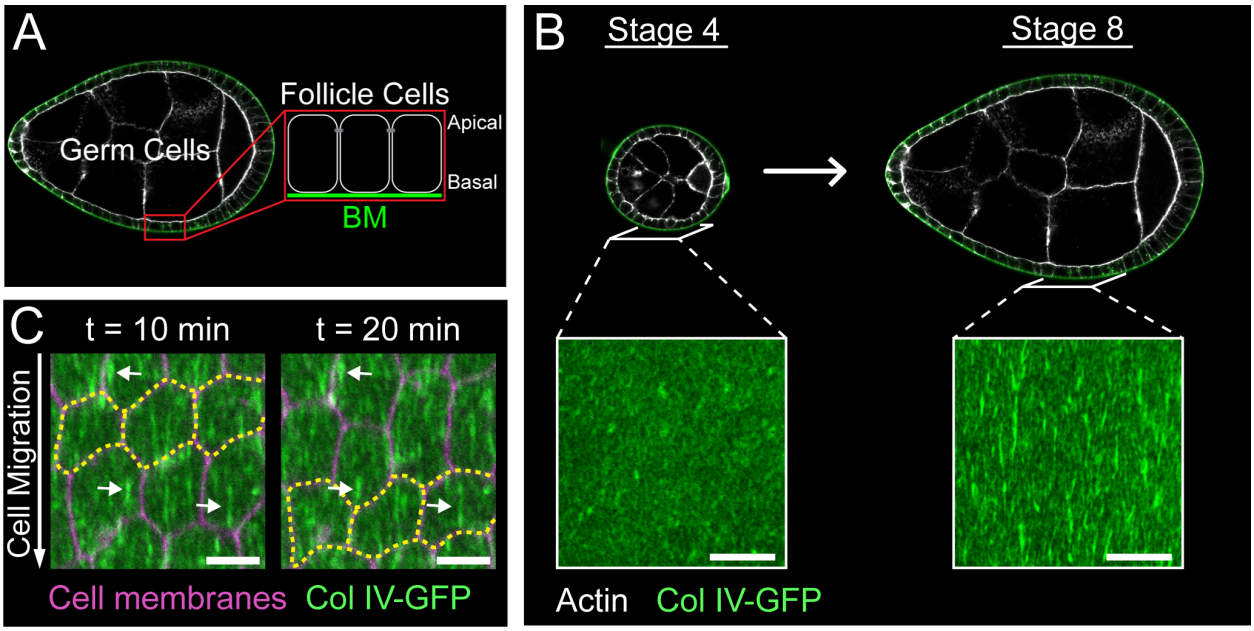

Figure 3.1. Introduction to BM fibrils
(A) Egg chamber structure. (B) Stage 4 egg chambers are round and have BMs that are largely uniform in structure; stage 8 egg chambers are elongated and their BMs contain polarized fibrils. Scale bars = 10 μm. (C) Time-lapse of follicle cell migration. Follicle cells migrate along the stationary BM in the direction of fibril polarity. Yellow outline marks three cells moving over time; arrows mark three stationary fibrils over time. Stage 7. Scale bars = 5 μm.

Egg chamber elongation coincides with a dramatic change in BM structure (Gutzeit et al., 1991; Haigo and Bilder, 2011b). Before elongation, the BM is largely uniform; between stages 5 and 8, however, linear, fibril-like structures are added to the pre-existing planar matrix (Figure 3.1 B). All major BM proteins thus far examined – Col IV, Laminin, and Perlecan – exhibit this structure (Gutzeit et al., 1991; Haigo and Bilder, 2011b; Schneider et al., 2006). BM fibrils align perpendicular to the A-P axis, polarizing the matrix. The construction of this new matrix architecture was reported to depend on collective migration of the follicle cells along the BM (Figure 3.1 C) (Haigo and Bilder, 2011b); this movement causes the entire egg chamber to rotate within the BM in the same direction that it becomes polarized. Although rotation appears to be necessary for BM fibril formation, it is not sufficient, as the follicle cells begin migrating ~20

hours before fibrils appear (Cetera et al., 2014). Thus, the mechanisms underlying BM fibril formation are still unclear.

The polarized BM is thought to function as part of a molecular corset that anisotropically constrains egg chamber growth to promote elongation (Figure 3.2 B) (Gutzeit et al., 1991). The main evidence supporting this idea comes from experiments in which collective follicle cell migration is blocked (Haigo and Bilder, 2011b). Inhibiting this migration prevents BM fibril formation and blocks elongation; however, migration feeds into other cellular process that may contribute to the elongation program independently of BM structure (Cetera et al., 2014; Viktorinová and Dahmann, 2013). Thus, to show that BM fibrils play a role in elongation, we must identify a more specific way to affect their assembly.

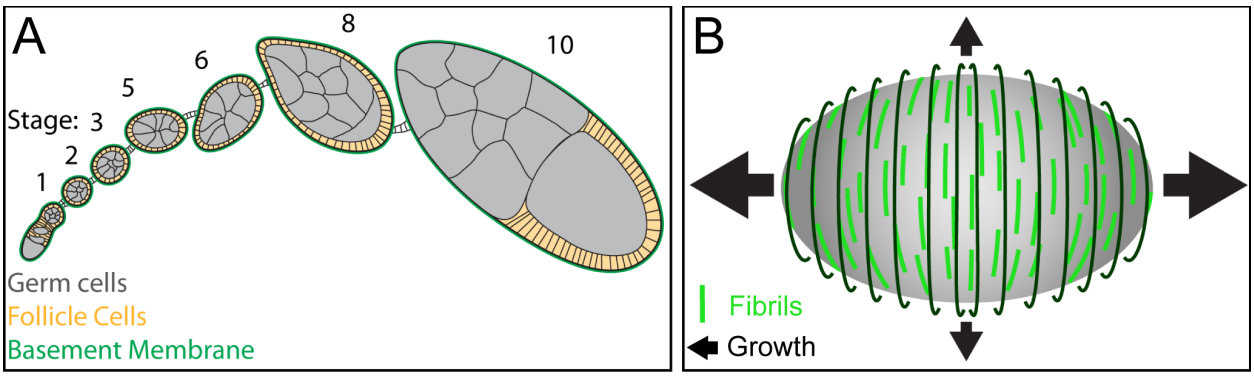

Figure 3.2. Introduction to egg chamber elongation
(A) Illustration showing a developmental array of egg chambers (ovariole). Stage 1 egg chambers arise as small, spherical structures, which grow and elongate as they develop. (B) The molecular corset model for egg chamber elongation. It is hypothesized that the polarized BM constrains egg chamber growth in the direction of polarity, thereby driving elongation along the orthogonal axis. Arrows represent direction and relative magnitude of growth.

Here, we use live imaging and genetic manipulations to determine how BM fibrils form. We find that BM fibrils are generated de novo from newly synthesized proteins. Our data suggest a model in which new BM proteins are secreted through a basal region of the lateral plasma membrane and aggregate into cohesive structures within the pericellular space between

follicle cells. They are then inserted into the BM in the correct orientation by the directed migration of the tissue. We further show that the small GTPase Rab10 and its effector EH domain binding protein 1 (Ehbp1) promote BM fibril formation via this pericellular secretion pathway. Finally, we use Rab10/Ehbp1 mis-expression to selectively alter BM structure and show that increasing BM fibril formation influences egg chamber elongation. This work shows how coordinated cellular behaviors can regulate BM structure during development, and how the matrix remodeling can play an instructive role in shaping the tissue.

3.4 RESULTS

BM fibrils form from newly synthesized proteins

The fibrillar structures that form in the follicular BM are best visualized with a GFP protein trap in the Col IV α2 chain Viking (Col IV-GFP) (Haigo and Bilder, 2011b). To visualize BM fibril formation, we performed live imaging of stage 7 BMs labeled with Col IV-GFP. This process coincides with a period of increased BM protein production (Haigo and Bilder, 2011b); thus, we reasoned that fibrils might arise from newly synthesized proteins. To test this idea, we photo-bleached a large rectangular region of the BM, which allowed us to assess the contribution of newly synthesized Col IV-GFP to fibril formation (Figures 3.3 A, B and 3.4 A). Over the course of a 39-minute time lapse, two populations of Col IV-GFP can be seen moving relative to the static BM (Figures 3.3 A and 3.4 A). The first population appears as punctae that move steadily throughout the time lapse. This signal likely represents Col IV within the secretory pathway of the migrating cells. The second population includes structures that often appear linear - these initially move with the follicle cells but eventually integrate into the BM as new fibrils. We will refer to these structures as “nascent fibrils”. Newly incorporated fibrils always exhibit

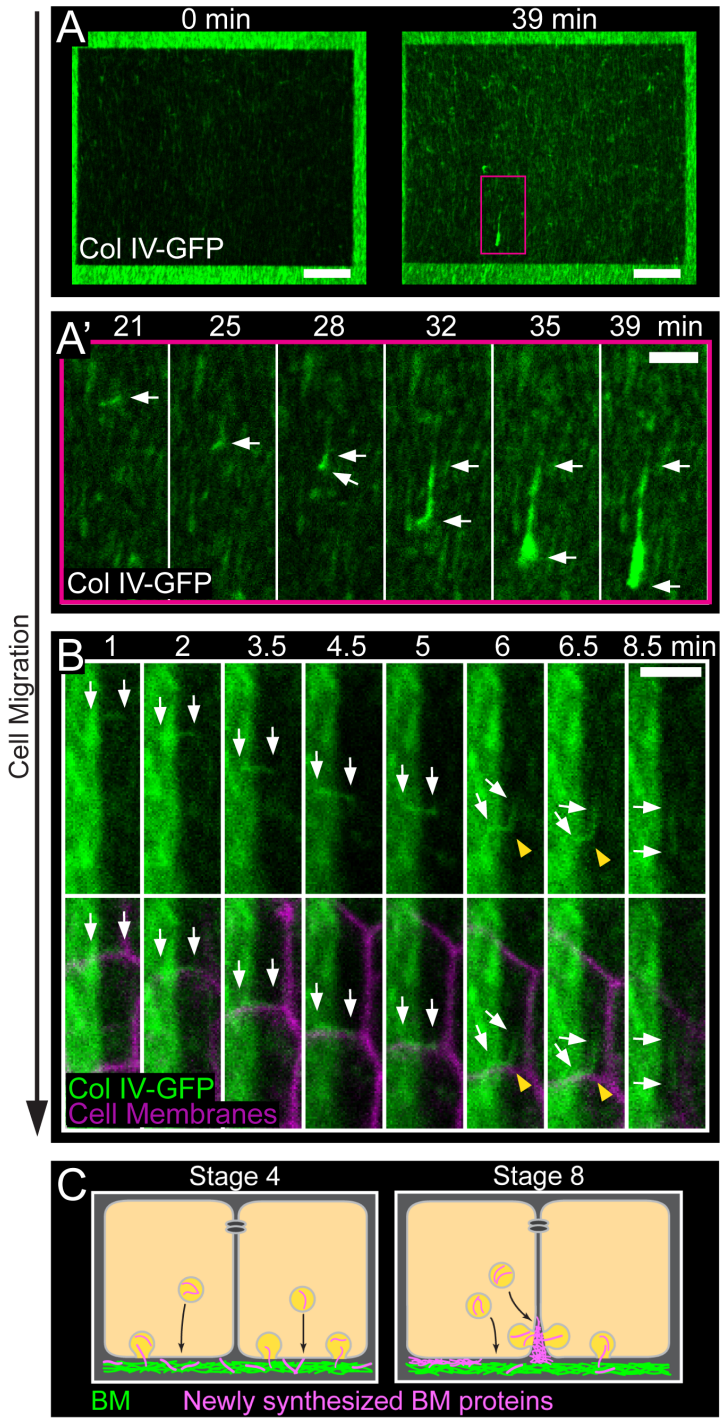

Figure 3.3. Live imaging of BM fibril formation

(A) Still images from a time lapse showing fibril incorporation into the BM. (A) First and last frames. The dark rectangle is the photobleached region. The pink box corresponds to the region shown in (A'). (A') Montage showing an individual nascent fibril with full GFP fluorescence moving in the direction of cell migration and then incorporating into the BM. Arrows mark both ends of the nascent fibril. Scale bars = 10 µm (A), 3 µm (A'). (B) Time lapse montage showing fibril incorporation into the BM. The dark portion on the right of each panel is the photobleached region. A nascent fibril travels with the migrating cell-cell interface until it is drawn away from this location and inserted into the BM. BM insertion causes the fibril to bend (yellow arrowheads) and then become properly aligned in the BM. Arrows mark both ends of the nascent fibril. Scale bar = 3 µm. (C) Model for BM fibril formation. Prior to fibril formation (represented by stage 4), we envision that new BM proteins (pink) exit through the basal surface and directly incorporate into the planar BM (green). During fibril formation (represented by stage 8), a portion of the BM traffic may be redirected to a basal region of the lateral surface. BM proteins would then aggregate in the pericellular space before being deposited in the BM as fibrils. Experiments performed at stage 7.

bright GFP fluorescence relative to the photo-bleached BM, indicating that they form from newly synthesized proteins (Figures 3.3 A and 3.4 A). Additionally, although the shapes of nascent fibrils are highly variable, from globules that appear to unfurl during insertion (Figure 3.3 A') to wispy, linear structures that insert with little shape change (Figures 3.3 B and 3.4 A'), their cohesiveness suggests that they are assembled prior to deposition into the BM.

Performing the same experiment with follicle cell plasma membranes marked suggested that BM fibrils form at cell-cell interfaces (Figure 3.3 B). At the beginning of the movie shown in Figure 3.3 B, a linear nascent fibril sits at the interface between two follicle cells, where it is oriented perpendicular to the mature fibrils within the BM. As the nascent fibril moves with the migrating tissue, it maintains association with the cell-cell interface. After 8 minutes, one side of the nascent fibril stops moving, likely due to adhesion to the BM, while the other side stays associated with the cell-cell interface. Continued cell migration draws the nascent fibril away from the interface, first inducing a 90° bend and then rotating it into the proper orientation. The fibril ultimately loses contact with the moving interface and takes up its final position in the BM (Figure 3.3 B). We made 19 such movies, and observed 88 fibril formation events. In all cases, new fibrils were incorporated into the BM as a cohesive structure from a cell-cell interface.

We observed that only a fraction of newly synthesized Col IV is incorporated into the BM as easily visualized fibrils at stage 7, while the rest continues to undergo constitutive deposition into the planar BM. Live total internal reflection fluorescence (TIRF) microscopy of a photobleached BM revealed Col IV-GFP incorporation into regions containing new fibrils and into regions where no obvious fibrils appear (Figure 3.4 B). Thus, new proteins

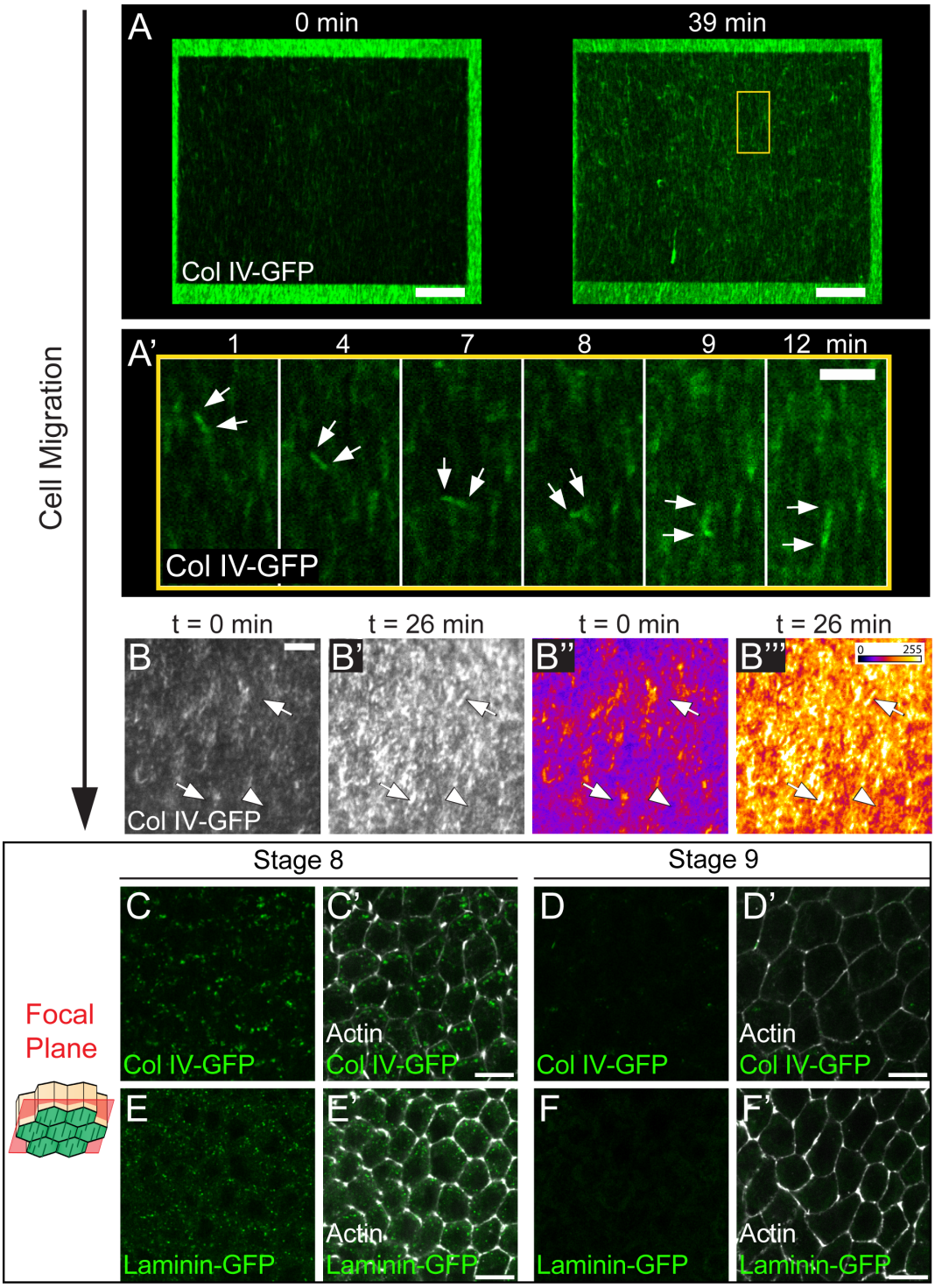

Figure 3.4. BM Col IV deposition during fibrillogenesis
(A) Still time lapse images showing fibril incorporation into the BM. Cell migration direction is down. (A) First and last frames from time lapse. The dark rectangle is the photobleached region. The yellow box corresponds to the region shown in (A'). (A') Montage showing individual fibril incorporation event. A nascent fibril with full GFP fluorescence moves in the direction of cell migration and then incorporates into the BM. Arrows mark the two ends

Figure 3.4. Continued, BM Col IV deposition during fibrillogenesis
of the nascent fibril. Scale bars = 10 μm (A), 3 μm (A'). (B) Cropped still time lapse images. (B'' and B''') represent heat maps of images in (B and B'), respectively. In TIRF imaging of a photobleached BM, Col IV-GFP fluorescence increases across the entire BM – both in regions containing new fibrils (arrows) and in the planar matrix (arrowhead). Thus, during BM fibril formation, only a fraction of the newly synthesized Col IV is incorporated as fibrils, while the remainder is deposited into the planar BM. Scale bar = 5 μm. (A and B) Experiments performed at stage 7. (C-F) BM protein production appears to cease at the end of stage 8. At stage 8, intracellular levels of Col IV (C) and Laminin (E) are high, while at stage 9 they are low (D and F). The focal plane illustration indicates the rough distance from the BM (green) at which the images were taken. Scale bars = 10 μm.

appear to be apportioned between these two BM populations. BM protein secretion appears to largely cease between stages 8 and 9, concurrent with the end of rotational migration, as we observe a sharp drop in intracellular Col IV and Laminin levels at this time (Figures 3.4 C-F).

These live imaging experiments led us to generate a model for how BM fibrils form (Figure 3.3 C). Prior to stage 5, we envision that newly synthesized BM proteins are trafficked to the basal cell surface. Immediate contact with the BM upon secretion would promote even incorporation across the BM and expansion of the isotropic planar matrix. In contrast, during fibril formation, a portion of the BM traffic may be redirected to a basal region of the lateral cell surface. This would cause BM proteins to accumulate in the pericellular spaces between follicle cells and promote their aggregation into nascent fibrils. The migration of the epithelium would then provide the directional information to orient fibrils perpendicular to the A-P axis as they incorporate into the BM.

BM fibrils form in the pericellular space between follicle cells

To test our model, we first asked whether Col IV accumulates in the pericellular space between follicle cells during fibril formation. We stained non-permeabilized tissue expressing Col IV-GFP with an anti-GFP antibody to selectively label extracellular Col IV. Because pericellular

Col IV-GFP is dim relative to intracellular Col IV-GFP, it is difficult to see without enhancing the signal with a non-permeabilized stain. Images were obtained at a focal plane ~1-1.5 μm apical to the BM. Very little Col IV is present in the pericellular space at stage 4, before fibril formation begins; however, we detected significant pericellular Col IV at stage 8 when fibrils are forming (Figures 3.5 A-C).

Although linear structures can often be seen in individual focal planes at stage 8 (Figure 3.5 B), 3D reconstruction of pericellular Col IV-GFP across the tissue reveals that nascent fibrils have diverse shapes and orientations (Figure 3.5 D). Many nascent fibrils, including the one highlighted in Figure 3.5 D, make contact with the BM at one end, suggesting that they are in the early stages of BM deposition.

To ensure that the pericellular Col IV is newly synthesized protein, we examined stage 8 epithelia in which some cells express Col IV-GFP and some express unmarked Col IV. Due to follicle cell migration, the BM typically becomes uniformly labelled with GFP under these conditions. We envisioned two possible outcomes from this experiment. (1) Col IV-GFP could be present in the pericellular space throughout the epithelium, which would suggest that at least some of this population is derived from the BM, via diffusion and/or endocytic recycling. (2) Col IV-GFP could be restricted to the pericellular space around Col IV-GFP-expressing cells, a scenario that can only be achieved by direct secretion of new protein into this location. We observed the latter, indicating that pericellular Col IV-GFP is new material that has not yet reached the BM (Figure 3.6 A).

Further support for our model comes from changes in BM structure that occur when follicle cell migration is blocked. We previously showed that loss of the Ste20-family kinase Misshapen (Msn) blocks follicle cell migration (Lewellyn et al., 2013). Under these conditions,

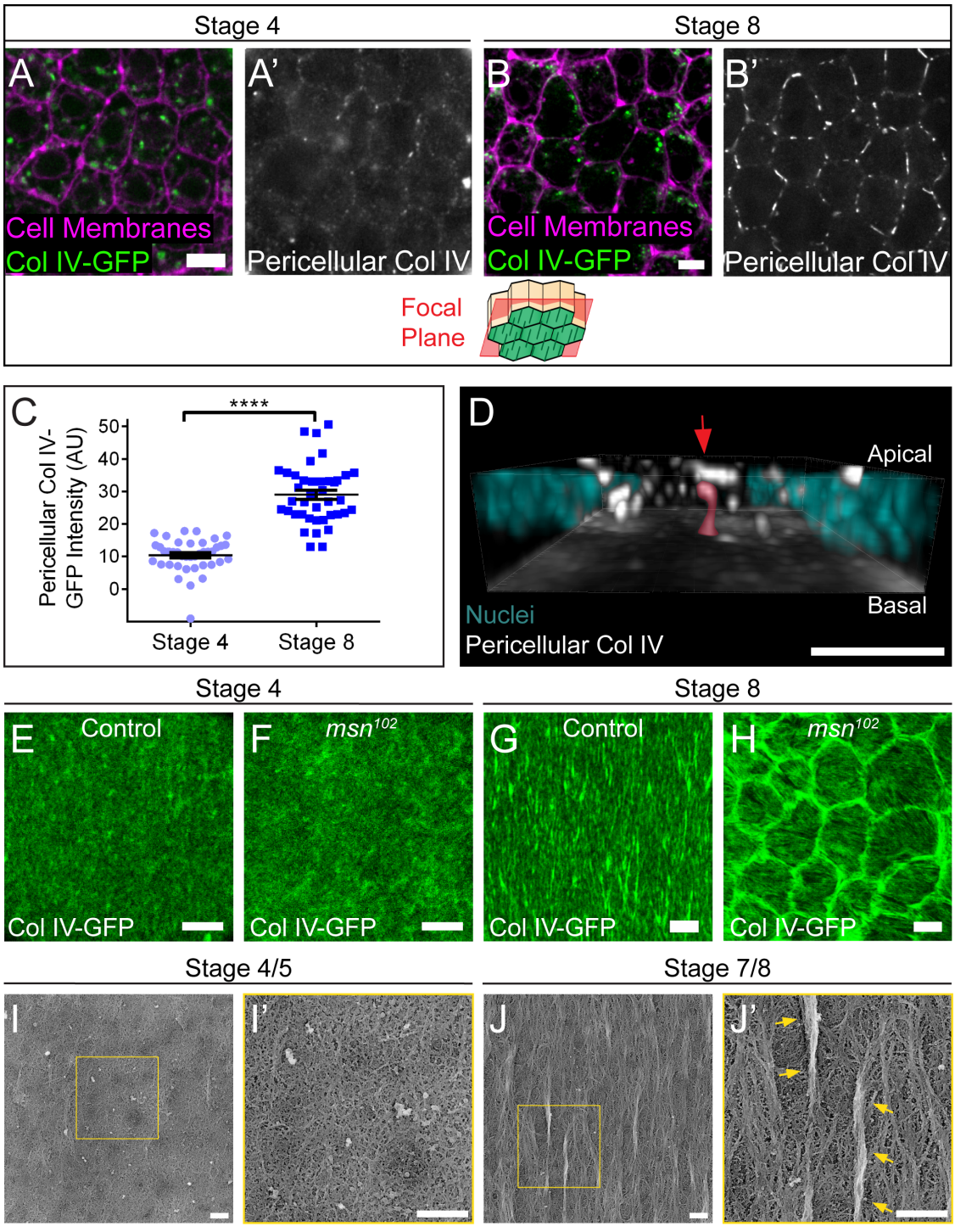

Figure 3.5. BM fibrils form in the pericellular space between follicle cells
(A and B) Representative images of Col IV in the pericellular space. Staining non-permeabilized tissue expressing Col IV-GFP with a GFP antibody reveals pericellular Col IV (white) and does not label intracellular Col IV-GFP (green). The illustration shows the rough distance from the BM (green) at which the images were taken. Pericellular Col IV is low at stage 4 (A) but high at stage 8 (B). Scale bars = 5 μm. (C) Quantification of pericellular Col IV. Data represent mean

Figure 3.5. Continued, BM fibrils form in the pericellular space between follicle cells ± s.e.m. t-test: **** = P<0.0001. (D) 3D reconstruction of the basal half of a stage 8 follicular epithelium, showing pericellular Col IV aggregates. The image is oriented with the BM down; most BM fluorescence has been removed to allow visualization of nascent fibrils. The highlighted nascent fibril (red highlight and arrow) contacts the BM and is likely in the process of BM incorporation. Scale bar = 5 μm. (E-H) At stage 4, the BMs of non-migrating *msn*^{102} epithelia (F) show little difference from controls (E). However, at stage 8, the BMs of non-migrating *msn*^{102} epithelia (H) show ring-like aggregates around cells, which likely represent nascent fibrils that could not exit the pericellular space. Scale bars = 5 μm. (I-J) Platinum replica electron micrographs of the inner surface of de-cellularized follicular BMs. (I) Stage 4/5 BMs are primarily composed of an isotropic planar matrix. (J) Stage 7/8 BMs contain large linear aggregates that lie atop the planar matrix (arrows), as well as small polarized regions that appear to be integrated within the planar matrix. (I' and J') Blow-ups of the boxed regions in (I and J). Scale bars = 500 nm.

Col IV-GFP forms ring-like aggregates around the edges of non-motile cells. These rings show the same stage-specificity as pericellular Col IV accumulation – they are absent at stage 4, but strongly apparent at stage 8 (Figures 3.5 E-H). Because loss of Msn increases integrin levels at the basal cell surface, we initially proposed that this phenotype might be due to heightened adhesion to the BM (Lewellyn et al., 2013). However, we have now found that two conditions that block collective follicle cell migration by other means – loss of the Fat2 cadherin (Viktorinová and Dahmann, 2013) and RNAi knockdown of the SCAR complex component Abelson interacting protein (Abi) (Cetera et al., 2014) – cause the same change in BM structure (Figures 3.6 B-D). We also observed that the rings extend up to 2 μm into the pericellular space, consistent with the idea that BM proteins exit the cell at the lateral surface during fibril formation (Figure 3.6 D). Thus, the rings likely represent the subset of BM proteins that would have formed fibrils, but were unable to exit the pericellular space in the absence of follicle cell migration. Collectively, these data support a model in which nascent fibrils are assembled in the pericellular space between follicle cells and are then drawn into the BM by directed epithelial motility.

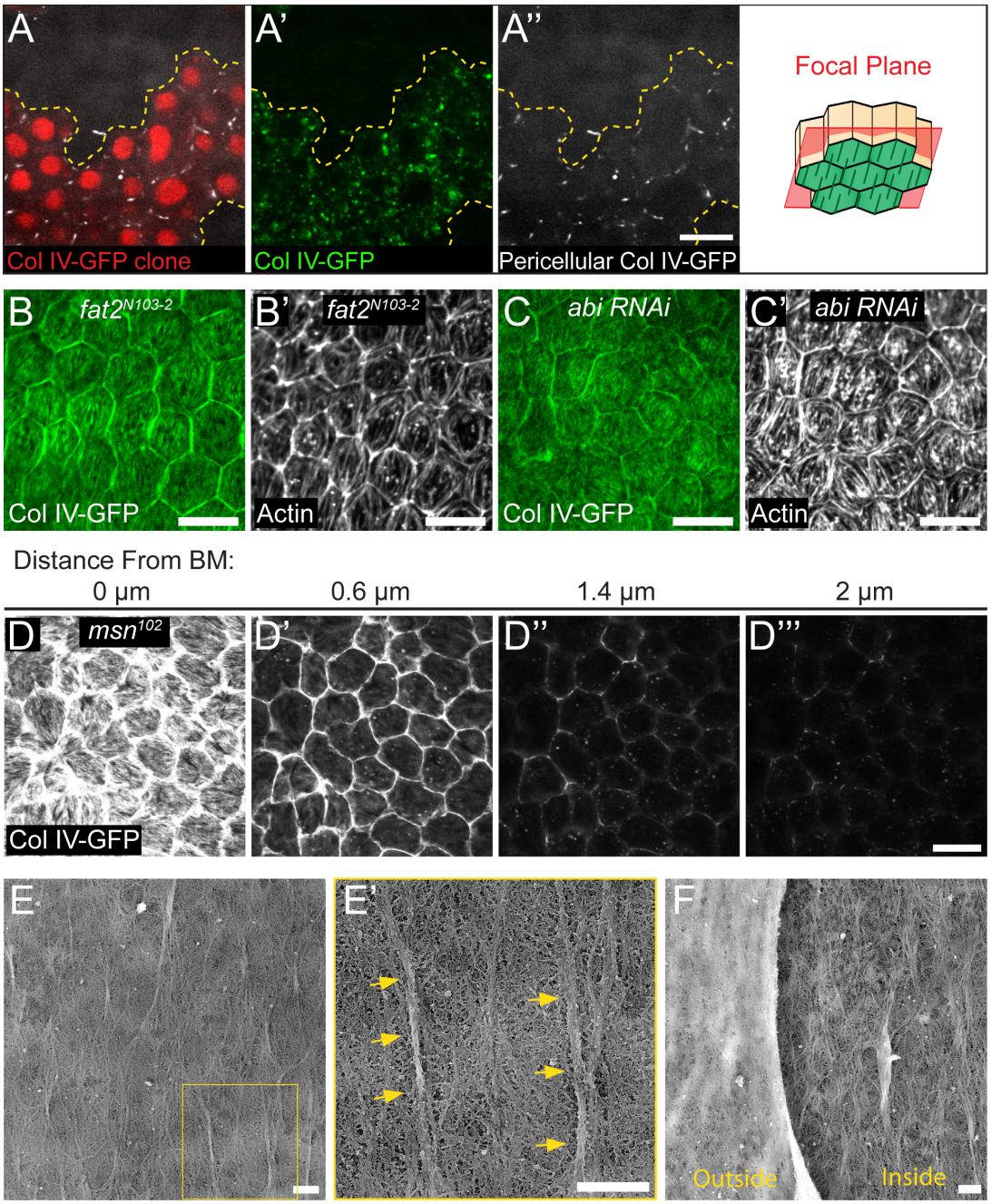

Figure 3.6. BM polarization in migrating and non-migrating epithelia
(A) Mosaic epithelium in which some cells express Col IV-GFP and some cells express unlabeled Col IV. Pericellular Col IV signal can only be seen around Col IV-GFP-expressing cells. Because follicle cell migration distributes Col IV-GFP evenly throughout the BM in this condition, any pericellular Col IV-GFP derived from the BM would accumulate around all cells. Accumulation of pericellular Col IV only around Col IV-GFP-expressing cells indicates that this protein is directly secreted to this location. The illustration shows the rough distance from the BM (green) at which the images were taken. Scale bar = 10 µm. (B and C) Two additional conditions (other than loss of Msn) that block follicle cell migration – mutation of *fat2* (B) or expression of *abi RNAi* throughout the follicular epithelium (C) – also cause ring-like

Figure 3.6. Continued, BM polarization in migrating and non-migrating epithelia accumulations of Col IV around cell edges. In addition to the prominent Col IV rings, small ridges can be seen in in the planar BM overlying each cell. These ridges show the same general orientation as linear actin bundles at the basal follicle cell surfaces (B' and C'). Scale bars = 10 μm. (D) In *msn* epithelia, the Col IV rings penetrate up to 2 μm into the pericellular space, suggesting that they arise from pericellular Col IV. Scale bars = 10 μm. (E and F) Platinum replica electron micrographs of stage 7/8 de-cellularized follicular BMs. (E) A second example of the inner surface of a BM that contains large linear aggregates that lie atop the planar matrix (arrows), as well as small polarized regions that appear to be integrated within the planar matrix. (E') Blow-up of the boxed region in (E). (F) The BM is folded to reveal both the outer and inner surfaces. Polarized structures can only be observed on the inner surface of the BM. Scale bar = 500 nm. Experiments Performed at Stage 8 except where otherwise noted.

Notably, in our non-migratory conditions small, polarized ridges can be seen in the planar BM overlaying individual follicle cells (Figures 3.5 H, 3.6 B-C). This suggests that the epithelium has an alternate method to induce BM polarity, perhaps by reorganizing the planar matrix. To more closely examine BM structure, we generated platinum replicas of de-cellularized BMs for electron microscopic (EM) analysis. As expected, stage 4/5 BMs exist as a largely isotropic planar meshwork (Figure 3.5 I), while large fibrils - generally 1-3 μm in length - are distributed throughout the BM at stage 7/8 (Figures 3.5 J and 3.6 E). These fibrils appear as distinct aggregates of aligned proteins that sit atop the planar matrix, and can only be seen on the inner, cell-facing surface of the BM (Figure 3.6 F). In addition to fibrils, there are also smaller regions of local alignment that appear to be integrated within, rather than on top of, the planar matrix (Figures 3.5 J and 3.6 E). While we cannot rule out that these regions simply represent very small fibrils, these data open the possibility that there may be two levels of polarization in the follicular BM - large fibrils that are deposited on top of the pre-existing planar matrix and smaller regions of local alignment within the planar matrix itself.

Rab10 promotes BM fibril formation

Given that BM fibrils form during a specific developmental time period from newly secreted proteins, we reasoned that there must be a regulated change in the BM secretion machinery that promotes their formation. We previously identified the small GTPase Rab10 as a central regulator of polarized BM protein transport and showed that this protein labels membrane-bound compartments in the basal region of the cell (Lerner et al., 2013). This Rab10 population could represent endosomal sorting compartments and/or exocytic carriers, but the location of these structures is not necessarily indicative of where BM proteins exit the cell. Further examination showed that Rab10 also accumulates on the follicle cells' lateral surfaces. We observed this pattern with both a *UAS-RFP-Rab10* transgene (Figure 3.7 A) and a construct in which *YFP* was inserted into the endogenous *Rab10* locus (Figure 3.7 B). This localization could reflect fusion of Rab10 vesicles with lateral cell membranes, as Rab10 can function with the exocyst to control late stages of secretion (Babbey et al., 2010; Sano et al., 2015; Taylor et al., 2015; Zou et al., 2015). Endogenous Rab10 levels also increase significantly between stages 4 and 6 (Figures 3.8 A-B). Thus, Rab10 might direct BM protein traffic to the lateral plasma membranes, and thereby promote BM fibril formation.

Consistent with this idea, Rab10 over-expression increases both the amount of Col IV in the pericellular space (Figures 3.7 C-D) and the fibrillar nature of the BM (Figures 3.7 E-F) at stage 8. We considered two possible explanations for this effect. Increased Rab10 activity might cause more Col IV to be secreted. Alternatively, it might cause a shift in protein distribution, such that more Col IV is directed into fibrils at the expense of the planar matrix. To distinguish between these ideas, we measured Col IV-GFP levels in the BM, and then determined the percentage of that Col IV that is in fibrils (fibril fraction) vs. the planar matrix

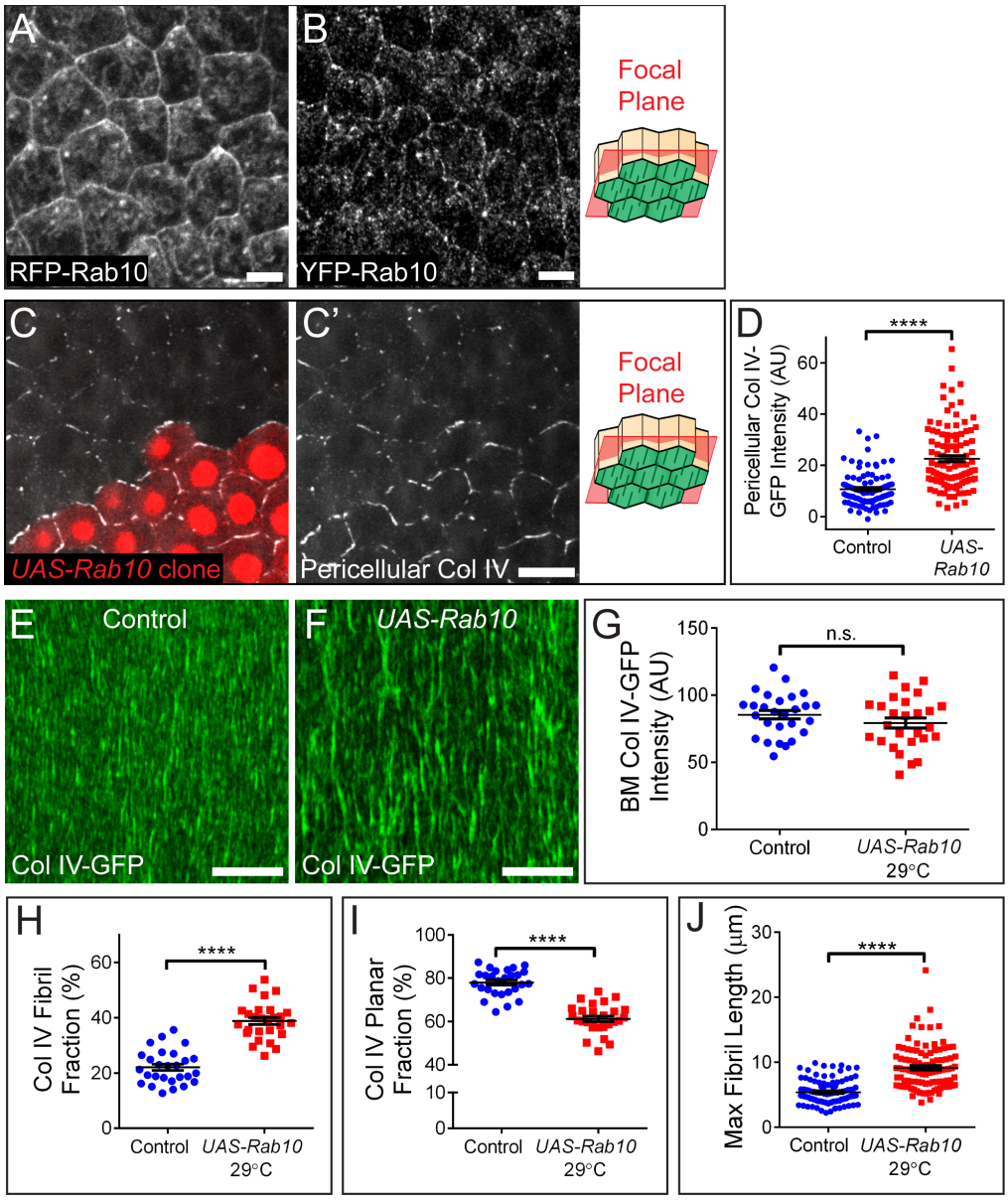

Figure 3.7. Rab10 promotes BM fibril formation
(A and B) RFP-Rab10 produced from a UAS transgene (A) and endogenous YFP-Rab10 (B) both localize to lateral membranes. Antibody staining was used to enhance YFP-Rab10 signal. Scale bars = 5 µm. (C) Representative image showing that clonal *UAS-Rab10* expression (red cells) increases pericellular Col IV relative to wild-type cells. Scale bars = 10 µm. (A-C) The illustrations show the rough distance from the BM (green) at which the images were taken. (D) Quantification of the condition shown in (C). (E and F) Representative images showing that *UAS-Rab10* expression in all follicle cells at 29°C enhances the incorporation of Col IV into fibrils. Scale bars = 10 µm. (G) *UAS-Rab10* does not alter Col IV-GFP levels in the BM. (H) *UAS-Rab10* increases the fraction of BM Col IV-GFP contained within fibrils. (I) *UAS-Rab10* decreases the fraction of BM Col IV-GFP in the planar matrix. (J) *UAS-Rab10* increases maximum BM fibril length. (D and G-J) Data represent mean ± s.e.m. t-test: n.s. = P>0.05, **** = P<0.0001. Experiments performed at stage 8.

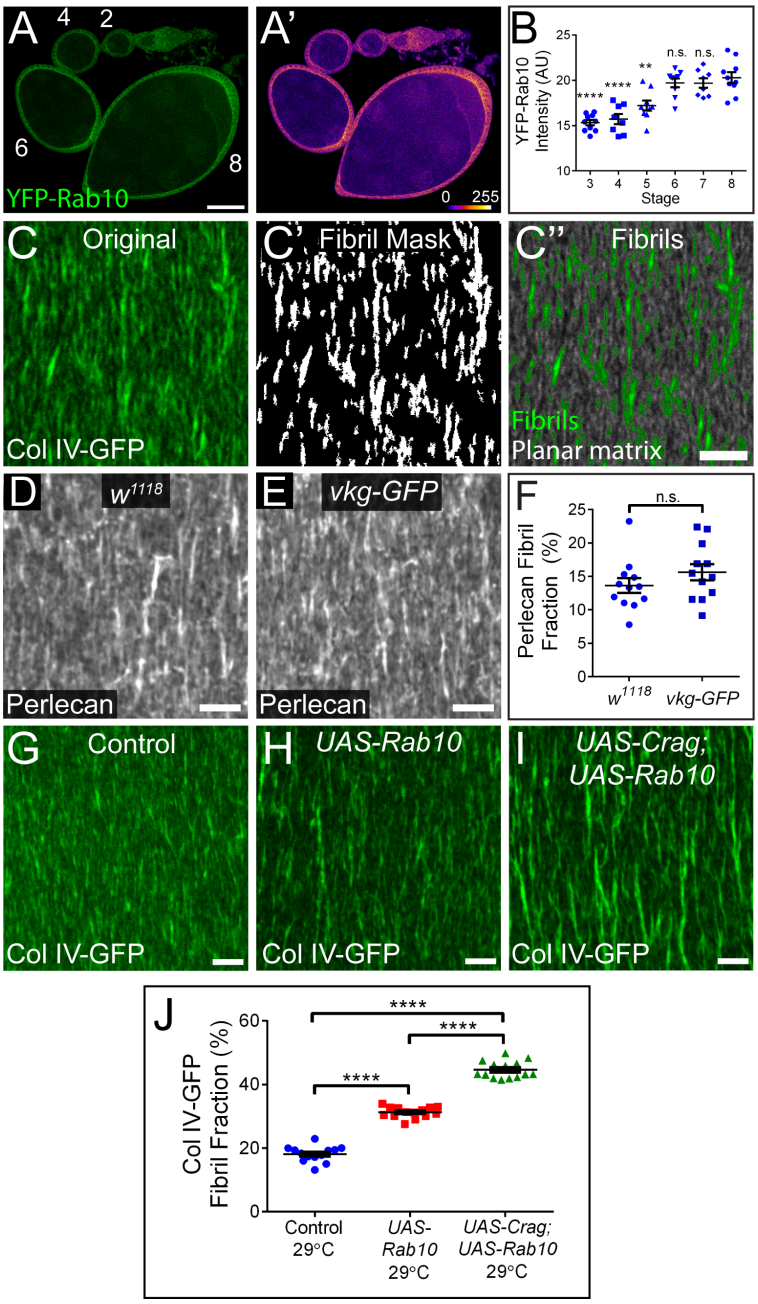

Figure 3.8. Rab10 activity enhances BM fibril formation
(A and B) Rab10 protein levels increase between stages 4 and 6. (A) Image of endogenously tagged YFP-Rab10 across stages. Numbers indicate egg chamber stages. Scale bar = 50 μm. (A') Heat map of image shown in (A). (B) Quantification of YFP-Rab10 protein levels across stages. Asterisks indicate significance relative to stage 8. (C) Images depicting our method for determining the BM fibril fraction. Original images, as shown in (C), were thresholded by pixel intensity and size to generate masks of fibrillar pixels (C'). (C'') Original image modified to show fibrillar pixels in green and pixels contained within the planar matrix in grey. See

Figure 3.8. Continued, Rab10 activity enhances BM fibril formation
supplemental experimental procedures for more information. Scale bar = 5 μm. (D-F) The GFP tag on the Viking protein does not alter BM fibril structure. (D and E) representative stage 8 w^{1118} (D) and *vkg-GFP* (E) BMs immunostained with anti-Perlecan antibody. Scale bars = 5 μm. (F) The Perlecan fibril fraction is not different between these two genotypes. (G-I) Representative images of Control (G), *UAS-Rab10* (H), and *UAS-Crag; UAS-Rab10* double over-expression (I) BMs. Over-expression of the Rab10 GEF *Crag* enhances the effect of *Rab10* over-expression on BM fibril fraction. Scale bar = 5 μm. (J) Quantification of data shown in (G-I). (B, F, and J) Data represent mean ± s.e.m. t-test: n.s. = P>0.05, ** = P<0.01, **** = P<0.0001. Experiments performed at stage 8 unless otherwise noted in figure.

(planar fraction) (Figure 3.8 C). Given the resolution limits of light microscopy and our image processing algorithm, this method likely underestimates the fibril fraction of the matrix, as very small fibrils will elude detection and be assigned to the planar fraction. This method does, however, provide a sensitive metric to compare relative changes to BM structure between conditions. For example, it allowed us to confirm that the fibrillar structure of the BM is not altered by the GFP tag on Col IV (Figures 3.8 D-F).

Using this strategy, we found that Rab10 over-expression does not change the amount of Col IV in the BM at stage 8 (Figure 3.7 G); instead, the fibril fraction increases at the expense of the planar fraction (Figures 3.7 H-I). This condition also produces longer BM fibrils (Figure 3.7 J). The fibril fraction is further increased by co-over-expressing Rab10's GDP/GTP exchange factor (GEF) *Crag* (Denef et al., 2008; Lerner et al., 2013); thus, the active, GTP-bound form of Rab10 is responsible for this effect (Figures 3.8 G-J). We were unable to determine whether the opposite occurs under Rab10 loss of function, as BM proteins are mis-trafficked to the apical surface under these conditions (Lerner et al., 2013). However, our data strongly suggest that Rab10 helps to guide newly synthesized Col IV into a laterally-directed, fibril-forming pathway.

Thus far, we have primarily used Col IV-GFP to study BM fibril formation. However, Laminin and Perlecan also form fibrils (Gutzeit et al., 1991; Schneider et al., 2006). We

therefore examined whether these proteins do so via the same mechanism as Col IV. We first examined GFP-tagged versions of the Perlecan homolog Terribly reduced optic lobes (Perlecan-GFP) and the Laminin β subunit LanB1 (Laminin-GFP). Although it is difficult to observe Perlecan-GFP before it reaches the BM, Laminin-GFP accumulates in the pericellular space weakly at stage 4 and strongly at stage 8 (Figures 3.9 A-B). Moreover, Rab10 over-expression increases the BM fibril fraction of Laminin-GFP and Perlecan-GFP at stage 8 without altering the amount of these proteins in the BM, similarly to Col IV (Figures 3.9 C-J). Finally, we simultaneously visualized Col IV-GFP, Laminin, and Perlecan in the BM and found that all three co-localize in individual fibrils (Figure 3.9 K). These data show that fibrils are compositionally similar to the planar BM, and that a common mechanism governs the secretion and fibrillogenesis of Col IV, Laminin, and Perlecan.

Modulating Rab10 activity provides a tunable mechanism to control BM structure

Our discovery that Rab10 over-expression increases pericellular BM protein accumulation and fibril formation without affecting bulk BM protein composition suggests that the Rab10 pathway may exist in competitive balance with another pathway that directs secretion to the planar matrix. If true, the fibril fraction should scale with Rab10 activity. We utilized the fact that UAS transgene expression increases with temperature to examine the fibril fraction across a range of Rab10 expression levels. Although temperature-independent in controls, the stage 8 fibril fraction rises with temperature in the *UAS-Rab10* condition (Figure 3.10 A). The amount of Rab10 in the follicle cells, therefore, provides a tunable mechanism to control the relative distribution of BM proteins into the fibrillar vs. planar BM populations.

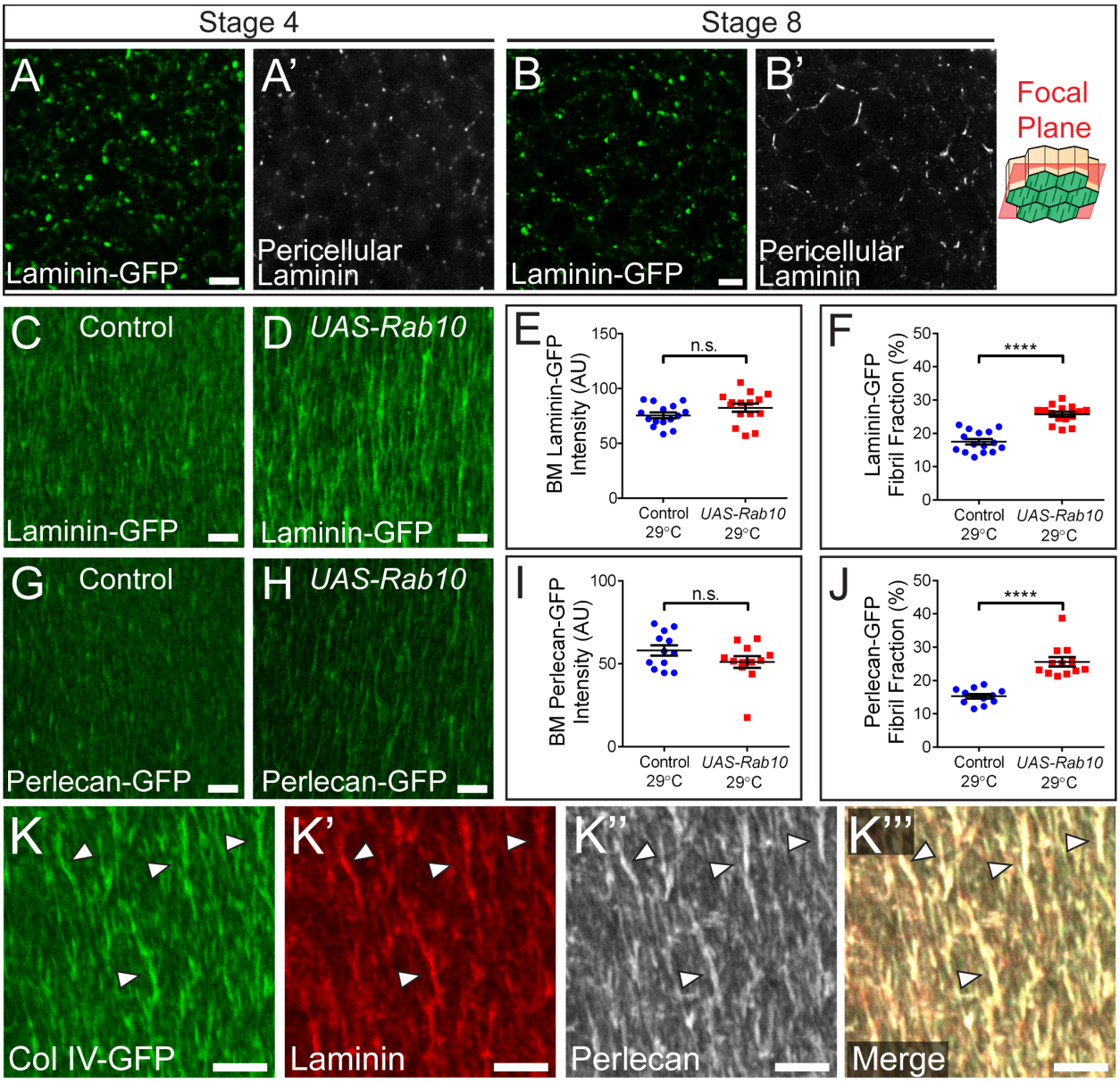

Figure 3.9. Rab10 also targets Laminin and Perlecan into BM fibrils
(A and B) Laminin is low in the pericellular space at stage 4 (A) but high at stage 8 (B). Scale bars = 5 µm. The illustration shows the rough distance from the BM (green) at which the images were taken. (C-D) Representative images showing that *UAS-Rab10* expression in all follicle cells at 29°C enhances the incorporation of Laminin into fibrils. Scale bars = 5 µm. (E) *UAS-Rab10* does not alter Laminin-GFP levels in the BM. (F) *UAS-Rab10* increases the fibril fraction of Laminin-GFP. (G-H) Representative images showing that *UAS-Rab10* expression in all follicle cells at 29°C enhances the incorporation of Perlecan into fibrils. Scale bars = 5 µm. (I) *UAS-Rab10* does not alter Perlecan-GFP levels in the BM. (J) *UAS-Rab10* increases the fibril fraction of Perlecan-GFP. (E,F, I and J) Data represent mean ± s.e.m. t-test: n.s. = P>0.05, **** = P<0.0001. (K) Col IV, Laminin, and Perlecan co-localize in individual fibrils (arrowhead). Scale bars = 5 µm. Experiments performed at stage 8 unless otherwise noted in figure.

As an alternative approach to enhancing Rab10-based secretion, we over-expressed Ehbp1, which is a Rab10 effector in *C. elegans* (Shi et al., 2010). This role appears to be conserved, as Ehbp1 depletion phenocopies loss of Rab10 (Figures 3.10 B-D), and Ehbp1 over-expression tunably increases the stage 8 BM fibril fraction and maximum BM fibril length (Figures 63.11 A-D and 3.10 A) without altering BM Col IV levels (Figure 3.10 E). In fact, over-expressing *Ehbp1* increases fibril formation to an even greater extent than *Rab10* over-expression (Figure 3.10 A). Ehbp1 over-expression also increases pericellular Col IV (Figures 3.11 E-F) at stage 8. 3D reconstruction of this pericellular pool revealed extremely long aggregates that span multiple cell lengths, consistent with the extremely long BM fibrils seen in this condition (Figure 3.11 G). These observations strengthen the link between pericellular Col IV and BM fibril formation. Further, although it is unclear why manipulating Ehbp1 has a stronger effect on BM protein trafficking than Rab10, it provides us with a practical means to increase the fibril fraction beyond what can be accomplished by over-expressing Rab10.

BM fibrils play an instructive role in egg chamber elongation

We next asked how altering BM architecture affects egg chamber elongation. Having identified conditions that allow us to control the extent of BM fibril formation over a large range, we examined the effects of both a modest (*UAS-Rab10* 23°C) and a strong (*UAS-Ehbp1* 29°C) increase in fibril fraction. Modestly increasing the fibril fraction leads to an increase in the egg's aspect ratio (length/width) (Figures 3.12A-C). This enhanced elongation is first seen at stage 7 (Figure 3.12 A), indicating that increasing the fibrillar nature of the BM is sufficient to augment the egg chamber's morphogenetic program. Conversely, strongly increasing the fibril fraction

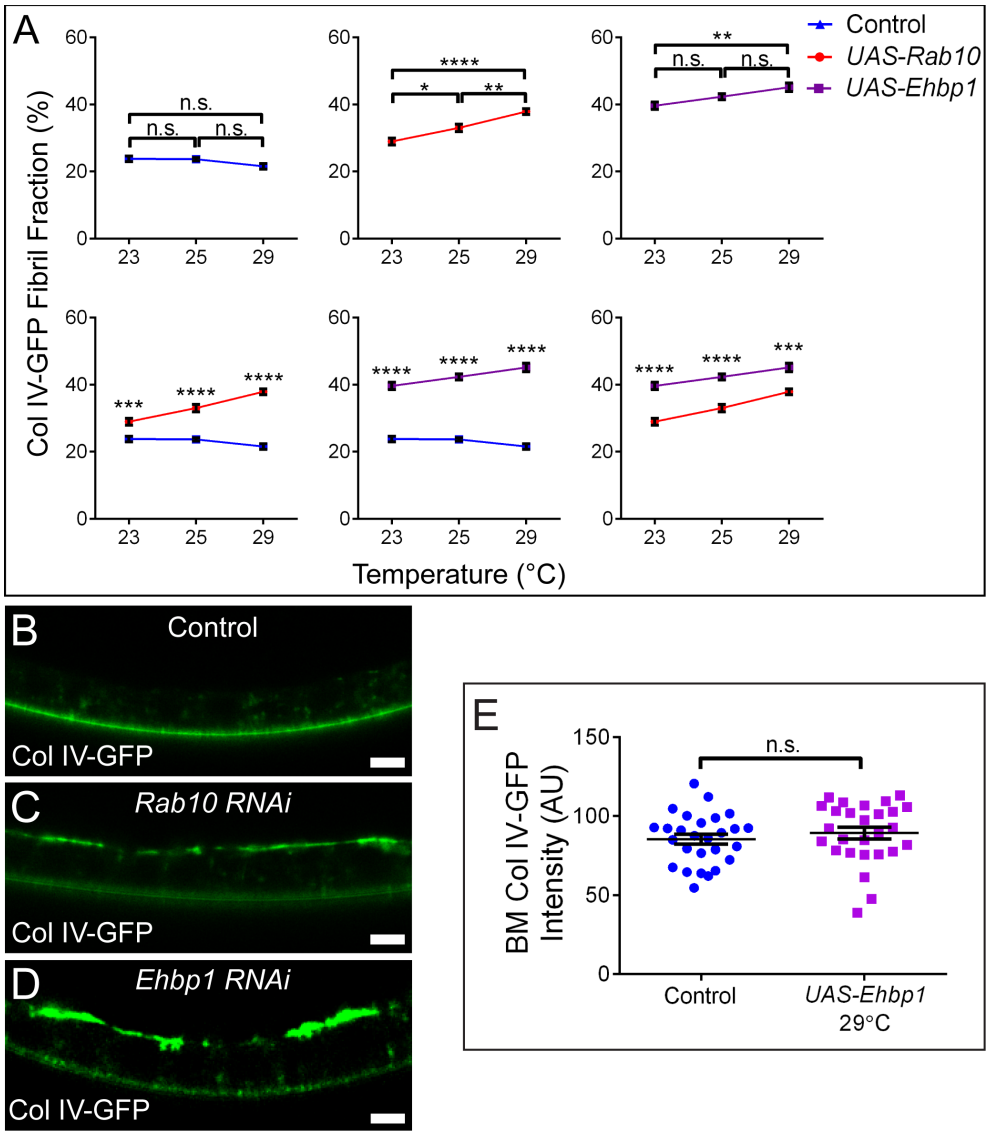

Figure 3.10. BM fibril formation is sensitive to Rab10 and Ehbp1 levels
(A) The Col IV-GFP Fibril fraction is sensitive to levels of Rab10 and the putative Rab10 effector Ehbp1. Increasing the temperature – which increases UAS transgene expression – has no effect on the fibril fraction in control egg chambers, but significantly increases fibril formation in the *UAS-Rab10* and *UAS-Ehbp1* conditions (top row). Additionally, *UAS-Rab10* and *UAS-Ehbp1* expression significantly increase fibril fraction relative to control at all temperatures, and *UAS-Ehbp1* causes a greater increase in fibril fraction than *UAS-Rab10* at all temperatures (bottom row). n = 14-27 egg chambers/data point. (B-D) Although control epithelia display no apical Col IV accumulation (B), apical Col IV can be seen upon expression of *Rab10 RNAi* (C) and, to an even greater extent, *Ehbp1 RNAi* (D). Scale bars = 5 µm. (E) 29°C *UAS-Ehbp1* expression does not alter the total amount of Col IV present in the BM. Graph uses same control data as Figure 4G. (A and E) Data represent mean ± s.e.m. t-test: n.s. = P>0.05, * = P<0.05, ** = P<0.01, *** = P<0.001, **** = P<0.0001. Experiments performed at stage 8.

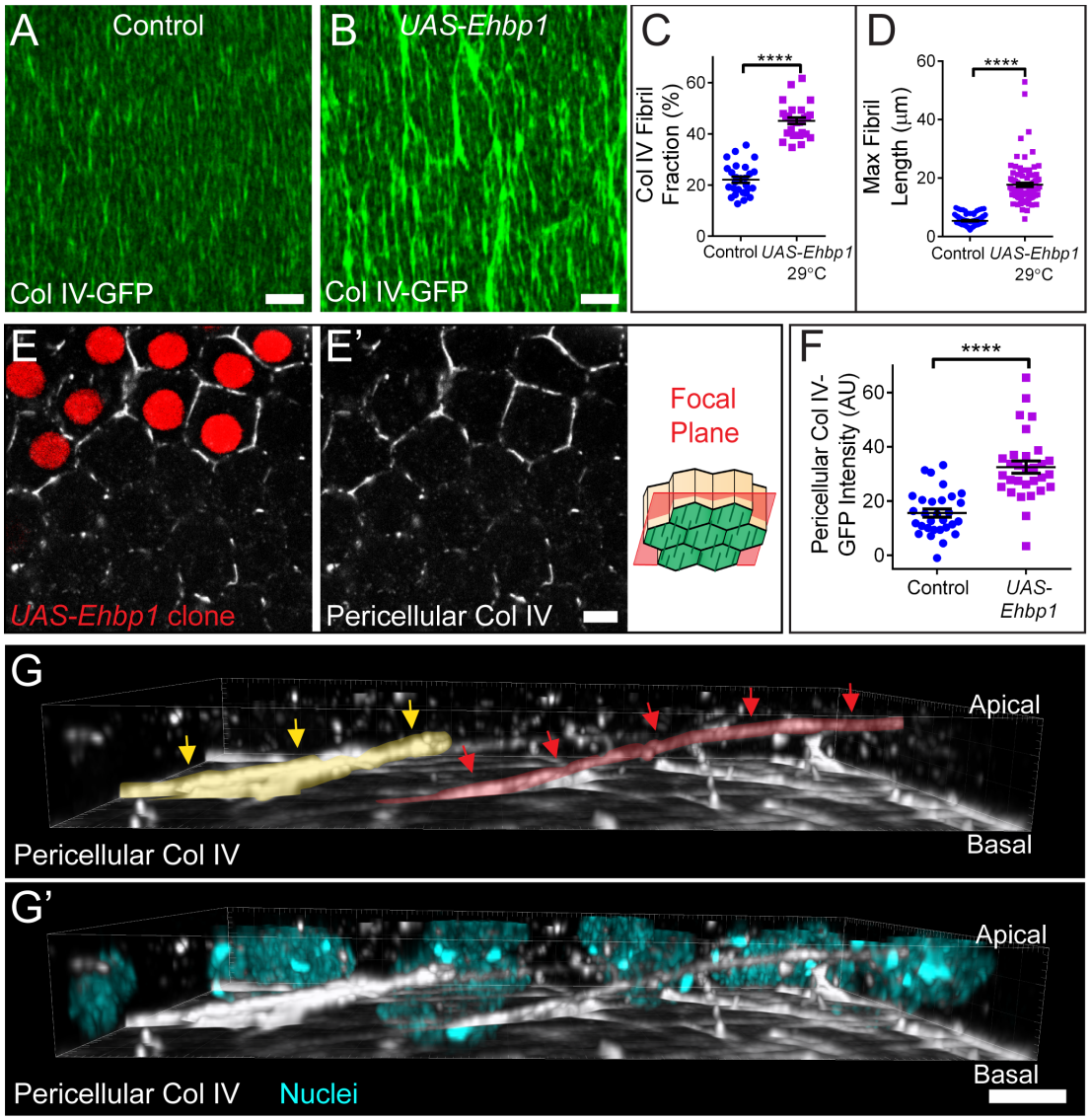

3.11. Ehbp1 promotes BM fibril formation

(A and B) Representative images showing that *UAS-Ehbp1* expression at 29°C in all follicle cells enhances BM fibril formation. Scale bars = 5 µm. (C and D) *UAS-Ehbp1* expression increases BM fibril fraction (C) and maximum BM fibril length (D). Graphs use same control data as Figures 4H and J. (E) Representative image showing that clonal *UAS-Ehbp1* expression (red cells) increases pericellular Col IV relative to neighboring wild-type cells. The illustration shows the rough distance from the BM (green) at which the images were taken. Scale bar = 5 µm. (F) Quantification of the condition shown in (E). (C, D, and F) Data represent mean ± s.e.m. t-test: **** = P<0.0001. (G-G') 3D reconstruction of the basal 3/4 of the follicular epithelium, showing pericellular Col IV in the *UAS-Ehbp1* condition. Extremely long pericellular aggregates can be seen, consistent with the long BM fibrils seen in (B and D). Two nascent fibrils are indicated by red and yellow arrows and highlights. Image is oriented with BM down; most BM fluorescence has been removed to allow visualization of nascent fibrils. Scale bars = 5 µm. Experiments performed at stage 8.

decreases the egg's aspect ratio (Figures 3.12 D-F). In this case, the egg chamber elongates normally, but fails to maintain its shape after stage 10 (Figure 3.12 F). These changes are not due to an indirect effect on egg chamber rotation, as follicle cell migration rates are unaffected by changes in the BM's fibril fraction (Figures 3.13 A-E). These data show that differing BM architectures can influence both the establishment and maintenance of the egg chamber's elongated shape.

The interplay between BM architecture and elongation can best be seen by plotting the aspect ratios of eggs across the full range of fibril fractions that we can generate (Figures 3.12 G and 3.13 F). Under control conditions, the fibril fraction ranges from 22-25%. Increasing the fibril fraction to 30-33%, via moderate *Rab10* over-expression (23°C and 25°C), maximally increases the egg's aspect ratio compared to controls, whereas increases above 37% via *Epbh1* or 29°C *Rab10* over-expression ultimately decrease the egg's aspect ratio compared to controls. These observations demonstrate how fine regulation of BM structure, in this case by tunable regulation of Rab10 pathway activity, can precisely influence morphogenesis. They also reveal the importance of tightly controlling BM structure during development.

3.5 DISCUSSION

BMs are often viewed as largely static structures that provide mechanical support for tissues. However, the changes in tissue size and shape that occur during development necessitate that BMs be similarly malleable. Regulated changes in BM structure may also actively promote tissue deformation. Thus, understanding morphogenesis will require that we know how tissues dynamically remodel their BMs, and how differing BM architectures affect tissue shape.

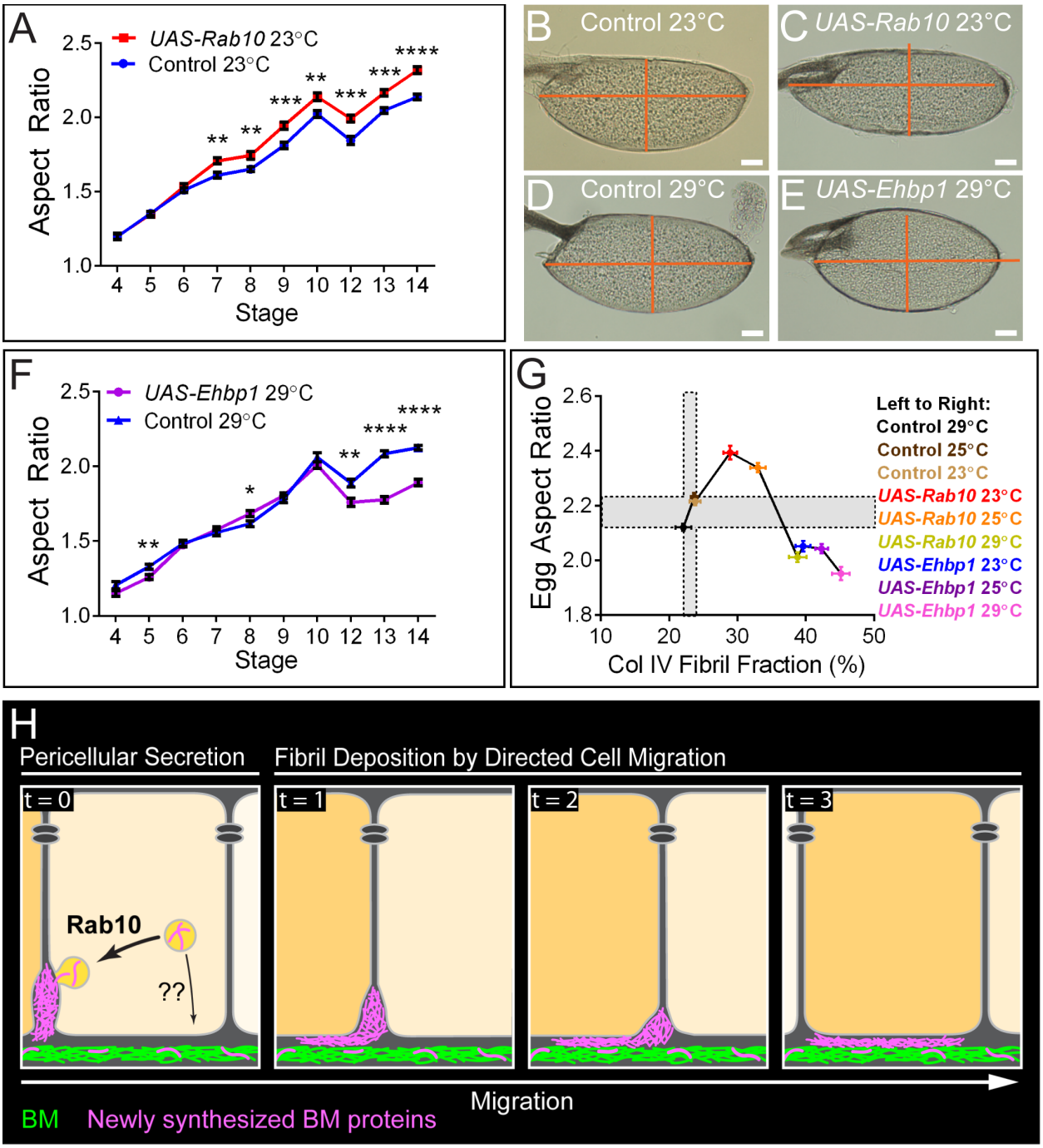

Figure 3.12. BM fibrils play an instructive role in egg chamber elongation
(A) *UAS-Rab10* expression at 23°C increases the egg chamber's aspect ratio. This effect is first seen at stage 7, suggesting that this BM structure augments elongation morphogenesis. n = 25-32 egg chambers/data point. (B and C) Representative images showing that 23°C *UAS-Rab10* expression results in eggs that are longer and narrower than controls. (D and E) Representative images showing that 29°C *UAS-Ehbp1* expression results in eggs that are shorter and wider than controls. (B-E) For each pair of eggs, the length and width of the control egg (orange lines) is mapped onto the experimental egg for reference. Scale bars = 50 µm. (F) *UAS-Ehbp1*

Figure 3.12. Continued, BM fibrils play an instructive role in egg chamber elongation expression at 29°C reduces the egg's aspect ratio. This effect is not seen until stage 12, suggesting that this BM structure is defective in maintaining the elongated state. n = 23-27 egg chambers/data point. (A and F) Data represent mean ± s.e.m. t-test: * = P<0.05, ** = P<0.01, *** = P<0.001, **** = P<0.0001. (G) Graph showing how egg aspect ratio changes as a function of Col IV fibril fraction. Fibril fractions of 30-33% increase egg aspect ratio compared to controls, whereas fibril fractions of 38% and above reduce it. Grey bars show control ranges for both measurements. X axis: n = 14-27 stage 8 egg chambers/condition. Y axis: n = 40-60 stage 14 egg chambers/condition. Both axes: data represent mean ± s.e.m. t-test values are in Figure S6F. Fibril fraction values represent same data shown in Figures 4H, 6C and S5A. (H) Proposed model for BM fibril formation. During fibril formation, Rab10 directs a portion of newly synthesized BM proteins to a basal region of the lateral plasma membrane for secretion. It may do so in competition with an unidentified pathway that directs BM protein secretion to the basal surface for incorporation into the planar matrix. Secretion to the lateral surface causes BM proteins to aggregate in the pericellular space between follicle cells. Directed follicle cell migration then inserts the nascent fibrils into the BM in the correct orientation. Cell migration direction is to the right.

Focusing on the fibrillar BM that surrounds the *Drosophila* egg chamber, we used live imaging to watch this matrix being remodeled in real time. The resulting information allowed us to determine how BM fibrils form, and to establish a direct role for these structures in egg chamber elongation.

We found that fibril formation begins when newly synthesized BM proteins aggregate in the pericellular space between follicle cells. These nascent fibrils then incorporate into the BM by first making a single point of contact with the planar matrix, and then being pulled out of the pericellular space as the follicle cells migrate away from this site. In this way, the motion of the migrating epithelium also provides the directional information needed to align BM fibrils perpendicular to the egg chamber's A-P axis and polarize the matrix (Figure 3.12 H).

3D reconstructions of nascent fibrils in the pericellular space showed that they often appear globular, despite the fact that most mature fibrils are linear. In rare cases, we have seen globules deposited into the BM; however, most eventually resolve into linear structures. The globules could be aggregation intermediates that will fuse into linear structures in the pericellular

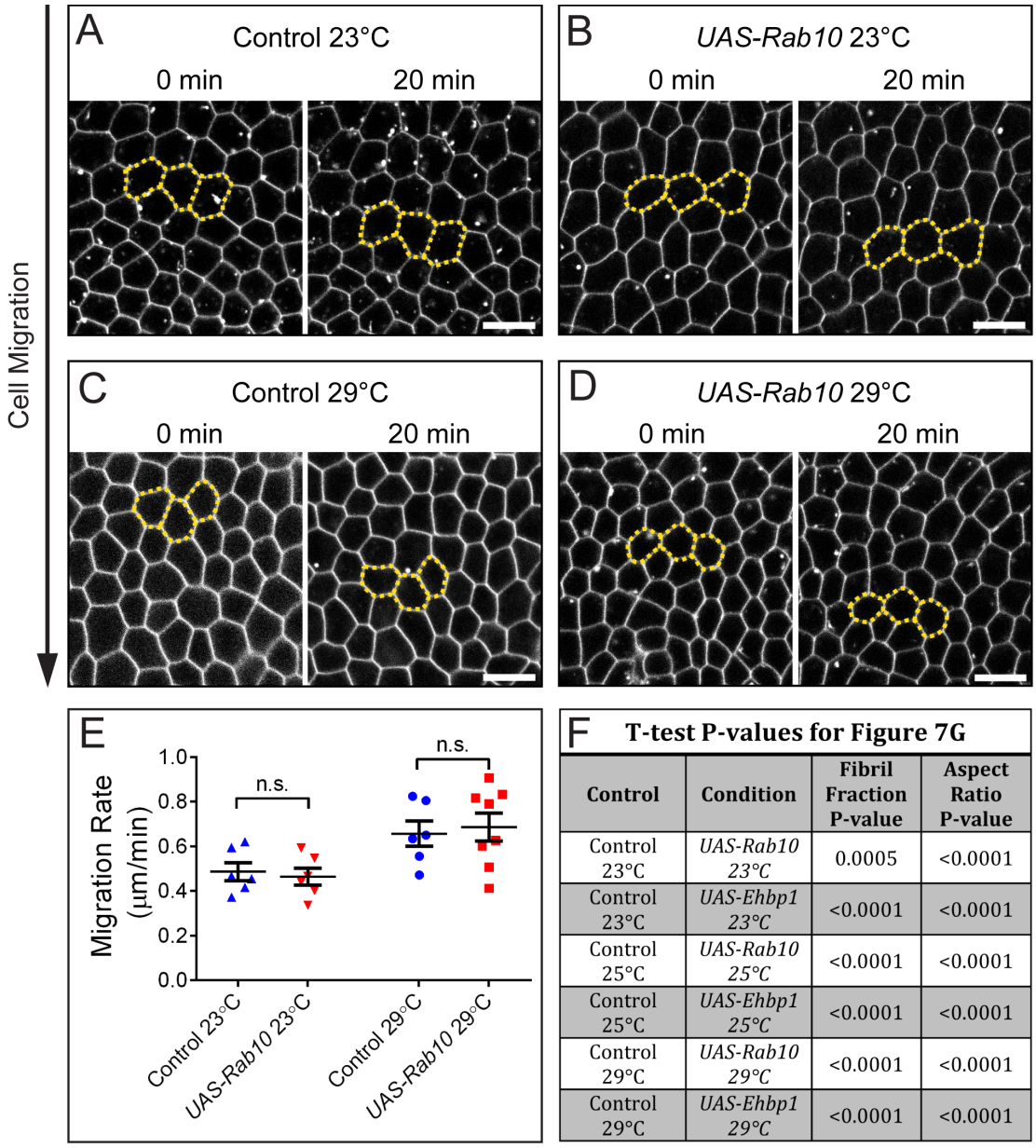

F **T-test P-values for Figure 7G**

Control	Condition	Fibril Fraction P-value	Aspect Ratio P-value
Control 23°C	*UAS-Rab10 23°C*	0.0005	<0.0001
Control 23°C	*UAS-Ehbp1 23°C*	<0.0001	<0.0001
Control 25°C	*UAS-Rab10 25°C*	<0.0001	<0.0001
Control 25°C	*UAS-Ehbp1 25°C*	<0.0001	<0.0001
Control 29°C	*UAS-Rab10 29°C*	<0.0001	<0.0001
Control 29°C	*UAS-Ehbp1 29°C*	<0.0001	<0.0001

Figure 3.13. BM fibril fraction affects elongation but not epithelial migration
(A-E) Follicle cell migration rates are not affected by increasing the fibril fraction in the BM, either under conditions that increase the egg's aspect ratio (*UAS-Rab10* 23°C) or decrease the egg's aspect ratio (*UAS-Rab10* 29°C). (A-D) First and last frames from a representative movie for each condition, showing follicle cell migration. Yellow outlines indicate the same cells over time. Cell migration direction is down. Scale bars = 10 µm. (E) Quantification of follicle cell migration rates for the conditions shown in (A-D). Differences in migration rates between 23°C and 29°C controls may indicate that temperature influences migration rates. Data represent mean ± s.e.m. t-test: n.s. = P>0.05. (F) T-test results for fibril fraction and aspect ratio data reported in Figure 7G. All conditions exhibit significantly different aspect ratios and fibril fractions relative to their respective controls. (A-E) Experiments performed at stage 7.

space. Alternatively, tension placed on a globule during the deposition process by the migrating cells may cause its elongation, similar to pulling two sides of a cotton ball in opposite directions. In either case, the model that emerges is that BM fibril formation occurs through a series of seemingly disordered events that, through bulk action, produce a robustly polarized matrix.

Although nascent fibril deposition appears to be the main way that the follicular BM becomes polarized, other mechanisms may contribute to this process. Although impeding collective follicle cell migration blocks the fibril formation, the resulting BMs still exhibit small, aligned ridges that tend to be oriented in the same direction as the actin bundles at the basal surface of each adjacent follicle cell. A seemingly similar phenomenon was also recently reported by another group (Aurich and Dahmann, 2016). Because the actin bundles are contractile elements that interact with the BM through integrin-based adhesions (Bateman et al., 2001; Cetera et al., 2014; Delon and Brown, 2009), these ridges could form via physical deformation of the planar matrix. Whether such a mechanism contributes to BM polarity under wild-type conditions is currently unclear, although it could produce the small-scale alignment we observed by EM.

We found that Rab10 and its putative effector Ehbp1 promote BM fibril formation. We previously showed that Rab10 prevents improper sorting of BM proteins into an apically-directed secretory pathway (Lerner et al., 2013). Our data now suggest that Rab10 may perform this function, in part, by targeting BM proteins to a basal region of the lateral plasma membrane for secretion. In support of this notion, Rab10 accumulates on lateral membranes and its over-expression increases the amount of BM proteins in the pericellular space. Work from other systems has shown that Rab10 localizes to exocytic vesicles bound for a basal region of the lateral plasma membrane (Cao et al., 2008), and that this protein functions with the exocyst to

control the docking of exocytic vesicles at the cell surface (Babbey et al., 2010; Sano et al., 2015; Taylor et al., 2015; Zou et al., 2015). Altogether, these data suggest a model wherein Rab10 promotes BM fibril formation by determining the location where new BM proteins exit the cell.

Our data further suggest that Rab10 functions in competitive balance with a second BM secretion pathway. New BM material is deposited into the planar matrix at the same time that fibrils are generated. That Rab10 (or Ehbp1) over-expression can increase pericellular BM protein accumulation and fibril formation without altering bulk protein levels in the BM indicates that a portion of BM proteins – likely those bound for the planar matrix – are normally secreted via a different pathway. We propose that there may be two distinct pathways for BM deposition – one directed to the basal surface for planar matrix assembly and one directed to the lateral surface for fibril formation (Figure 3.12 H). This model offers a simple mechanism to control the allocation of BM proteins into distinct populations by tuning activity levels of the two pathways.

What sets the developmental timing of BM fibril formation remains an open question. Although this process coincides with increased Col IV incorporation into the BM (Haigo and Bilder, 2011b), this does not appear to be the initiating factor, as we have previously shown that abrogating this increase does not inhibit BM fibril formation (Isabella and Horne-Badovinac, 2015b). Instead, because this phenomenon coincides with an increase in Rab10 expression and is sensitive to Rab10 levels, we propose that a regulated increase in Rab10 pathway activity may specify both the timing and extent of fibril formation; however, future work is required to test this hypothesis.

It has been speculated that polarization of the follicular BM allows it to function as a molecular corset for egg chamber elongation (Gutzeit et al., 1991). In this model, the aligned fibrils provide an anisotropic constraining force that channels egg chamber growth along the A-P axis. Our finding that a modest increase in fibril formation enhances elongation supports this idea. It is becoming increasingly clear, however, that fibril formation is only one of many structural changes that must occur in the BM for it to exert this corset function. For example, we recently showed that a temporally regulated increase in Col IV levels and concomitant decrease in Perlecan levels are also necessary for proper egg chamber elongation (Isabella and Horne-Badovinac, 2015b). Moreover, we have found that BM architecture influences egg chamber shape beyond the active elongation phase. When the fibril fraction in the BM exceeds 37%, egg chambers elongate normally, but this matrix can no longer maintain the elongated state. We envision that this failure is due not to increased fibril formation per se, but to a global weakening of the BM caused by the accompanying depletion of the planar matrix. This idea is consistent with previous work showing that collagenase-mediated digestion of the BM causes the egg chamber to round up during this maintenance phase (Haigo and Bilder, 2011b). Altogether, these observations suggest that the ways in which the follicular BM influences the shape of the egg are complex, and that there is still much to be learned about this process.

To our knowledge, a polarized BM structure akin to that of the follicular BM has not been seen outside of insects, although there is currently very little data describing *in vivo* BM architecture with sufficient detail to reveal such structure. However, the fibrillar BM is one instance of what appears to be a common strategy of using a surrounding ECM to provide a stabilizing/constraining force during morphogenesis. For instance, the developing *Xenopus* notochord is ensheathed by an oriented network of Collagen fibrils that channel its elongation

along the A-P axis (Adams et al., 1990). Additionally, thickening of the BM around epithelial ducts in mouse mammary and salivary glands is believed to stabilize these structures (Fata et al., 2004; Harunaga et al., 2014); whether these BMs also exhibit circumferential polarity has not been examined. Further understanding the roles of BMs in morphogenesis will require detailed examination of BM structure in other tissues.

In conclusion, this work highlights how coordinated tissue behaviors – in this case regulated protein secretion and tissue movement – can synergize to remodel BM architecture during development, and how matrix remodeling can play an active role in tissue morphogenesis.

3.6 METHODS

Drosophila genetics

Experimental genotypes are in supplemental experimental procedures. Experimental crosses were raised at 25°C and females aged on yeast for 3 days at 29°C with exceptions listed in supplemental experimental procedures. UAS transgenes were driven with *traffic jam-Gal4* or *traffic jam-Gal4, Mef2.mb247-Gal80* for follicle cell expression or *hs-Flp;Act5c>>Gal4* for FLP-out. FLP-out was induced by 37°C heat shock for 1 hour, twice daily for 3 days on yeast with intermittent periods at 25°C. Mitotic clones were generated using *FRT80B* or *FRT40A* and *e22c-Gal4* or *T155-Gal4*, respectively, to drive *UAS-Flp* expression. Most lines were obtained from the Bloomington *Drosophila* stock center except: *nls-mRFP, vkg, FRT40* is from (Haigo and Bilder, 2011b). *vkg-GFP* and *Trol-GFP* are from Flytrap (Buszczak et al., 2007). *abi RNAi* and *traffic jam-Gal4* are from the *Drosophila* Genetic Resource Center (Kyoto Institute of Technology, Kyoto, Japan). $fat2^{N103\text{-}2}$ is from (Horne-Badovinac et al., 2012). *UAS-flag-Rab10 and UAS-RFP-Rab10* are from this study. *Mef2.mb247-Gal80* was a gift from Martin

Heisenberg. Endogenous *YFP-Rab10* is from (Dunst et al., 2015). *UAS-flag-Ehbp1* is from (Giagtzoglou et al., 2012). *LanB1-GFP* (Sarov et al., 2016) and *UAS-Ehbp1 RNAi* are from Vienna *Drosophila* Resource center (Vienna, Austria). *UAS-Crag* is from (Denef et al., 2008).

Table 3.1. Experimental Genotypes

Figure	Panel	Genotype
3.1	C	*w; traffic jam-Gal4, vkg-GFP/+*
3.3	A	*w; traffic jam-Gal4, vkg-GFP*
	B	*w; traffic jam-Gal4, vkg-GFP; UAS-mCD8-RFP/+*
3.4	A	*w; traffic jam-Gal4, vkg-GFP*
	B	*w; traffic jam-Gal4, vkg-GFP/+; UAS-mCD8-RFP/+*
	C D	*w; traffic jam-Gal4, vkg-GFP*
	E F	*w; traffic jam-Gal4; LanB1-GFP*
3.5	A B C	*w; traffic jam-Gal4, vkg-GFP/+; UAS-mCD8-RFP/+*
	D	*w; traffic jam-Gal4, vkg-GFP/+*
	E G	*w; traffic jam-Gal4, vkg-GFP/+*
	F H	*w; e22c-Gal4, UAS-Flp/vkg-GFP; msn^{102}, FRT80/ubi-eGFP, FRT80*
	I J	*w; traffic jam-Gal4, vkg-GFP*
3.6	A	*w; nls-mRFP, vkg-GFP, FRT40A/FRT40A; T155-Gal4, UAS-Flp/+*
	B	*w; e22c-Gal4, UAS-Flp/vkg-GFP; $fat2^{N103-2}$, FRT80/ubi-eGFP, FRT80*
	C	*w; traffic jam-Gal4, vkg-GFP/+; UAS-abi $RNAi^{NIG9749R-3}$/+*
	D	*w; e22c-Gal4, UAS-Flp/vkg-GFP; msn^{102}, FRT80/ubi-eGFP, FRT80*
	E F	*w; traffic jam-Gal4, vkg-GFP*
3.7	A	*w; traffic jam-Gal4, Mef2.mb247-Gal80/UAS-RFP-Rab10*
	B	*YFP-Rab10;;*
	C D	*hsflp/+; vkg-GFP/+; act5c>>Gal4, UAS-RFP/UAS-flag-Rab10*
	E	*w; traffic jam-Gal4, vkg-GFP/+*
	F	*w; traffic jam-Gal4, vkg-GFP/UAS-RFP-Rab10*
	G H I J	*w; traffic jam-Gal4, vkg-GFP/+*
		w; traffic jam-Gal4, vkg-GFP/UAS-RFP-Rab10
3.8	A B	*YFP-Rab10;;*
	C	*w; traffic jam-Gal4, vkg-GFP/+*
	D F	*w^{1118}; ;*
	E F	*; vkg-GFP;*
	G J	*w; traffic jam-Gal4, vkg-GFP/+*
	H J	*w; traffic jam-Gal4, vkg-GFP/+; UAS-RFP-Rab10/+*
	I J	*w; traffic jam-Gal4, vkg-GFP/UAS-HA-Crag A-46; UAS-RFP-Rab10/+*
3.9	A B	*w; traffic jam-Gal4/+; LanB1-GFP/+*
	C E F	*w; traffic jam-Gal4/+; LanB1-GFP/+*
	D E F	*w; traffic jam-Gal4/UAS-RFP-Rab10; LanB1-GFP/+*
	G I J	*trol-GFP/+; traffic jam-Gal4/+*

Table 3.1. Experimental Genotypes, Continued

Figure	Panel	Genotype
3.9	H I J	*trol-GFP/+; traffic jam-Gal4/UAS-RFP-Rab10*
	K	*w; traffic jam-Gal4, vkg-GFP*
3.11	A	*w; traffic jam-Gal4, vkg-GFP/+*
	B G	*w; traffic jam-Gal4, vkg-GFP/+; UAS-flag-Ehbp1/+*
	C D	*w; traffic jam-Gal4, vkg-GFP/+* *w; traffic jam-Gal4, vkg-GFP/+; UAS-flag-Ehbp1/+*
	E F	*hsflp/+; vkg-GFP/+; act5c>>Gal4, UAS-RFP/UAS-flag-Ehbp1*
3.10	A	*w; traffic jam-Gal4, vkg-GFP/+* *w; traffic jam-Gal4, vkg-GFP/UAS-RFP-Rab10* *w; traffic jam-Gal4, vkg-GFP/+; UAS-flag-Ehbp1/+*
	B	*w; traffic jam-Gal4, vkg-GFP/+*
	C	*w; traffic jam-Gal4, vkg-GFP/+; UAS-Rab10 RNAi$^{TRiP.JF02058}$/+*
	D	*w; traffic jam-Gal4, vkg-GFP/UAS-Ehbp1 RNAi^{v109413}*
	E	*w; traffic jam-Gal4, vkg-GFP/+* *w; traffic jam-Gal4, vkg-GFP/+; UAS-flag-Ehbp1/+*
3.12	A	*w; traffic jam-Gal4, Mef2.mb247-Gal80/+* *w; traffic jam-Gal4, Mef2.mb247-Gal80/UAS-RFP-Rab10*
	B D	*w; traffic jam-Gal4, Mef2.mb247-Gal80/+*
	C	*w; traffic jam-Gal4, Mef2.mb247-Gal80/UAS-RFP-Rab10*
	E	*w; traffic jam-Gal4, Mef2.mb247-Gal80/+; UAS-flag-Ehbp1/+*
	F	*w; traffic jam-Gal4, Mef2.mb247-Gal80/+* *w; traffic jam-Gal4, Mef2.mb247-Gal80/+; UAS-flag-Ehbp1/+*
	G (X-axis)	*w; traffic jam-Gal4, vkg-GFP/+* *w; traffic jam-Gal4, vkg-GFP/UAS-RFP-Rab10* *w; traffic jam-Gal4, vkg-GFP/+; UAS-flag-Ehbp1/+*
	G (Y-axis)	*w; traffic jam-Gal4, Mef2.mb247-Gal80/+* *w; traffic jam-Gal4, Mef2.mb247-Gal80/UAS-RFP-Rab10* *w; traffic jam-Gal4, Mef2.mb247-Gal80/+; UAS-flag-Ehbp1/+*
3.13	A C E	*w; traffic jam-Gal4, vkg-GFP/+ OR w; traffic jam-Gal4, vkg-GFP/+; UAS-mCD8-RFP/+*
	B D E	*w; traffic jam-Gal4,vkg-GFP/UAS-RFP-Rab10 OR w; traffic jam-Gal4/UAS-RFP-Rab10; UAS-mCD8-RFP/+*

Table 3.2. Experimental conditions

For most experiments, females were aged on yeast for 3 days at 29°C. Experiments using different conditions are detailed here.

Figure	Panels	Females on yeast	
		Temp	No. days
3.5	A B C	25	3
3.5	I J	25	3
3.6	A E F	25	3
3.6	B C	25	4
3.7	A B	25	3
3.8	A B D E F	25	3
3.9	A B	25	4
3.9	K	29	2
3.10	A	variable, noted in Figure	3
3.12	A B C	23	3
3.12	G	variable, noted in Figure	3
3.13	A B C D E F	variable, noted in Figure	3

Staining and microscopy

Ovaries were dissected in S2 medium and fixed for 15 minutes in PBS + 0.1% Triton (PBT) + 4% EM-grade formaldehyde (Polysciences), then separated from the muscle sheath by gentle pipetting. Antibody stains were performed in PBT and detected with Alexa Fluor-conjugated secondary antibodies (1:200, Invitrogen). Actin was labeled with TRITC-Phalloidin (1:200, Sigma) or Alexa-647 Phalloidin (1:50, Invitrogen), and nuclei labeled with DAPI (1:1000, Sigma). For non-permeabilized stains, ovarioles were dissected from the muscle sheath in S2 medium and fixed for 6 minutes in PBS + 4% EM-grade formaldehyde. GFP antibody stains were performed as above using PBS instead of PBT. Antibodies used: guinea pig α-Laminin (1:400) (Harpaz and Volk, 2012), rabbit α-Trol (1:1000) (Friedrich et al., 2000), rabbit α-GFP (1:200, Molecular Probes A21311 and A31852). Fluorescent images were obtained using Zeiss LSM 510 or LSM 880 confocal microscopes. Images for stage 14 aspect ratios were obtained

using a Leica DM550B microscope with a Leica DFC425C camera. Image processing and custom image analysis were performed using ImageJ and Python. For 3D reconstructions, confocal Z-stacks were deconvolved (Huygens) and 3D images made in Imaris (Bitplane). Graphing and statistical analysis were performed in Prism (GraphPad). For all graphs, error is presented as mean ± s.e.m. and statistical differences between conditions were determined with 2-tailed, unpaired t-tests.

Live imaging

Live imaging was performed as described (Prasad et al., 2007), with the following modifications. Dissected egg chambers were placed on a pad of 0.4% NuSieve GTG low melt agarose (Lonza) in live imaging medium, and follicle cell membranes marked with CellMask (1:1000, Molecular Probes) or *UAS-mCD8-RFP*. The coverslip was cushioned with vacuum grease at each corner. For confocal imaging of BM fibril formation, a region of the Col IV-GFP in the BM was photobleached with a 488nm laser at 100% power for 10 iterations, 10 minutes prior to imaging. TIRF movies were taken on an Olympus IX-50 microscope equipped with an iXon EMCCD camera (Andor) and a 100x objective fitted with through-the-objective TIRF illumination. TIRF photobleaching was achieved by exposing the BM to the 488nm TIRF laser at 50% power for ~2 minutes, 10-15 minutes before imaging. Movies were processed using ImageJ.

Platinum replica electron microscopy

To decellularize the follicular BM, egg chambers were dissected as for live imaging in HL3.1 (70mM NaCl, 5mM KCl, 1.5mM CaCl, 4mM $MgCl_2$, 10mM $NaHCO_3$, 5mM trehalose, 115mM sucrose, 5mM HEPES), adhered to poly-lysine (Sigma) coated slides, incubated 10-20 minutes

in PBT, sonicated, and washed in PBS. BMs were then prepared for EM using the protocol in (Svitkina, 2009). Briefly, BMs were fixed with 2% Glutaraldehyde (Electron Microscopy Sciences), tannic acid, and uranyl acetate; critical point dried; coated with platinum and carbon; and transferred onto EM grids for observation. Samples were imaged using a FEI Tecnai Spirit G2 transmission electron microscope (FEI Company, Hillsboro, OR) operated at 80 kV. Images were captured by Eagle 4k HR 200kV CCD camera and presented in inverted contrast.

Production of* UAS-RFP-Rab10 *and* UAS-Flag-Rab10 *transgenic flies

The Rab10 coding sequence was PCR-amplified from genomic DNA isolated from ;*UAS-YFP-Rab10;* flies (Zhang et al., 2006). The PCR product was gel extracted, digested with BamHI and Xhol and cloned into the Gateway pENTR3C Dual Selection Entry Vector (Invitrogen). It was then recombined (LR clonase reaction, Invitrogen) into pTRW (uasT promoter, N-terminal mRFP tag) or pTFW (uasT promoter, N-terminal 3xFLAG tag) (Carnegie *Drosophila* Gateway Vector Collection). Transgenic flies were generated via P-element-mediated transformation (Best Gene).

Measurement of Pericellular Col IV-GFP intensity

Confocal sections were acquired 1-1.5 μm apical of the BM. For wild-type measurements, 5 cells/egg chamber (n = 8 egg chambers/stage) were randomly selected for analysis. When measuring the effect of transgene expression on pericellular signal, experiments were performed in mosaic epithelia via FLP-out, allowing us to collect data for the control and experimental condition from the same tissues. In this case, 1-10 cells of each genotype/egg chamber (n = 20 egg chambers (Ehbp1), 27 egg chambers (Rab10)) were randomly selected for analysis. The

edges of each cell were manually outlined with 3 pixel-thick lines; mean intensity of all pixels contained within the line was measured. For each cell, background fluorescence values were measured over cell centers and subtracted from outline intensity. All images were acquired with the same settings.

Measurement of fibril fraction and BM fluorescence intensity

A confocal section capturing the entire thickness of the BM was acquired. All images were obtained at the same settings. Because the BM generally did not take up the entire imaging frame, the largest possible representative rectangle was cropped to remove background pixels. Mean intensity of all pixels in the cropped image was measured to determine overall GFP intensity. Pixels contained within fibrils were isolated by successive intensity and size thresholds. To determine appropriate thresholding parameters, 10 Col IV-GFP BMs from each of the control, *UAS-Rab10,* and *UAS-Ehbp1* conditions were manually thresholded by eye to maximally include fibrils and exclude the planar matrix. A conservative threshold was used to ensure exclusion of all non-fibrillar pixels, meaning our analysis likely underestimates the fibril fraction. By analyzing our by-eye thresholds, we found that we consistently applied an intensity cutoff corresponding to 1.35x the median image intensity independently for all conditions, and used this value for subsequent analysis. We then applied an object size threshold of 20 pixels to remove image noise. Using custom Python and ImageJ scripts, we applied these thresholds to all experimental images to isolate pixels within fibrils and, inversely, in the planar matrix. Fibril fraction was measured by dividing the sum intensity of all fibrillar pixels by the sum intensity of all pixels in the image. Planar fraction was measured by dividing the sum intensity of all non-fibrillar pixels by the sum intensity of all pixels in the image. By definition, fibril fraction +

planar fraction = 100%. This method was used for analysis of Col IV-GFP, Laminin-GFP, and Perlecan-GFP egg chambers.

Measurement of maximum fibril length

In each of 10 cropped images/condition from our fibril fraction analysis, length of the 10 longest fibrils was manually measured in ImageJ.

Measurement of Rab10 protein levels

In central transverse sections of stage 3-8 egg chambers with endogenously tagged YFP-Rab10, the entire epithelium of each egg chamber was manually outlined and its mean fluorescence intensity measured in ImageJ. All images were acquired with the same settings.

Measurement of egg chamber aspect ratios

In central transverse sections, egg chamber length (anterior to posterior tip) and width (widest region perpendicular to anterior-posterior axis) were measured, and ratio of length:width was calculated. Dorsal appendages were excluded from measurements.

Measurement of follicle cell migration rates

20 minute time-lapse movies were acquired from egg chambers labeled with CellMask or *UAS-mCD8-RFP*. The leading edge of a single follicle cell was marked at the start and end of the movie and distance traveled was measured and divided by movie length (minutes). Three distant cells were measured and their rates averaged for each egg chamber.

CHAPTER 4: PLANAR POLARIZED SECRETION OF BASEMENT MEMBRANE PROTEINS DURING COLLECTIVE CELL MIGRATION IN THE *DROSOPHILA* EGG CHAMBER

4.1 PREFACE

This chapter is unpublished work examining the precise site of Rab10-dependent basement membrane protein secretion. This project is a direct continuation of, and was largely carried out in conjunction with, the work presented in Chapter 3.

4.2 INTRODUCTION

It has long been known that BM proteins accumulate specifically on the basal side of epithelial tissues, indicating that mechanisms exist to ensure polarized trafficking of this material. There is growing knowledge about how polarized BM trafficking is controlled, as several factors required to prevent secretion of BM proteins to the apical cell surface – most notably Rab10 (Lerner et al., 2013) – have been identified. It has generally been assumed that BM proteins are secreted through the basal cell surface, although to my knowledge the actual site of BM protein exocytosis has not been identified in any system. Further, my previous work on Rab10 has challenged current assumptions regarding BM protein secretion, as it suggests that these proteins can also be secreted through the lateral cell surface (see chapter 3). Thus, understanding polarized BM protein secretion will be facilitated by identifying the precise site at which BM proteins exit the cell, and how they are targeted to this location.

An additional consideration regarding polarized secretion is that cells in the follicular epithelium are polarized along two axes. Like all epithelia, follicle cells exhibit apical-basal

polarity. These cells, which migrate along the BM, also exhibit planar polarization at their basal surfaces, oriented orthogonally to the apical-basal axis, with distinct leading and trailing edges. Notably, Rab10 exhibits polarization along both of these axes. It is predominantly localized to the basal region of the cell, and the population of Rab10 present near the basal surface, which we speculated may represent the BM protein sorting population, is polarized along the epithelium's planar axis, localizing to the trailing edge of each cell (Lerner et al., 2013). This raises the possibility that Rab10-mediated BM protein secretion is also directed along the planar axis, although the exact site of BM protein secretion, and the functional implications of such a targeting scheme, remains unknown.

In this section, I will describe my work to identify the site of Rab10-dependent BM protein secretion. I have identified two factors – the exocyst complex and the putative Rab10 GTPase activating protein (GAP) Evi5 – that appear to regulate a late stage of BM vesicle exocytosis at the cell surface. Manipulating these components induces intracellular accumulation of BM proteins at a site that is constrained along the apical-basal and planar axes; I propose a preliminary model in which Rab10-dependent BM protein trafficking is regulated along both major epithelial axes.

4.3 RESULTS

Exocyst knockdown stalls BM protein secretion at the lateral plasma membrane

The exocyst is an octameric protein complex that mediates tethering of exocytic vesicles with the plasma membrane (He and Guo, 2009). It has been shown to function with Rab10 in multiple contexts (Babbey et al., 2010; Sano et al., 2015; Taylor et al., 2015; Zou et al., 2015). Consistent with these observations, I found that the exocyst component Sec15 co-localizes with Rab10.

This co-localization can be seen on both punctate compartments in the basal cytoplasm and on the lateral plasma membrane (Figure 4.1 A-B). Further, knockdown of the exocyst component Exo84 causes intracellular accumulation of the Rab10 cargo Col IV-GFP (Figure 4.1 C-D), suggesting a defect in secretion of this protein. This Col IV-GFP accumulation shows a specific and very intriguing pattern. In addition to the large punctae that are visible in control cells and likely represent protein in the ER, in the *Exo84 RNAi* condition Col IV-GFP can be seen just inside the lateral plasma membrane near the basal surface, often in the form of small punctae (Figure 4.1 C-D). Because these punctae are small, intracellular, and located near the membrane region that I had previously proposed as the site of Rab10-mediated BM protein secretion, they most likely represent Col IV-containing exocytic vesicles that have stalled at their docking site on the plasma membrane. Although more work is required to confirm these findings, these data suggest a model in which the exocyst functions with Rab10 to promote docking of BM protein-containing vesicles at a basal region of the lateral plasma membrane.

Evi5 over-expression stalls BM protein secretion at the trailing lateral plasma membrane

To further examine this model, I sought to replicate these results by locally disrupting Rab10 activity. Rab GTPases are inactivated by GAPs. The Tre-2/Bub2/Cdc16 (TBC) domain-containing protein Evi5 exhibits GAP activity towards Rab10 in mice (Itoh et al., 2006). Consistent with this relationship, I found that RNAi-mediated knockdown of *Evi5* phenocopies Rab10 hyper-activation – it enhances pericellular Col IV-GFP accumulation and fibril formation in the follicular BM (Figure 4.2 A-E). Evi5 additionally exhibits the same localization as Rab10 and the exocyst (Figure 4.2 F-G). I then asked what happens upon over-expression of *Evi5*. This condition does not appear to globally decrease Rab10 activity in the cells, as it does not result in

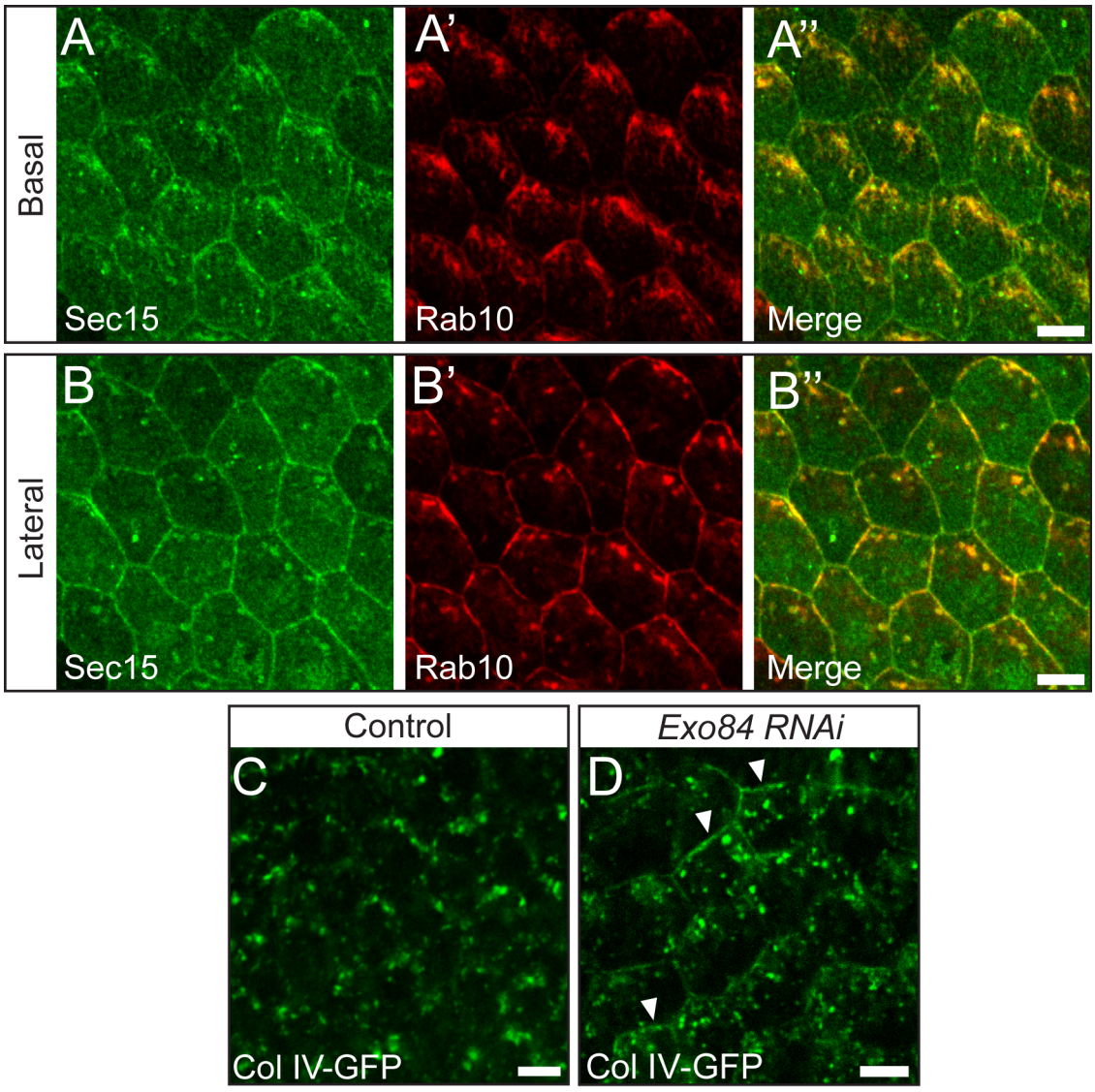

Figure 4.1. Exocyst knockdown stalls BM protein secretion at the lateral plasma membrane (A-B) The exocyst protein Sec15 co-localizes with Rab10 in the follicle cells. Co-localization can be seen on planar polarized compartments in the basal cytoplasm (A) and on the lateral plasma membrane (B). Images are Sec15-GFP and Rab10-RFP proteins produced from *UAS* transgenes. (C) In a focal plane 1-2 µm apical from the basal surface (lateral plane), Col IV-GFP can be seen in intracellular punctae in control egg chambers. (D) In a lateral focal plane, *RNAi* knockdown of the exocyst component *Exo84* causes aberrant accumulation of Col IV-GFP on the lateral plasma membrane. (A-D) Scale bars = 5 µm. Experiments performed at stage 8.

the apical Col IV-GFP accumulation seen upon Rab10 knockdown (Figure 4.2 H-I). However, like *Exo84 RNAi, Evi5* over-expression causes accumulation of Col IV-GFP punctae just inside a basal region of the lateral plasma membrane (Figure 4.2 J-K). It is likely that, in this condition,

premature inactivation of Rab10 is responsible for stalled Col IV-GFP secretion. These findings are consistent with my exocyst data, and strengthen the model that Rab10 and the exocyst function together to promote BM protein secretion at a basal region of the lateral plasma membrane.

Having identified conditions that appear to stall BM protein secretion at the site of exocytosis allows for a precise examination of where these proteins exit the cell. I observed accumulation of Col IV-GFP vesicles on lateral membranes within 1-2 μm of the basal surface. The lab's previous observation that Rab10 exhibits planar-polarized localization to the trailing edge of each follicle cell led us to hypothesize that BM protein secretion may also be planar polarized. By clonally over-expressing *Evi5*, I observed that the Col IV-GFP puntae that accumulate inside the cell are specifically enriched at the trailing edge of each follicle cell (Figure 4.2 L). These observations suggest that the site of BM protein secretion may also be regulated along the planar cell axis.

4.4 DISCUSSION

In this chapter, I have identified the exocyst and the putative Rab10 GAP Evi5 as factors that regulate BM protein secretion. Manipulating these components - specifically knocking down the exocyst and over-expressing Evi5 - induces intracellular accumulation of Col IV-GFP at a basal region of the trailing lateral plasma membrane. Based on these results, I propose the following model: Rab10 targets BM protein-containing vesicles to this membrane region for secretion, where it interacts with the exocyst to promote vesicle tethering; Evi5 then inactivates Rab10 at this site to promote its recycling. These data suggest that BM protein secretion is regulated along both the apical-basal and planar axes.

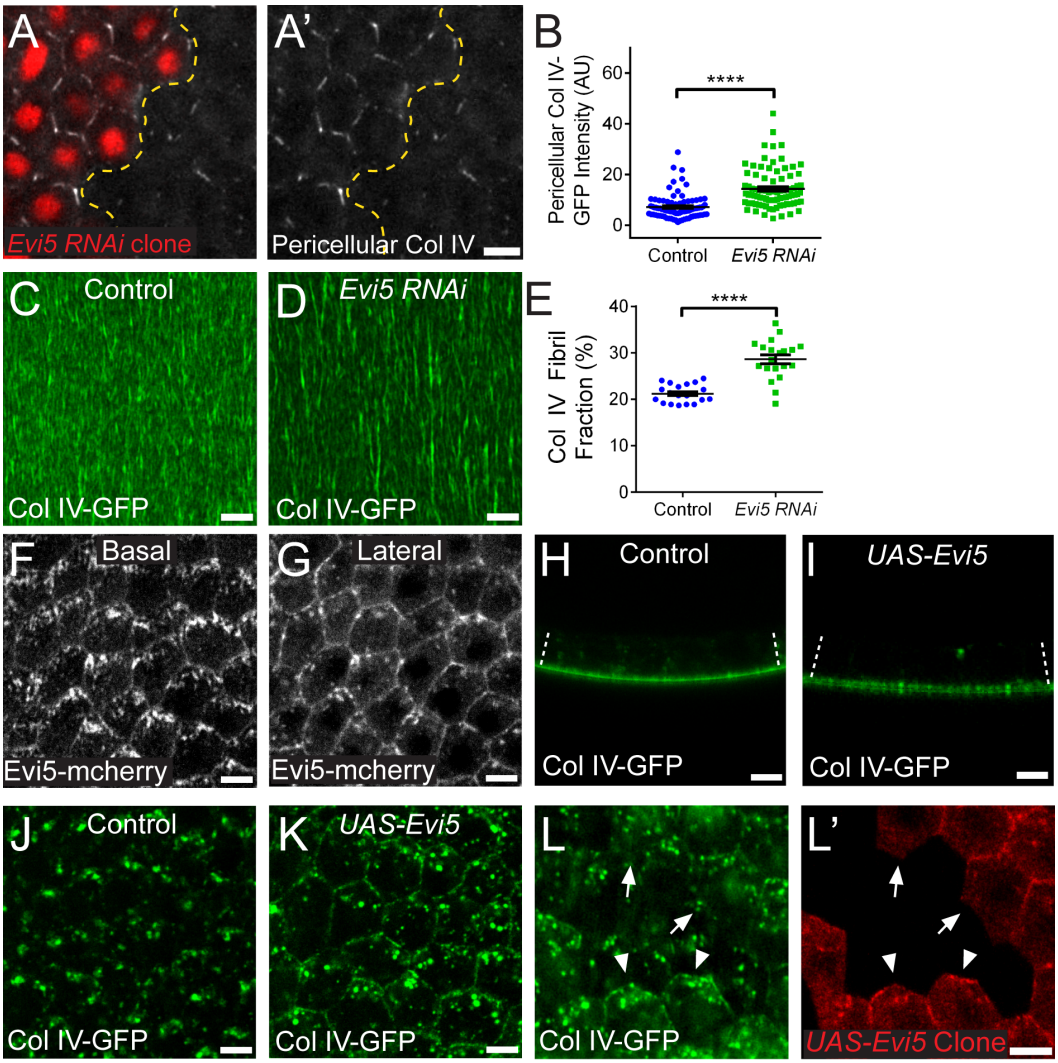

Figure 4.2. Evi5 over-expression stalls BM protein secretion at the trailing lateral plasma membrane

(A) Representative image showing that clonal *Evi5 RNAi* expression (red cells) increases pericellular Col IV relative to neighboring wild-type cells. Yellow line indicates clone boundary. (B) Quantification of the condition shown in (A). (C-D) *Evi5 RNAi* expression increases fibril formation in the BM. (E) *Evi5 RNAi* expression increases the BM fibril fraction. (B and E) Data represent mean ± s.e.m. t-test: **** = P<0.0001. (F-G) Evi5 localizes to planar polarized compartments in the basal cytoplasm (F) and to the lateral plasma membrane (G). Images represent Evi5-mcherry protein produced from a *UAS* transgene. (H-I) *Evi5 RNAi* expression does not disrupt polarized trafficking of Col IV-GFP along the apical-basal axis. The epithelium is oriented with the apical surface up. Dotted lines indicate the apical-basal axis. (J) In a focal plane 1-2 µm apical from the basal surface, Col IV-GFP can be seen in intracellular punctae in control egg chambers. (K) In a lateral focal plane, *RNAi* knockdown of *Evi5* causes aberrant punctate accumulation of Col IV-GFP on the lateral plasma membrane. (L) Mosaic over-expression of *Evi5* (red cells) reveals that this condition causes aberrant punctate accumulation of Col IV-GFP at the trailing edges of follicle cells (arrowheads) but not at the leading edges (arrows). Scale bars = 5 µm. Experiments performed at stage 8.

While my data are consistent with this preliminary model, further work will be required to confirm it. Most importantly, electron microscopy will be needed to show that the Col IV-GFP accumulation I observe represents an accumulation of secretory vesicles near the plasma membrane; immuno-EM could also confirm the presence of Rab10 and Col IV on and in these vesicles, respectively. It will also be important to carry out biochemical experiments to confirm my proposed protein interactions – does active Rab10 bind to an exocyst component? Does Evi5 function specifically as a Rab10 GAP in this system? The latter question is especially important. Evi5 has also been shown to act as a GAP for Rab11 in *Drosophila* (Laflamme et al., 2012). Additionally, I have observed that Rab8 shows similar localization to Rab10 in this system and may play some role in BM protein secretion. Although the function of Rab8 is unclear, the manipulations described here could also affect Rab8 function, requiring that it be considered as well.

The functional implications of such precise control over where BM proteins exit the cell are not clear. The need to prevent apical secretion of these proteins is clear, as BMs are not assembled on the apical surface. I also previously found that secretion to the lateral membrane is a regulated event that allows for generation of fibrils in the follicular BM. However, the importance of polarizing secretion along the planar axis, if any, is not obvious. Narrowing the secretion site could serve to increase the local concentration of BM proteins in the pericellular space, thus promoting polymerization of this material into fibrils; however, pericellular Col IV-GFP does not exhibit planar polarized localization (data not shown), suggesting that it quickly diffuses around the cells upon secretion. It is possible that planar polarized secretion is dispensable for BM proteins, but important for some other Rab10 cargo. It will therefore be

important to identify other proteins trafficked through the Rab10 pathway and determine whether they exhibit planar polarized localization and function.

It is also unclear how vesicles would be trafficked specifically to this site. Planar polarity at the basal follicle cell surface appears to be highly dependent on follicle cell migration, which aligns actin and microtubule bundles at the basal surface in the direction of cell migration (Cetera and Horne-Badovinac, 2015; Viktorinová and Dahmann, 2013). In the follicle cells, microtubules near the basal epithelial surface show a biased orientation, with their plus ends towards the trailing edge (Viktorinová and Dahmann, 2013). Therefore, association with a plus end-directed motor could promote transport of Rab10 vesicles to the trailing edge. Preliminary data from Allison Zajac, a postdoc in the lab, suggests that Rab10-positive compartments are indeed trafficked on microtubules near the basal surface. It will be interesting to further examine whether Rab10 vesicles exhibit directional transport on microtubules; identification of such a transport mechanism could also lead to the discovery of additional components that exhibit planar polarized localization, as a large amount of intracellular trafficking occurs on microtubules.

Finally, this study also elucidates additional aspects of the Rab10 pathway. Our previous work suggested that Rab10 functions in post-Golgi trafficking of BM proteins, to ensure that they are sorted away from an apically-directed pathway (Lerner et al., 2013). I also identified a role for Rab10 in targeting BM protein secretion to a basal region of the lateral plasma membrane for secretion. It now appears that Rab10 activity may be required for docking of vesicles at the plasma membrane as well, likely in coordination with the exocyst complex. Thus, Rab10 may act at every major step of the trafficking process.

4.5 METHODS

Drosophila genetics

Experimental genotypes are in table 4.1. Experimental crosses were raised at 25°C and females aged on yeast for 3 days at 29°C. FLP-out was induced by 37°C heat shock for 1 hour, twice daily for 3 days on yeast with intermittent periods at 25°C. Most lines were obtained from the Bloomington *Drosophila* stock center except: *UAS-evi5 RNAi* is from the Vienna *Drosophila* resource center (Vienna, Austria). *UAS-evi5-mCherry* is from (Laflamme et al., 2012). *Traffic jam-Gal4* is from the *Drosophila* Genetic Resource Center (Kyoto Institute of Technology, Kyoto, Japan). *vkg-GFP* is from Flytrap (Buszczak et al., 2007). For RFP-Rab10, see section 3.6.

Table 4.1 Experimental Genotypes

Figure	Panel	Genotype
4.1	A B	*w; traffic jam-Gal4, mb247-Gal80/UAS-sec15-GFP; UAS-RFP-Rab10/+*
	C	*w; traffic jam-Gal4, vkg-GFP/+*
	D	*w; traffic jam-Gal4, vkg-GFP/+; UAS-exo84 RNAi $^{TRiP.JF03139}$/+*
4.2	A B	*hs-FLP; vkg-GFP/+; Act5c>>Gal4, UAS-RFP/UAS-evi5 RNAi^{V17549}*
	C E H J	*w; traffic jam-Gal4, vkg-GFP/+*
	D E	*w; traffic jam-Gal4, vkg-GFP/+; UAS-evi5 RNAi^{V17549}/+*
	F I K	*w; traffic jam-Gal4, vkg-GFP/+; UAS-evi5-mCherry/+*
	L	*hs-FLP; vkg-GFP/+; Act5c>>Gal4, UAS-GFP/UAS-evi5-mCherry*

Staining and microscopy

Ovaries were dissected in S2 medium and fixed for 15 minutes in PBS + 0.1% Triton (PBT) + 4% EM-grade formaldehyde (Polysciences), then separated from the muscle sheath by gentle pipetting. Antibody stains were performed in PBT and detected with Alexa Fluor-conjugated secondary antibodies (1:200, Invitrogen). Actin was labeled with TRITC-Phalloidin (1:200,

Sigma) or Alexa-647 Phalloidin (1:50, Invitrogen). For non-permeabilized stains, ovarioles were dissected from the muscle sheath in S2 medium and fixed for 6 minutes in PBS + 4% EM-grade formaldehyde. GFP antibody stains were performed as above using PBS instead of PBT. Antibodies used: rabbit α-GFP (1:200, Molecular Probes A21311 and A31852). Fluorescent images were obtained using Zeiss LSM 510 or LSM 880 confocal microscopes. Image processing and custom image analysis were performed using ImageJ and Python. Graphing and statistical analysis were performed in Prism (GraphPad). For all graphs, error is presented as mean ± s.e.m. and statistical differences between conditions were determined with 2-tailed, unpaired t-tests.

Measurement of fibril fraction and Pericellular Col IV-GFP intensity

See section 3.6.

CHAPTER 5: CONCLUSIONS AND FUTURE DIRECTIONS

5.1 PREFACE

In Section 5.2, I will summarize the conclusions that can be drawn from my work. In section 5.3, I will discuss remaining questions concerning basement membrane remodeling.

5.2 CONCLUSIONS

During my dissertation work, I have examined the mechanisms by which BMs are secreted, assembled, and remodeled by their adjacent epithelial tissues during development, and how such remodeling regulates tissue morphogenesis. This work has been largely motivated by the following assumptions: 1) because epithelia undergo dynamic movements during development, the BMs that adhere to these tissues must exhibit similarly dynamic properties. 2) The physical properties of the BM will modulate the morphogenetic dynamics of associated epithelia. In this section, I will summarize my conclusions regarding these concepts.

BMs have historically been, and often still are, regarded as merely static scaffolds for their associated tissues, and are frequently disregarded in studies of epithelial biology. However, reports from a variety of organisms have indicated that BMs are in fact dynamic structures with important roles in determining tissue structure and function (Daley and Yamada, 2013; Fata et al., 2004; Harunaga et al., 2014; Morrissey and Sherwood, 2015). The *Drosophila* egg chamber stood out as a powerful system to probe the mechanisms underlying BM remodeling. Two dramatic, stage-specific changes in the BM had been previously described – a strong increase in the amount of Col IV in the BM, and polarization of the matrix by generation of oriented fibrils (Gutzeit et al., 1991; Haigo and Bilder, 2011b). Notably, both of these changes coincide with

egg chamber elongation, suggesting they may regulate this process. During my dissertation work, I identified the mechanisms underlying these two instances of BM remodeling, and elucidated their contributions to morphogenesis. I also identified a new remodeling event – a regulated decrease in BM Perlecan levels – and demonstrated its contribution to morphogenesis.

Regulation of BM composition during egg chamber elongation

I first identified a mechanism that promotes the stage-specific increase in Col IV levels that occurs between oogenic stages 5 and 8. I observed that expression of the BM protein SPARC inversely correlates with the rise in BM Col IV levels, and that developmental down-regulation of SPARC protein levels between stages 4 and 6 is necessary to permit the rise in Col IV levels. I found that SPARC and Col IV physically interact in this system, and that SPARC and Col IV likely are co-trafficked within the secretory pathway. Because I could find no evidence that SPARC disrupts Col IV secretion, my observation that SPARC decreases Col IV levels suggest a model in which SPARC promotes extracellular Col IV solubility; I propose that SPARC binds Col IV and prevents its adhesion to cellular receptors and/or proteins within the BM. This role for SPARC was recently independently verified in *C. elegans* (Morrissey et al., 2016) and is consistent with previous observations in *Drosophila* that loss of SPARC causes aberrant adhesion of Col IV to cell surfaces in the fat body (Pastor-Pareja and Xu, 2011; Shahab et al., 2015). These data clarify the role of SPARC in the BM and will aid in understanding its function in development and disease processes.

I also further characterized the changes in BM composition that occur during egg chamber elongation and their implications for this process. In addition to increased Col IV levels, the follicular BM exhibits decreased Perlecan levels during elongation stages. I found

that both of these changes promote elongation, suggesting that Col IV promotes this process while Perlecan inhibits it. This is consistent with the observation that Col IV and Perlecan have opposing effects on development of other *Drosophila* organs (Pastor-Pareja and Xu, 2011). Due to Col IV's high tensile strength, this protein likely promotes elongation by enhancing the strength of the BM corset. Perlecan appears to increase elasticity of the matrix (Pastor-Pareja and Xu, 2011), which likely counters its ability to constrain growth. These data reveal the importance of finely regulating the composition the BM.

Regulation of BM structure during elongation

I also identified the mechanism by which the polarized fibrillar BM network is assembled by the follicle cells (Isabella and Horne-Badovinac, 2016). Using live imaging analysis of Col IV-GFP in the BM, I observed that fibrils are assembled from newly synthesized material in the pericellular space between lateral follicle cell membranes, and subsequently undergo oriented insertion into the BM by the migrating follicle cells. I found that Rab10 directs secretion of BM proteins to the pericellular region, and that Rab10 activity levels within the cells determine the extent of fibril formation. Finally, by manipulating this pathway, I discovered an important role for BM fibrils in directing egg chamber morphogenesis.

The dynamics of the fibrillar BM suggest that the mechanics of BM assembly and remodeling are sufficiently flexible to allow for a diversity of structure. This differs from the textbook view of a uniform static matrix. In the egg chamber, the ability to generate a polarized BM appears to result from two characteristic properties of the follicle cells: The flexibility to secrete BM proteins to the basal or lateral surface, and collective migration of the epithelium. This study indicates how various properties of an epithelium can synergize to regulate BM

structure. My work also suggests that the epithelium can regulate BM structure via direct remodeling of the existing matrix. Even in the absence of fibril formation, such as I observe in non-migrating epithelia, a low level of polarity is observed within the matrix. This polarity always orients with adjacent stress fiber-like actin bundles at the basal cell surface. These actin bundles are contractile elements that interact with the BM through integrin-based adhesions (Bateman et al., 2001; Cetera et al., 2014; Delon and Brown, 2009). It is therefore likely that this structure results from physical deformation of the BM due to contraction of the actin bundles. Altogether, these observations suggest that multiple means to influence BM structure exist.

My live imaging analysis offers a paradigm for examining BM remodeling in other tissues. Elucidation of the fibril formation mechanism was dependent on my observations of this process in living egg chambers. These observations were made possible by the presence of GFP protein trap tags in the *Drosophila viking* and *trol* genes, which encode the Col IV α2 subunit and Perlecan proteins, respectively. Successful generation of these protein traps will be instructive in functional tagging of these components in other organisms, and current genome editing techniques make this goal eminently achievable. Because so little is known of BM dynamics in developing systems, live imaging offers the opportunity to rapidly reveal the dynamic properties of these matrices, and simultaneously gain insights into the underlying mechanisms in a variety of organisms.

Elucidating the BM protein secretion pathway

My work offers new insights into the mechanism by which cells regulate BM protein secretion. It has long been known that BM proteins must be prevented from exiting at the apical cell surface, and long been assumed that their site of secretion is the basal cell surface. We

previously identified Rab10 as a critical factor in sorting BM proteins away from a Rab11-dependent apical secretion pathway (Lerner et al., 2013). I have clarified the role of Rab10 in this circumstance and revealed more complex control over BM protein secretion than initially thought. I found that Rab10 promotes secretion of BM proteins to the lateral, rather than the basal, cell surface. It appears to do so by promoting not just the sorting, but subsequent targeting to and docking at the correct plasma membrane domain. The observation that BM proteins exit at the lateral cell surface is surprising, and highlights how much is unknown about this process – to my knowledge, it has never been expressly demonstrated that BM proteins exit through the basal cell surface. It will therefore be important to reexamine our assumptions regarding BM protein secretion and more carefully probe this process. Interestingly, I found that, under normal circumstances, only a portion of BM proteins are sorted into the laterally-directed Rab10 pathway. Therefore, a second BM secretion pathway must exist. This pathway carries the portion of BM proteins that incorporate into the planar, rather than the fibrillar, matrix; it most likely targets BM proteins to the basal cell surface for secretion, although further study will be required to confirm this proposition. Further, this pathway appears to exist in competitive balance with the Rab10 pathway, as modulating Rab10 activity levels seems to shift the relative distribution of BM proteins between these pathways. My observations suggest the following model: BM protein sorting occurs as a competitive event between these two pathways, with their relative activity levels determining the distribution of BM proteins between them. The two pathways then direct their contents to different membrane regions: Rab10 to the lateral cell surface, and the alternate pathway to the basal cell surface. In the follicle cells, these pathways distinguish two BM populations, with Rab10 promoting fibril formation and the alternate pathway promoting incorporation into the planar matrix. While my data strongly support the

existence of a second BM secretion pathway, further study will be required to identify its molecular components and assess its function. It will also be important to determine whether these principles are generally applicable to BM protein secretion in other tissues.

Complex inputs of the BM into morphogenesis

The prevailing model for the role of the BM in egg chamber elongation is that of a molecular corset: the polarized BM anisotropically constrains egg chamber growth to promote elongation. This model suggests that the BM affects egg chamber shape during the active elongation period, which occurs during stage stages 5-10. My data support a corset role for the matrix, as increasing fibril formation enhances elongation during these stages, while decreasing Col IV levels inhibits it. However, this model is not sufficient to fully explain the role of the BM in regulating egg shape, as I have observed that altered BM structure can also affect egg chamber shape after stage 10. For instance, drastically increasing fibril formation causes rounding between stages 10 and 12. Thus, the BM also plays an important role in maintaining the elongated shape of the egg chamber. This finding is consistent with the previous observation that treating stage 13 egg chambers with Collagenase causes rapid rounding (Haigo and Bilder, 2011b). Intriguingly, this time period corresponds with an event within the egg chamber that may place particularly high mechanical strain on the organ. During stage 11, the nurse cells undergo actiomyosin-based contractions that squeeze their cytoplasmic contents into the posteriorly-localized oocyte. This process may use the BM as a stable substrate for force generation, and it is likely that the forces experienced by the matrix – both a contractile force in the anterior and an expansive force from the oocyte in the posterior – are strong. Extremely hyper-fibrillar BMs, which fail to maintain egg chamber shape at this stage, exhibit a depleted

planar matrix that may not be sufficiently strong to handle these forces. While it remains to be determined how the BM maintains egg chamber shape at late stages, these data indicate the complex and varied inputs that the BM has on egg shape. It is also noteworthy that identifying the complexity of this system required a careful stage-by-stage quantitative analysis of elongation; it is now clear that there are many ways to make a round egg, and simply examining the final product would not have been sufficient to recognize the complex regulation of this morphogenetic process.

Broad relevance of my work

This work was motivated by the idea that dynamic tissue development requires dynamic regulation of BM structure. My findings serve, in part, as a proof of principle of this concept – I have shown that the BM of the *Drosophila* egg chamber is highly dynamic during development, that cellular strategies have been devised to tightly regulate the composition and structure of this matrix, and that its properties influence the morphogenesis of its associated tissue. It is likely that these are general characteristics of BMs in developing tissues.

Although few BMs have been sufficiently examined to confirm this idea, existing evidence suggests that the BM is a common regulator of morphogenesis in vertebrates and invertebrates, although by varied means. For instance, in developing epithelial ducts, such as the mouse mammary and salivary glands, BM thickness appears to regulate several aspects of tissue shape: the BM is thin and porous at ductal tips to promote tissue outgrowth (Harunaga et al., 2014), while thickening of the BM around more mature ducts is believed to stabilize these structures; local BM thickenings may also act as an impeding force to promote ductal branching (Fata et al., 2004). It remains to be determined, in this case, to what extent the compositional

makeup of the BM is regulated, and whether structural specificities beyond thickness also contribute to tissue shape regulation.

This dissertation has focused primarily on morphogenesis; however, as outlined in chapter 1, the developmental contributions of the BM are many. For instance, BMs also regulate most major secreted cell signaling molecules. Virtually nothing is known of how specific aspects of BM structure or composition alter cell signaling, although it is likely that they do. For example, it is easy to imagine that adjusting the levels of a given BM protein would alter the diffusion of a signaling molecule to which it binds, or alter the ability of such a molecule to interact with cellular receptors through the BM. Therefore, examining BM remodeling will likely offer insights beyond its mechanical roles in morphogenesis.

In conclusion, studying the dynamic structure and function of BMs will be an important aspect of understanding principles of tissue development, and this work provides a blueprint for elucidating mechanisms of BM remodeling, and their functions, *in vivo*.

5.3 FUTURE DIRECTIONS

How is BM protein composition regulated?

My findings have revealed several outstanding questions that will provide opportunities for future research. First, what are the mechanisms that regulate the relative levels of different BM proteins within the matrix? I identified SPARC as an important regulator of Col IV incorporation into the BM, but it is likely that several other mechanisms exist. Although *SPARC* downregulation is necessary to increase Col IV levels, it is not sufficient, as *SPARC* knockdown does not appear to cause a precocious increase in Col IV levels. This observation, in fact,

indicates that we do not understand why SPARC is expressed in the follicular epithelium at all. It could be one of multiple redundant mechanisms controlling BM Col IV levels, or it could play additional roles in egg chamber development that I have not identified. My preliminary results suggest that expression of Col IV protein is also increased during stages 5-8. This likely occurs at the transcriptional level, as Darcy McCoy, a technician in the lab, has observed increased levels of mRNA for the Col IV subunits *viking and Cg25C* by in *situ* hybridization. However, a more thorough examination of Col IV expression is required, and the developmental signals that regulate this purported increase, as well as the down-regulation of SPARC expression, are unclear (see below). How BM Perlecan protein levels are regulated is even less clear. The decreased Perlecan levels observed during elongation stages could also be a product of transcriptional control, although I have yet to explore this possibility. In addition to protein production and incorporation, BM protein levels could be regulated by modifying their turnover rate within the BM. I do not know the extent to which BM proteins are removed from the matrix in this system, how turnover is controlled, or how turnover rates might be developmentally modulated. Genome editing to attach photo-convertible tags to BM proteins will allow for precise measurement of the rates of incorporation into, and removal of these proteins from, the BM.

How is BM protein secretion regulated?

My work supports the previous observation that BM proteins are sorted into a Rab10-dependent pathway, but it remains unclear how BM proteins are recognized and sorted. I found that Col IV and SPARC are likely co-secreted, and there are indications that the same mechanisms regulate the secretion of all major BM proteins. However, the extent of co-regulation is unclear. Are

these proteins independently recognized and sorted into the same pathway, or do they exist in such close association as to be co-sorted, perhaps even with multiple proteins sorted into the same individual vesicles; if this is the case, might a master factor exist that coordinates the secretion of these proteins? I present some evidence for this concept in Addendum B.

I have found that, in addition to initial sorting of BM proteins, Rab10 appears to regulate targeting and docking/fusion of BM protein-containing vesicles. BM proteins appear to be secreted at a basal region of the trailing lateral plasma membrane, but how they are targeted to this specific location is unclear. The basolateral polarity protein Lgl1 regulates Rab10-dependent trafficking in neurons (Wang et al., 2011), and the laterally-localized PIP2 plays some role in targeting of BM protein secretion (Devergne et al., 2014), but the localization of these factors is broader than the site where I propose BM proteins exit the cell. Because BM proteins are secreted close to the interface between basal and lateral cell membranes, it may be that the confluence of factors at this site provides such specificity, although the identity of such factors is unknown. We have observed that a large number of proteins accumulate at the trailing basal-lateral interface, suggesting that a distinct membrane identity may exist at this location; we do not, however, understand what causes the accumulation of certain proteins at this site. Identification of the factors responsible for Rab10 vesicle transport, and additional factors that function with Rab10, such as the exocyst, may aid in further elucidating this pathway.

My work indicates that only a portion of BM protein secretion occurs through the Rab10 pathway. My characterization of fibril formation dynamics suggests that the laterally-directed Rab10 pathway exists in competition with a second pathway that may direct BM protein secretion to the basal cell surface. I speculate that another Rab GTPase regulates this pathway, and although I do not know its identity, I can make several hypotheses about its behavior. Like

the Rab10 pathway, this pathway should function predominantly in the basal region of the cell. Additionally, there is reason to believe that this pathway acts redundantly with Rab10 to prevent apical BM protein secretion. Rab10 knockdown causes only a weak apical accumulation of BM proteins, indicative of some redundancy. Further, the apical accumulation seen upon Rab10 knockdown indicates that the alternate pathway is not sufficient to handle 100% of BM protein traffic on its own; the principles of competitive balance suggest that the inverse is also true. Thus, knocking down components of this pathway would be expected to cause BM protein secretion to the apical surface. Finally, while increasing Rab10 activity increases BM fibril formation, increasing the activity of a competitive pathway should decrease fibril formation. These experimental hypotheses should allow us to identify the second pathway by screening the existing collection of Rab over-expression and RNAi lines (Zhang et al., 2006). Rab8 is a good candidate to regulate this pathway: this protein is the closest evolutionary relative of Rab10 (Zhang et al., 2006), and has been shown to be partially redundant with Rab10 in multiple contexts (Schuck et al., 2007; Shi et al., 2010). Our preliminary evidence also suggests that Rab8 may specify this alternate pathway, as I have observed that this protein shows localization similar to that of Rab10, and expression of a Rab8 dominant negative construct causes apical accumulation of Col IV-GFP. However, further examination of this protein is required.

How is the timing of BM remodeling specified?

The increase in BM Col IV levels and the formation of BM fibrils occur at a precise time in egg chamber development – specifically, they both occur between stages 5 and 8. It is unclear, however, how the timing of these events is regulated. My work addressed this question at one level – the timing of the increase in Col IV levels is set, in part, by down-regulation of SPARC,

and fibril formation likely results from a stage-specific increase in Rab10 activity. However, the more fundamental question of what developmental signal is responsible for these changes remains unanswered. That these two events occur in the same timeframe indicates that they may both be regulated by the same signal. The best candidate for an initiating signal is Notch. At stage 6, a Delta signal from the germline activates Notch signaling in the follicle cells; this signal is proposed to promote follicle cell differentiation and is known to induce a transition from mitosis to endocycling (Horne-Badovinac and Bilder, 2005). However, because Notch signaling appears to induce changes at stage 6, and BM remodeling begins at stage 5, it is unclear whether these events are related.

Termination of this process at stage 9 may be regulated by ecdysone signaling. This stage is characterized by a cessation of egg chamber rotation and the subsequent migration of the follicle cells, as well as a small group of border cells at the anterior tip of the egg chamber, posteriorly to cover the oocyte. A peak of ovarian ecdysone synthesis occurs at stage 9, and appears to promote border cell migration(Bai et al., 2000). Because this signal also correlates with the end of BM remodeling, it may regulate this process as well, although such a relationship remains to be elucidated.

A-P differences in these remodeling events may also be informative in identifying their regulation. BM Col IV levels are higher in the anterior of the egg chamber, while fibril formation occurs to a greater extent in the posterior. Therefore, characteristic differences along the A-P axis may be tied to BM remodeling. Exploratory manipulation of signaling pathways in the follicle cells will likely be necessary to elucidate how the timing of BM remodeling is regulated. Stage-specific transcriptional profiling may also aid in understanding the changes that occur at stages 5 and 9.

Electron microscopy-based examination of different BM structures

In chapter 3, I utilized platinum replica electron microscopy (EM) to analyze the structure of the de-cellularized follicular BM at high resolution. This approach led to significant insights into the structural organization of the BM. First, I saw that fibrils localize to the inner surface of the BM, where they sit atop a planar matrix. Additionally, I observed that smaller regions of the planar matrix also appear to be polarized, supporting my other findings that a second mechanism may exist to polarize the BM by reorganization of the planar matrix. My genetic and fluorescence microscopy analysis has revealed several conditions that alter BM structure; examining these BMs with the resolution of EM could similarly reveal important details about BM structure. For instance, I proposed that increasing Rab10 activity increases fibril formation at the expense of the planar matrix – EM could confirm the presence of less material in the planar matrix, and determine whether the fibrils formed in this condition show any structural distinctions form wild-type fibrils. I also found that the BMs of non-migrating epithelia lack fibrils, but maintain local polarity over each individual cell that likely results from reorganization of the planar matrix. EM would allow us to examine this level of polarity, determine its structure, and ask whether it is similar to the apparent polarized regions of planar matrix I observe in the wild-type BM. Additionally, I found that loss of the Dystropyin/Dystroglycan ECM receptor complex decreases fibril formation (see Addendum A). With EM, I could assess the structure of this matrix as well – does it more closely resemble stage 4 BMs, which are primarily composed of an isotropic planar matrix? And does the remaining polarity exist as small fibrils, or is does it appear to be generated primarily via remodeling of the planar BM? Finally, this approach could be used to examine intracellular structures at the basal cell surface. If, instead of complete de-

cellularization of the BM, cells were unroofed to reveal the basal cortex, the organization of the basal cell surface could be examined at high resolution as well.

Biophysical studies of BM and tissue development

The model for how BM structure regulates egg shape is largely mechanical; however, this model currently relies purely on inferred mechanical properties of the BM. I have made several assumptions regarding how changes in BM composition and structure alter the physical properties of the matrix, but it will eventually be necessary to directly measure the physical properties of the BM, both in wild type egg chambers and under conditions that alter BM composition or structure.

One example of the value of this approach is in addressing the question of how the BM maintains the elongated shape of the egg chamber. In the previous section, I discussed the possibility that the BM maintains egg chamber shape by stabilizing the tissue against strain generated by other cellular processes, such as nurse cell contractions. Confirming these hypotheses will require rigorous biophysical studies of egg chamber development. What are the mechanical properties of the matrix? What forces are generated by these intracellular processes? And how do differences in BM structure and composition affect the generation of and/or response to such forces? Techniques to directly measure mechanical properties of live samples, such as laser severing to measure the magnitude and anisotropy of tension, and atomic force microscopy to measure other mechanical properties, will provide crucial insights into these questions.

Characterization of BM structure and function in other tissues

I believe that the principles of BM structure and function elucidated here are broadly applicable to developing epithelia. However, it will be necessary to carry out similar studies in other tissues to gain a deeper understanding of the roles of BMs in development. This will require characterization of the structure, composition, and dynamic properties of BMs during development, as well as detailed studies of the effect that manipulating these properties has on the behaviors of associated tissues.

Any developing BM is a good target for such studies. One strategy would be to examine BMs associated with a variety of morphogenetic events. For example, what are the dynamics of a BM in a tissue undergoing invagination? Convergent extension? Isotropic and anisotropic growth? It will also be interesting to examine the BMs of several tissues undergoing one event, to determine whether characteristic BM properties are conserved across given morphogenetic movements. Finally, it will be intriguing to determine whether individual remodeling mechanisms are conserved across different BMs, or different species. Take, for example, fibril formation. Thus far, the *Drosophila* egg chamber is the only fibrillar BM of which I know. However, the cell behaviors underlying this event – BM protein secretion and collective cell migration – are common. Do other migrating epithelia generate polarized BMs? One good system in which to ask this question is mammalian epithelial cysts. It has been observed that mammalian epithelial cells in 3D culture self-organize into polarized acini that spontaneously rotate, similarly to the egg chamber (Tanner et al., 2011). The acinar BM appears to play a role in this process, but its structure has not be examined (Wang et al., 2013). This would be a good system in which to examine whether the mechanisms identified in the egg chamber are conserved in other tissues.

Because BMs regulate many developmental processes, it will be important to broadly examine the effects of altered BMs beyond simply tissue shape. Once experimental procedures for precisely manipulating BM structure and function have been worked out, many alterations to cell behavior may ensue. For instance, will such manipulations alter intercellular signaling and downstream gene expression patterns? Will they impact the behaviors of stem cells, which often rely on niche signals from the BM? Such studies could have broad-ranging implications for various aspects of cell behavior.

ADDENDUM A: THE DYSTROPHIN/DYSTROGLYCAN COMPLEX PROMOTES BASEMENT MEMBRANE FIBRIL FORMATION AND EGG CHAMBER ELONGATION

Introduction

During early elongation stages, the follicle cells incorporate oriented fibrils into their BM. In chapter 3, I describe the process by which this polarized BM is built; in short, BM proteins are secreted, via a Rab10-dependent pathway, to the pericellular space between follicle cells, where they polymerize into nascent fibrils and are subsequently inserted into the BM by the migrating follicle cells. I further found that increasing Rab10 activity increases the amount of BM material secreted to the pericellular space, leading to polymerization and incorporation of larger BM fibrils. It has been proposed that the polarized BM acts as a molecular corset, anisotropically constraining egg chamber growth to promote elongation (Gutzeit et al., 1991). My data are consistent with this hypothesis, as modestly increasing fibril formation enhances elongation (See chapter 3). The current data suggest that fibril formation is required for egg chamber elongation, and leads to the hypothesis that decreasing fibril formation will inhibit elongation. However, we were unable to specifically decrease fibril formation by manipulating the Rab10 pathway, as decreasing Rab10 activity causes aberrant secretion of BM proteins to the apical surface (Lerner et al., 2013). Thus, identification of another mechanism to manipulate fibril formation is required to address this hypothesis.

The Dystrophin (Dys)/Dystroglycan (Dg) complex is a good candidate to regulate BM assembly and structure. Dg is a transmembrane ECM receptor that binds the BM components Laminin and Perlecan; its intracellular binding partner, Dys, interacts with the actin cytoskeleton, providing a functional link between the BM and the cytoskeleton (Ibraghimov-Beskrovnaya et

al., 1992; Schneider et al., 2006). *Dys* and *Dg* mutant egg chambers also exhibit elongation defects (Mirouse et al., 2009)[1]. Whether these conditions alter BM structure, however, has not been examined.

Here, I present my work identifying the Dys/Dg complex as a positive regulator of BM fibril formation. I find that knockdown of this complex inhibits BM fibril formation and disrupts maintenance, but not establishment, of egg chamber elongation.

Results

Maureen Cetera, a previous graduate student in the lab, observed that Dys exhibits a localization very similar to that of Rab10 – it localizes to the trailing edge of the basal cell surface, and on the basal region of the lateral cell membranes (Figure A.1 A-B). I therefore asked whether this complex, like Rab10, regulates BM fibril formation. *Dys* knockdown results in a strong inhibition of BM fibril formation (Figure A.1 C-E). I also observed this phenotype via *Dg* knockdown and in a *Dys* mutant background (Figure A.1 F-G). Therefore, the Dys/Dg complex promotes BM fibril formation. Because the extent of fibril formation has, thus far, always scaled with the amount of Col IV accumulation in the pericellular space, I hypothesized that *Dys* knockdown somehow inhibits the accumulation of pericellular Col IV. Surprisingly, however, I observed no effect of *Dys* knockdown on the amount or distribution of pericellular Col IV-GFP (Figure A.1 H-I). Fibril formation also requires collective follicle cell migration; however, I found that this process is minimally affected by *Dys* knockdown (Figure A.1 J). Thus, this

[1] Mirouse et al. 2009 has been retracted (Haack et al., 2013). The authors mistakenly interpreted damaged tissue as mutant clones, leading to the erroneous conclusion that *Dys* and *Dg* are required for apical-basal polarity. The analysis of egg shape, however, was not performed in mosaic tissue, suggesting that these data may be valid. Additionally, we have independently confirmed that these proteins are required for elongation (see below).

complex promotes fibril formation via a mechanism that is distinct from that of Rab10 and follicle cell migration.

I next addressed the hypothesis that decreasing fibril formation inhibits egg chamber elongation. I did observe that *Dys RNAi* results in eggs that are rounder than wild-type (Figure A.1 K). However, this condition does not affect egg chamber shape until stage 10, at the very end of elongation (Figure A.1 K). Therefore, Dys/Dg appears to be dispensable for the majority of egg chamber elongation. Additionally confounding these results, I observed that the defect in egg shape cause by *Dys RNAi* expression is independent of BM structure. By co-expressing *UAS-Rab10*, which enhances fibril formation, and *Dys RNAi*, which lowers it, I was able to rescue fibril formation to around wild-type levels (Figure A.1 L-N). This condition, however, does not rescue the elongation defect caused by *Dys RNAi* (Figure A.1 O). It can still be concluded that decreasing fibril formation in the BM has no effect, prior to stage 10, on establishing the elongated shape of the egg chamber; however, the cause of the eventual failure in elongation is not clear.

Discussion

Here, I report several confounding results. First, the Dys/Dg complex localizes to lateral follicle cell membranes. Because the BM blankets only the basal cell surface, localization of a BM adhesion molecule to any other location would seem counter-intuitive. These data are likely reconciled by my observation that BM components do accumulate in the pericellular space between lateral follicle cell membranes, providing a potential adhesion substrate for lateral Dg. My observation that the Dys/Dg complex promotes generation of fibrils, which derive from this

pericellular BM protein pool, further suggests an interaction between lateral Dg and pericellular BM proteins.

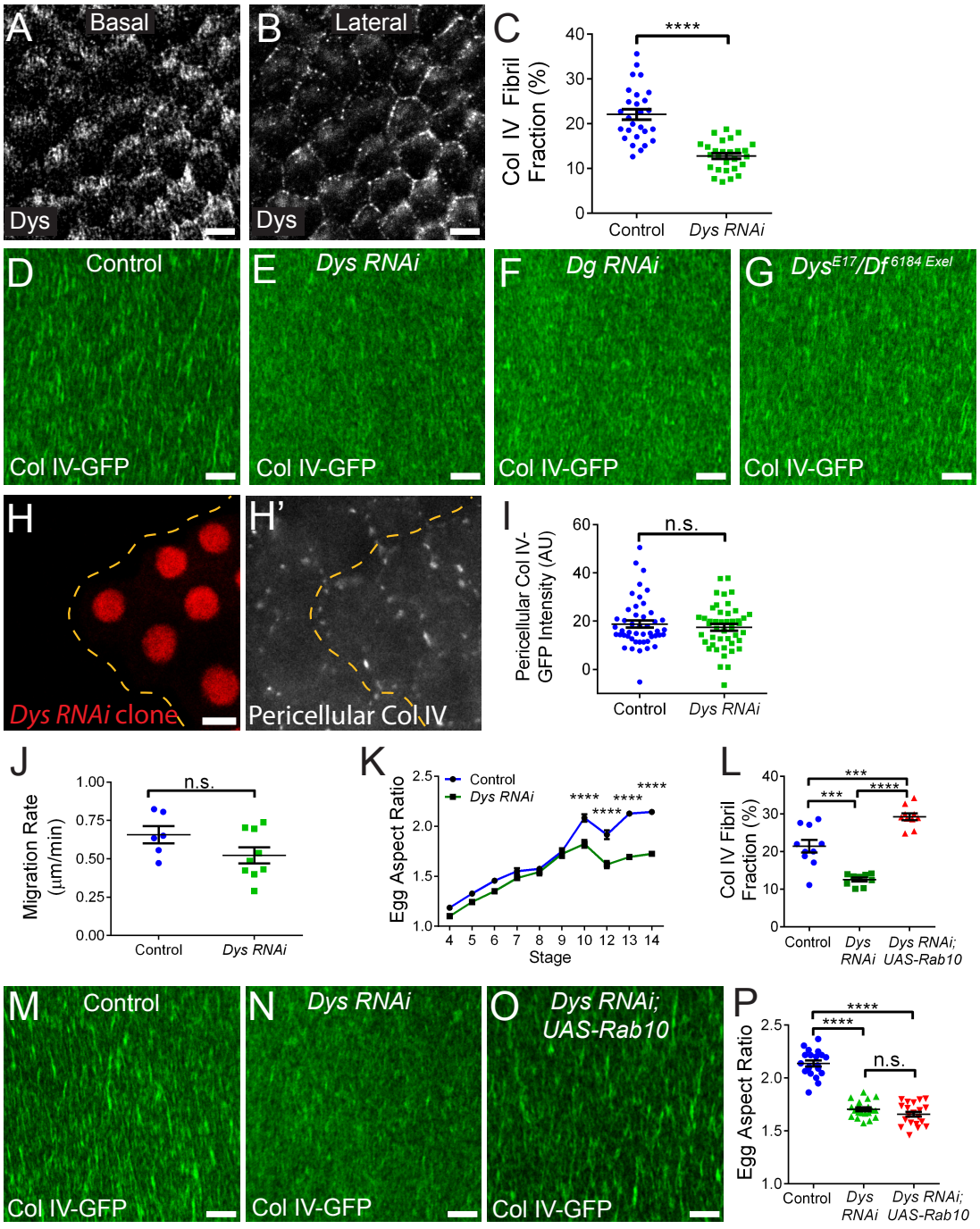

Figure A.1. The Dys/Dg complex promotes fibril formation and egg chamber elongation (A-B) Dys exhibits planar polarized localization at the basal follicle cell surface (A) and localizes to the lateral plasma membrane (B). Images represent endogenously tagged Dys

Figure A.1. Continued, The Dys/Dg complex promotes fibril formation and egg chamber elongation
protein. (C) *Dys RNAi* expression lowers the BM fibril fraction. (D-G) Representative images showing that expression of *Dys RNAi* or *Dg RNAi*, or generation of *Dys* null epithelia, decreases BM fibril formation. (H) Representative image showing that clonal *Dys RNAi* expression (red cells) does not alter the amount of pericellular Col IV relative to neighboring wild-type cells. Yellow line indicates clone boundary. (I) Quantification of the condition shown in (H). (J) *Dys RNAi* expression does not alter the rate of follicle cell migration. (K) *Dys RNAi* expression inhibits egg chamber elongation. In this condition, the failure in elongation occurs at stage 10. (L-O) The defect in fibrillogenesis does not explain the effect of *Dys RNAi* on egg chamber elongation. Over-expressing Rab10 in the *Dys RNAi* condition can rescue fibril formation to near control levels (L-O), but does not rescue egg shape (P). (C, I-L, O) Data represent mean ± s.e.m. t-test: n.s. = $P>0.05$, **** = $P<0.0001$. Scale bars = 5 μm. Experiments performed at stage 8 unless otherwise noted in figure.

My observations regarding the role of Dys/Dg in fibril formation also do not fit with the current conception of how BM fibrils are generated. My work with Rab10 suggested a simple model: the amount of BM proteins in the pericellular space determines the extent of fibril formation. That *Dys/Dg* knockdown inhibits fibril formation without decreasing pericellular BM protein accumulation suggests additional inputs to this process. It may be that binding of Dg to pericellular BM proteins promotes assembly of these structures, by preventing their rapid diffusion and/or increasing local concentrations of these proteins. My fluorescent images of pericellular Col IV-GFP may not have sufficient resolution to identify differences in such properties upon *Dys* knockdown. Alternatively, binding to Dg may stabilize nascent fibrillar aggregates as they are incorporated into the BM. It is likely that, during their deposition, nascent fibrils exhibit some affinity for both the BM and the pericellular space, meaning that they experience tension during the deposition process. It is possible that this tension acts to stabilize protein interactions within the fibril. In this case, loss of Dys/Dg would decrease affinity of the fibril for the pericellular space, thus decreasing tension and causing the fibril to fall apart during deposition. Tension-dependent stability has been observed for other protein complexes, most

notably integrin-based focal adhesion complexes that link the BM to the cytoskeleton at the basal cell surface (Schiller and Fässler, 2013). Additionally, some matrix proteins, such as fibronectin, have tension-dependent properties (Baneyx et al., 2002; Krammer et al., 2002). However, further work will be required to determine the mechanism by which Dys/Dg promote BM fibril formation.

Finally, many questions remain regarding my observations that *Dys* knockdown alters maintenance, but not establishment, of egg chamber elongation. First, my finding that decreasing fibril formation does not alter elongation prior to stage 10, which is the period during which the corset is proposed to function, requires that we modify our conception of how the BM regulates elongation. It remains likely that the BM exerts a corset effect during egg chamber elongation, as modestly increasing fibril formation enhances elongation and decreasing Col IV levels in the BM inhibits elongation. However, it appears as though, outside of a narrow range of fibril fractions, the extent of fibril formation has little ability to alter BM corset function. It should be noted that *Dys/Dg*-deficient BMs, though less fibrillar, remain polarized, suggesting that a base level of polarity may be sufficient for corset function. In fact, beyond such a potential requirement for some degree of polarity, it may be that the composition of the BM is more important in regulating the corset, as decreasing BM Col IV levels disrupts elongation to a greater extent than any change in fibril formation I have observed. It is also not clear what role Dys/Dg play in promoting elongation at stage 10. Because this effect appears to be independent of BM structure, it does not further our understanding of how the BM regulates egg shape. Between stages 9 and 10, stress fiber-like actin bundles at the basal follicle cell surfaces undergo oscillating myosin-based contractions, which drive the final stage of elongation (He et al., 2010). Dys/Dg play a well known role in stabilizing muscle tissue integrity against contraction forces

(Ervasti and Sonnemann, 2008). It may be that this complex also influences the generation of contractile force, or how that force is channeled into elongation, during this process.

Methods

Drosophila genetics

Experimental genotypes are in table A.1. Experimental crosses were raised at 25°C and females aged on yeast for 3 days at 29°C. FLP-out was induced by 37°C heat shock for 1 hour, twice daily for 3 days on yeast with intermittent periods at 25°C. Most lines were obtained from the Bloomington *Drosophila* stock center except: *UAS-dys RNAi* and *UAS-dg RNAi* are from the Vienna *Drosophila* resource center (Vienna, Austria). *Traffic jam-Gal4* and *dys-YFP* are from the *Drosophila* Genetic Resource Center (Kyoto Institute of Technology, Kyoto, Japan). *vkg-GFP* is from Flytrap (Buszczak et al., 2007). For RFP-Rab10, see section 3.6.

Table A.1 Experimental Genotypes

Figure	Panel	Genotype
A.1	A B	*;;Dys-YFP*
	C D L	*w; traffic jam-Gal4, vkg-GFP/+*
	C E M	*w; traffic jam-Gal4, vkg-GFP/UAS-dys RNAi^{V108006}*
	F	*w; traffic jam-Gal4, vkg-GFP/UAS-dg RNAi^{V107029}*
	G	*;;dys^{detE17}/Df3R$^{6184\ Exel}$*
	H I	*hs-FLP; vkg-GFP/ UAS-dys RNAi^{V108006}; Act5c>>Gal4, UAS-RFP/+*
	J	*w; traffic jam-Gal4/ +; UAS-mCD8-RFP/+*
		w; traffic jam-Gal4/UAS-dys RNAi^{V108006}; UAS-mCD8-RFP/+
	K	*w; traffic jam-Gal4, mb247-Gal80/+*
		w; traffic jam-Gal4, mb247-Gal80/UAS-dys RNAi^{V108006}
	N	*w; traffic jam-Gal4, vkg-GFP/UAS-dys RNAi^{V108006}; UAS-RFP-Rab10/+*
	O	*w; traffic jam-Gal4/+*
		w; traffic jam-Gal4/UAS-dys RNAi^{V108006}
		w; traffic jam-Gal4/UAS-dys RNAi^{V108006}; UAS-RFP-Rab10/+

Staining and microscopy

Ovaries were dissected in S2 medium and fixed for 15 minutes in PBS + 0.1% Triton (PBT) + 4% EM-grade formaldehyde (Polysciences), then separated from the muscle sheath by gentle pipetting. Antibody stains were performed in PBT and detected with Alexa Fluor-conjugated secondary antibodies (1:200, Invitrogen). Actin was labeled with TRITC-Phalloidin (1:200, Sigma) or Alexa-647 Phalloidin (1:50, Invitrogen). For non-permeabilized stains, ovarioles were dissected from the muscle sheath in S2 medium and fixed for 6 minutes in PBS + 4% EM-grade formaldehyde. GFP antibody stains were performed as above using PBS instead of PBT. Antibodies used: rabbit α-GFP (1:200, Molecular Probes A21311 and A31852). Fluorescent images were obtained using Zeiss LSM 510 or LSM 880 confocal microscopes. Image processing and custom image analysis were performed using ImageJ and Python. Graphing and statistical analysis were performed in Prism (GraphPad). For all graphs, error is presented as mean ± s.e.m. and statistical differences between conditions were determined with 2-tailed, unpaired t-tests.

Live imaging and measurement of migration rates

See section 3.6.

Measurement of fibril fraction, Pericellular Col IV-GFP intensity, and aspect ratios

See section 3.6.

ADDENDUM B: PERLECAN IS REQUIRED FOR POLARIZED COLLAGEN IV SECRETION

Introduction

BMs are assembled specifically on the basal surfaces of epithelia. Because of this fact, an important aspect of BM protein secretion by epithelia is ensuring polarized trafficking of these proteins to basal, and not apical, cell membranes. A few factors regulating the polarized trafficking of BM proteins have been identified, but this process is still not well understood. Most notably, the small GTPase Rab10 and its GEF, Crag, have been identified as necessary for polarized secretion of BM proteins to the basal cell surface (Denef et al., 2008; Lerner et al., 2013). In the absence of these proteins, BM proteins are aberrantly sorted into a Rab11-dependent pathway and secreted to the apical surface. Two other proteins – Phosphatidylinositol synthase (Pis), an enzyme involved in the production of phosphoinositides, and Scarface, a secreted serine protease-like protein that lacks catalytic activity, also appear to be required to prevent apical BM protein secretion, although the mechanisms by which they exert this effect is not clear (Devergne et al., 2014; Sorrosal et al., 2010). Understanding the mechanisms by which BM proteins are sorted and trafficked to the basal surface with high fidelity will require identification of additional factors that regulate this process.

Perlecan is a heparin sulfate proteoglycan that, along with Col IV, Laminin, and Nidogen, is a core component of the BM. Here, we report the identification of Perlecan as another protein required for polarized BM protein secretion.

Results

Examining egg chambers in which Perlecan had been knocked down with RNAi, I observed that Col IV-GFP accumulates on the apical epithelial surface (Figure B.1 A-B). The BM has been shown to act as an apicobasal polarizing cue for epithelial cells (Schneider et al., 2006); we therefore reasoned that Perlecan in the BM may act as a cue to polarize the BM secretory machinery. We addressed this hypothesis by examining Col IV-GFP localization in Perlecan mutant clones. Due to egg chamber rotation, epithelia clonally lacking Perlecan still distribute this protein evenly throughout the BM; we would therefore expect to observe no apical Col IV-GFP accumulation in this condition. However, in mosaic epithelia, Col IV-GFP shows a cell-autonomous accumulation at the apical surfaces of Perlecan null cells (Figure B.1 C). These results indicate that, contrary to my initial hypothesis, Perlecan is required cell-autonomously to prevent aberrant apical accumulation of Col IV.

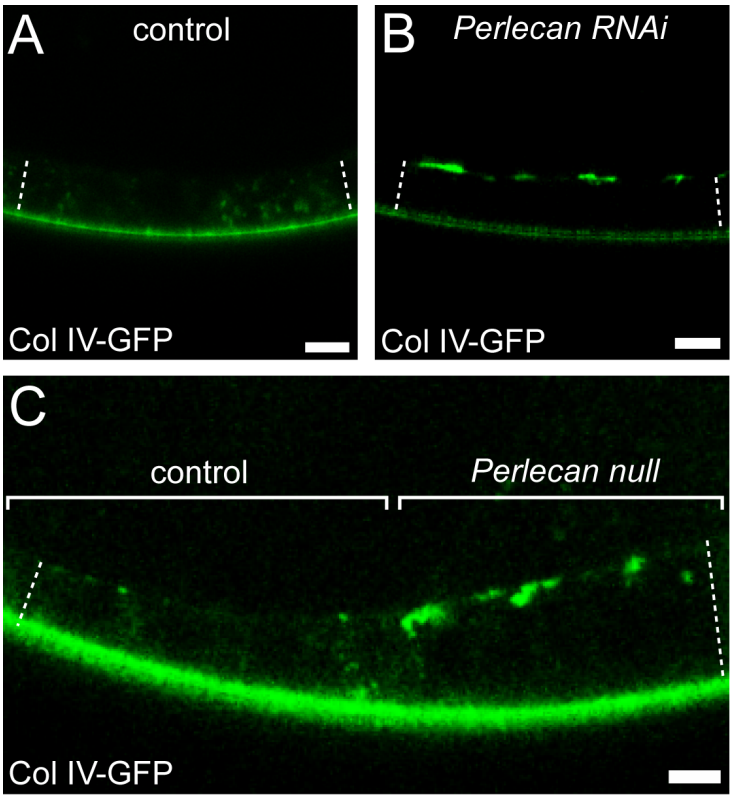

Figure B.1. Perlecan is required for polarized Col IV secretion
(A-B) *Perlecan RNAi* expression causes aberrant accumulation of Col IV-GFP on the apical follicle cell surface. (C) A mosaic *Perlecan* null epithelium. Loss of Perlecan causes cell-autonomous accumulation of Col IV-GFP at the apical epithelial surface. Brackets indicate control and *Perlecan* null tissue. (A-C) The epithelium is oriented with the apical surface up. Dotted lines indicate the apical-basal axis. Scale bars = 5 μm. Experiments performed at stage 8.

Discussion

Here, I report that the core BM protein Perlecan is required for the polarized secretion of another core BM protein, Col IV. There are several potential explanations for this observation. I initially though that Perlecan in the BM may provide a polarizing cue to the follicle cells that allows them to orient polarized trafficking. This, however, is not the case – due to egg chamber rotation, epithelia clonally lacking Perlecan still distribute this protein evenly throughout the BM. That this condition shows cell-autonomous apical Col IV accumulation indicates that Perlecan is required within the cell to direct Col IV secretion. The likeliest explanation for this phenotype is that Perlecan is required for the cell's secretory machinery to recognize and sort Col IV. The contents of a vesicle must be recognized by the exocytic machinery to ensure proper sorting. Our previous results indicate that the trafficking of all major BM proteins is co-regulated, and that Col IV and Perlecan may in fact be packaged into the same vesicles. In this case, it may be that Perlecan, and not Col IV, is the cargo that is recognized by the sorting machinery, and that Co IV is sorted indirectly by virtue of its association with Perlecan. This hypothesis posits that, in the absence of Perlecan, the sorting machinery is blind to the contents of Col IV-containing vesicles, causing them to be mis-sorted and trafficked to the apical surface. Finally, it is possible that Perlecan is required not for polarized secretion of Col IV, but for its transcytosis. It is assumed that BM proteins are trafficked to the basal surface with high fidelity because very little Col IV-GFP can be seen at the apical surface in wild-type egg chambers. However, this observation could also be explained by a model in which some Col IV is mis-trafficked to the apical surface, but a backup mechanism exists to rapidly endocytose this population and either degrade it or redirect (transcytose) it to the basal surface. In this scenario, much like in the previous one, Perlecan would be the protein that is recognized by the apical

endocytic machinery, and Col IV reuptake would result from its association with Perlecan. Thus, the absence of Perlecan would prevent recognition of apical Col IV for reuptake by the cells. In either of these cases, it will also be interesting to determine whether loss of Perlecan also causes apical accumulation of the other major BM components, Laminin and Nidogen. These data would help determine the extent to which the sorting and secretion of Col IV and other BM proteins is co-regulated. In conclusion, further work will be required to identify the cause of this phenotype, and the mechanisms by which Perlecan and other BM proteins are recognized and sorted by the cell.

Methods

Drosophila genetics

Experimental genotypes are in table B.1. Experimental crosses were raised at 25°C and females aged on yeast for 3 days at 29°C. Most lines were obtained from the Bloomington *Drosophila* stock center except: Traffic jam-Gal4 is from the *Drosophila* Genetic Resource Center (Kyoto Institute of Technology, Kyoto, Japan). *vkg-GFP* is from Flytrap (Buszczak et al., 2007).

Table B.1 Experimental Genotypes

Figure	Panel	Genotype
B.1	A	*w; traffic jam-Gal4, vkg-GFP/+*
	B	*w; traffic jam-Gal4, vkg-GFP/+; UAS-trol RNAi$^{TRiP.JF03376}$*
	C	*trol ^{null}, FRT101/ubi-GFP, FRT101; e22c-Gal4, UAS-FLP/vkg-GFP*

Staining and microscopy

Ovaries were dissected in S2 medium and fixed for 15 minutes in PBS + 0.1% Triton (PBT) + 4% EM-grade formaldehyde (Polysciences), then separated from the muscle sheath by gentle

pipetting. Fluorescent images were obtained using Zeiss LSM 510 or LSM 880 confocal microscopes. Image processing was performed using ImageJ.

REFERENCES

Adams, D.S., Keller, R., Koehl, M.A., 1990. The mechanics of notochord elongation, straightening and stiffening in the embryo of Xenopus laevis. Development 110, 115–130.

Andrew, D.J., Ewald, A.J., 2010. Morphogenesis of epithelial tubes: Insights into tube formation, elongation, and elaboration. Dev. Biol. 341, 34–55.

Anitei, M., Hoflack, B., 2011. Exit from the trans-Golgi network: from molecules to mechanisms. Curr. Opin. Cell Biol. 23, 443–51.

Aurich, F., Dahmann, C., 2016. A Mutation in fat2 Uncouples Tissue Elongation from Global Tissue Rotation. Cell Rep. 14, 2503–2510.

Babbey, C., Ahktar, N., Wang, E., Chen, C., Grant, B., Dunn, K., 2006. Rab10 Regulates Membrane Transport through Early Endosomes of Polarized Madin-Darby Canine. Mol. Biol. … 17, 3156–3175.

Babbey, C.M., Bacallao, R.L., Dunn, K.W., 2010. Rab10 associates with primary cilia and the exocyst complex in renal epithelial cells. Am. J. Physiol. Renal Physiol. 299, F495–F506.

Bai, J., Uehara, Y., Montell, D.J., 2000. Regulation of invasive cell behavior by taiman, a Drosophila protein related to AIB1, a steroid receptor coactivator amplified in breast cancer. Cell 103, 1047–1058.

Balla, T., 2013. Phosphoinositides: tiny lipids with giant impact on cell regulation. Physiol. Rev. 93, 1019–137.

Baneyx, G., Baugh, L., Vogel, V., 2002. Fibronectin extension and unfolding within cell matrix fibrils controlled by cytoskeletal tension. Proc. Natl. Acad. Sci. U. S. A. 99, 5139–5143. doi:10.1073/pnas.072650799

Barr, F.A., 2013. Rab GTPases and membrane identity: Causal or inconsequential? J. Cell Biol. 202, 191–9.

Bateman, J., Reddy, R.S., Saito, H., Van Vactor, D., 2001. The receptor tyrosine phosphatase Dlar and integrins organize actin filaments in the Drosophila follicular epithelium. Curr. Biol. 11, 1317–27.

Bernfield, M., Banerjee, S. Das, Koda, J.E., Rapraeger, A.C., 1984. Remodelling of the basement membrane: morphogenesis and maturation, in: Basement Membranes and Cell Movement. pp. 179–196.

Binari, R., Staveley, B., Johnson, W., Godavarti, R., Sasisekharan, R., Manoukian, A., 1997. Genetic evidence that heparin-like glycosaminoglycans are involved in wingless signaling. Development 124, 2623–2632.

Blümer, J., Rey, J., Dehmelt, L., Mazel, T., Wu, Y.-W., Bastiaens, P., Goody, R.S., Itzen, A., 2013. RabGEFs are a major determinant for specific Rab membrane targeting. J. Cell Biol. 200, 287–300.

Boll, W., Partin, J.S., Katz, a I., Caplan, M.J., Jamieson, J.D., 1991. Distinct pathways for basolateral targeting of membrane and secretory proteins in polarized epithelial cells. Proc. Natl. Acad. Sci. U. S. A. 88, 8592–6.

Bradshaw, A.D., 2009. The role of SPARC in extracellular matrix assembly. J. Cell Commun. Signal. 3, 239–46.

Bramham, C.R., Wells, D.G., 2007. Dendritic mRNA: transport, translation and function. Nat. Rev. Neurosci. 8, 776–89.

Broadus, J., Doe, C.Q., 1997. Extrinsic cues, intrinsic cues and microfilaments regulate asymmetric protein localization in Drosophila neuroblasts. Curr. Biol. 7, 827–835.

Brose, K., Bland, K., Wang, K., Arnott, D., Henzel, W., Goodman, C., Tessier-Lavigne, M., Kidd, T., 1999. Slit proteins bind Robo receptors and have an evolutionarily conserved role in repulsive axon guidance. Cell 96, 795–806.

Bunt, S., Hooley, C., Hu, N., Scahill, C., Weavers, H., Skaer, H., 2010. Hemocyte-secreted type IV collagen enhances BMP signaling to guide renal tubule morphogenesis in Drosophila. Dev. Cell 19, 296–306. doi:10.1016/j.devcel.2010.07.019

Buszczak, M., Paterno, S., Lighthouse, D., Bachman, J., Planck, J., Owen, S., Skora, A.D., Nystul, T.G., Ohlstein, B., Allen, A., Wilhelm, J.E., Murphy, T.D., Levis, R.W., Matunis, E., Srivali, N., Hoskins, R.A., Spradling, A.C., 2007. The Carnegie Protein Trap Library: A Versatile Tool for Drosophila Developmental Studies. Genetics 175, 1505–1531.

Cao, Z., Li, C., Higginbotham, J.N., Franklin, J.L., Tabb, D.L., Graves-Deal, R., Hill, S., Cheek, K., Jerome, W.G., Lapierre, L. a, Goldenring, J.R., Ham, A.-J.L., Coffey, R.J., 2008. Use of fluorescence-activated vesicle sorting for isolation of Naked2-associated, basolaterally targeted exocytic vesicles for proteomics analysis. Mol. Cell. proteomics 7, 1651–67.

Caplan, M., Stow, J., Newman, A., 1987. Dependence on pH of polarized sorting of secreted proteins. Nature.

Carey, D., 1997. Syndecans: multifunctional cell-surface co-receptors. Biochem. J 327, 1–16.

Cetera, M., Horne-Badovinac, S., 2015. Round and round gets you somewhere: collective cell migration and planar polarity in elongating Drosophila egg chambers. Curr. Opin. Genet. Dev. 32, 10–15.

Cetera, M., Ramirez-San Juan, G.R., Oakes, P.W., Lewellyn, L., Fairchild, M.J., Tanentzapf, G.,

Gardel, M.L., Horne-Badovinac, S., 2014. Epithelial rotation promotes the global alignment of contractile actin bundles during Drosophila egg chamber elongation. Nat. Commun. 5, 5511.

Charras, G., Sahai, E., 2014. Physical influences of the extracellular environment on cell migration. Nat. Rev. Mol. Cell Biol. 15, 813–824.

Chen, C., Schweinsberg, P., Vashist, S., Mareiniss, D., Lambie, E., Grant, B., 2006. RAB-10 Is Required for Endocytic Recycling in the Caenorhabditis elegans Intestine. Mol. Biol. Cell 17, 1286–1297.

Chlenski, A., Guerrero, L.J., Salwen, H.R., Yang, Q., Tian, Y., Morales La Madrid, A., Mirzoeva, S., Bouyer, P.G., Xu, D., Walker, M., Cohn, S.L., 2011. Secreted protein acidic and rich in cysteine is a matrix scavenger chaperone. PLoS One 6, e23880.

Cho, J.Y., Chak, K., Andreone, B.J., Wooley, J.R., Kolodkin, A.L., 2012. The extracellular matrix proteoglycan perlecan facilitates transmembrane semaphorin-mediated repulsive guidance. Genes Dev. 26, 2222–35.

Clark, C.J., Sage, E.H., 2008. A prototypic matricellular protein in the tumor microenvironment--where there's SPARC, there's fire. J. Cell. Biochem. 104, 721–32.

Cohen, D., Müsch, A., Rodriguez-Boulan, E., 2001. Selective control of basolateral membrane protein polarity by cdc42. Traffic 2, 556–64.

Conder, R., Yu, H., Zahedi, B., Harden, N., 2007. The serine/threonine kinase dPak is required for polarized assembly of F-actin bundles and apical-basal polarity in the Drosophila follicular epithelium. Dev. Biol. 305, 470–82.

Cummings, M., King, R., 1969. The Cytology of the Vitellogenic Stages of Oogenesis in Drosophila melanogaster I. General Staging Characteristics. J. Morphol. 128, 427–442.

Daley, W.P., Peters, S.B., Larsen, M., 2008. Extracellular matrix dynamics in development and regenerative medicine. J. Cell Sci. 121, 255–64.

Daley, W.P., Yamada, K.M., 2013. ECM-modulated cellular dynamics as a driving force for tissue morphogenesis. Curr. Opin. Genet. Dev. 23, 408–14.

Datta, M.W., Hernandez, A.M., Schlicht, M.J., Kahler, A.J., DeGueme, A.M., Dhir, R., Shah, R.B., Farach-Carson, C., Barrett, A., Datta, S., 2006. Perlecan, a candidate gene for the CAPB locus, regulates prostate cancer cell growth via the Sonic Hedgehog pathway. Mol. Cancer 5.

Datta, S., 1995. Control of proliferation activation in quiescent neuroblasts of the Drosophila central nervous system. Development 121, 1173–1182.

De Almeida, J.B., Stow, J.L., 1991. Disruption of microtubules alters polarity of basement membrane proteoglycan secretion in epithelial cells. Am. J. Physiol. 261, C691–700.

De Wit, J., De Winter, F., Klooster, J., Verhaagen, J., 2005. Semaphorin 3A displays a punctate distribution on the surface of neuronal cells and interacts with proteoglycans in the extracellular matrix. Mol. Cell. Neurosci. 29, 40–55.

Delon, I., Brown, N.H., 2009. The integrin adhesion complex changes its composition and function during morphogenesis of an epithelium. J. Cell Sci. 122, 4363–74.

Denef, N., Chen, Y., Weeks, S.D., Barcelo, G., Schüpbach, T., 2008. Crag regulates epithelial architecture and polarized deposition of basement membrane proteins in Drosophila. Dev. Cell 14, 354–64.

Denholm, B., 2013. Shaping up for action: the path to physiological maturation in the renal tubules of Drosophila. Organogenesis 9, 40–54.

Devergne, O., Tsung, K., Barcelo, G., Schupbach, T., 2014. Polarized deposition of basement membrane proteins depends on Phosphatidylinositol synthase and the levels of Phosphatidylinositol 4,5-bisphosphate. Proc. Natl. Acad. Sci. 111, 7689–7694.

Dickson, B.J., Gilestro, G.F., 2006. Regulation of commissural axon pathfinding by slit and its Robo receptors. Annu. Rev. Cell Dev. Biol. 22, 651–75.

Diehl, K.A., Foley, J.D., Nealey, P.F., Murphy, C.J., 2005. Nanoscale topography modulates corneal epithelial cell migration. J. Biomed. Mater. Res. A 75, 603–11.

Domínguez-Giménez, P., Brown, N.H., Martín-Bermudo, M.D., 2007. Integrin-ECM interactions regulate the changes in cell shape driving the morphogenesis of the Drosophila wing epithelium. J. Cell Sci. 120, 1061–71.

Dunst, S., Kazimiers, T., von Zadow, F., Jambor, H., Sagner, A., Brankatschk, B., Mahmoud, A., Spannl, S., Tomancak, P., Eaton, S., Brankatschk, M., 2015. Endogenously Tagged Rab Proteins: A Resource to Study Membrane Trafficking in Drosophila. Dev. Cell 33, 351–365.

Eastburn, D.J., Mostov, K.E., 2010. Laying the foundation for epithelia: insights into polarized basement membrane deposition. EMBO Rep. 11, 329–30.

Ervasti, J.M., Sonnemann, K.J., 2008. Biology of the Striated Muscle Dystrophin-Glycoprotein Complex, International Review of Cytology. Elsevier Masson SAS. doi:10.1016/S0074-7696(07)65005-0

Fata, J.E., Werb, Z., Bissell, M.J., 2004. Regulation of mammary gland branching morphogenesis by the extracellular matrix and its remodeling enzymes. Breast cancer Res. 6, 1–11.

Fessler, L., Nelson, R., Fessler, J., 1994. Drosophila Extracellular matrix. Methods Enzymol. 245, 271–294.

Fessler, L.I., Condic, M.L., Nelson, R.E., Fessler, J.H., Fristrom, J.W., 1993. Site-specific cleavage of basement membrane collagen IV during Drosophila metamorphosis. Development 117, 1061–9.

Folkman, J., Klagsbrun, M., Sasse, J., Wadzinski, M., Ingber, D., Vlodavsky, I., 1988. A Heparin-Binding Angiogenic Protein - Basic Fibroblast Growth Factor - Is Stored Within Basement Membrane. Am. J. … 130, 393–400.

Fölsch, H., Mattila, P.E., Weisz, O. a, 2009. Taking the scenic route: biosynthetic traffic to the plasma membrane in polarized epithelial cells. Traffic 10, 972–81.

Friedrich, M. V, Schneider, M., Timpl, R., Baumgartner, S., 2000. Perlecan domain V of Drosophila melanogaster. Eur. J. Biochem. 267, 3149–3159.

Frydman, H.M., Spradling, A.C., 2001. The receptor-like tyrosine phosphatase lar is required for epithelial planar polarity and for axis determination within drosophila ovarian follicles. Development 128, 3209–20.

García-Alonso, L., Fetter, R., Goodman, C., 1996. Genetic analysis of Laminin A in Drosophila: extracellular matrix containing laminin A is required for ocellar axon pathfinding. Development 122, 2611–2621.

Giagtzoglou, N., Yamamoto, S., Zitserman, D., Graves, H.K., Schulze, K.L., Wang, H., Klein, H., Roegiers, F., Bellen, H.J., 2012. dEHBP1 controls exocytosis and recycling of Delta during asymmetric divisions. J. Cell Biol. 196, 65–83.

Gonzalez, A., Rodriguez-Boulan, E., 2009. Clathrin and AP1B: key roles in basolateral trafficking through trans-endosomal routes. FEBS Lett. 583, 3784–95.

Grindstaff, K.K., Yeaman, C., Anandasabapathy, N., Hsu, S.-C., Rodriguez-Boulan, E., Scheller, R.H., Nelson, W.J., 1998. Sec6/8 Complex Is Recruited to Cell–Cell Contacts and Specifies Transport Vesicle Delivery to the Basal-Lateral Membrane in Epithelial Cells. Cell 93, 731–740.

Gu, Z., Liu, F., Tonkova, E. a, Lee, S.Y., Tschumperlin, D.J., Brenner, M.B., 2014. Soft matrix is a natural stimulator for cellular invasiveness. Mol. Biol. Cell 25, 457–69.

Guha, A., Lin, L., Kornberg, T.B., 2009. Regulation of Drosophila matrix metalloprotease Mmp2 is essential for wing imaginal disc:trachea association and air sac tubulogenesis. Dev. Biol. 335, 317–26.

Gunn, P.A., Gliddon, B.L., Londrigan, S.L., Lew, A.M., van Driel, I.R., Gleeson, P.A., 2011.

The Golgi apparatus in the endomembrane-rich gastric parietal cells exist as functional stable mini-stacks dispersed throughout the cytoplasm. Biol. cell 103, 559–72.

Guo, Z., Driver, I., Ohlstein, B., 2013. Injury-induced BMP signaling negatively regulates Drosophila midgut homeostasis. J. Cell Biol. 201, 945–61. doi:10.1083/jcb.201302049

Guo, Z., Wang, Z., 2009. The glypican Dally is required in the niche for the maintenance of germline stem cells and short-range BMP signaling in the Drosophila ovary. Development 136, 3627–35.

Gutzeit, H., 1990. The microfilament pattern in the somatic follicle cells of mid-vitellogenic ovarian follicles of Drosophila. Eur. J. Cell Biol. 53, 349–56.

Gutzeit, H., Eberhardt, W., Gratwohl, E., 1991. Laminin and basement membrane-associated microfilaments in wild-type and mutant Drosophila ovarian follicles. J. Cell Sci. 100, 781–788.

Haack, T., Bergstralh, D.T., St Johnston, D., 2013. Damage to the Drosophila follicle cell epithelium produces “false clones” with apparent polarity phenotypes. Biol. Open 2, 1313–20. doi:10.1242/bio.20134671

Haigo, S.L., Bilder, D., 2011b. Global tissue revolutions in a morphogenetic movement controlling elongation. Science 331, 1071–4.

Hanus, C., Ehlers, M.D., 2008. Secretory outposts for the local processing of membrane cargo in neuronal dendrites. Traffic 9, 1437–45.

Harpaz, N., Volk, T., 2012. A novel method for obtaining semi-thin cross sections of the Drosophila heart and their labeling with multiple antibodies. Methods 56, 63–68.

Harris, B.S., Zhang, Y., Card, L., Rivera, L.B., Brekken, R. a, Bradshaw, A.D., 2011. SPARC regulates collagen interaction with cardiac fibroblast cell surfaces. Am. J. Physiol. Heart Circ. Physiol. 301, H841–7.

Harunaga, J.S., Doyle, A.D., Yamada, K.M., 2014. Local and global dynamics of the basement membrane during branching morphogenesis require protease activity and actomyosin contractility. Dev. Biol. 394, 197–205.

Hayashi, Y., Kobayashi, S., Nakato, H., 2009. Drosophila glypicans regulate the germline stem cell niche. J. Cell Biol. 187, 473–80.

He, B., Guo, W., 2009. The exocyst complex in polarized exocytosis. Curr. Opin. Cell Biol. 21, 537–542. doi:10.1016/j.ceb.2009.04.007

He, L., Wang, X., Tang, H.L., Montell, D.J., 2010. Tissue elongation requires oscillating contractions of a basal actomyosin network. Nat. Cell Biol. 12, 1133–42.

He, Z., Wang, K.C., Koprivica, V., Ming, G., Song, H.-J., 2002. Knowing how to navigate: mechanisms of semaphorin signaling in the nervous system. Sci. STKE re1.

Horne-Badovinac, S., 2014. The Drosophila egg chamber-a new spin on how tissues elongate. Integr. Comp. Biol. 54, 667–76.

Horne-Badovinac, S., Bilder, D., 2005. Mass transit: epithelial morphogenesis in the Drosophila egg chamber. Dev. Dyn. 232, 559–74. doi:10.1002/dvdy.20286

Horne-Badovinac, S., Hill, J., Gerlach, G., Menegas, W., Bilder, D., 2012. A screen for round egg mutants in Drosophila identifies tricornered, furry, and misshapen as regulators of egg chamber elongation. G3 2, 371–8.

Horton, A.C., Rácz, B., Monson, E.E., Lin, A.L., Weinberg, R.J., Ehlers, M.D., 2005. Polarized secretory trafficking directs cargo for asymmetric dendrite growth and morphogenesis. Neuron 48, 757–71.

Hussain, S.-A., Piper, M., Fukuhara, N., Strochlic, L., Cho, G., Howitt, J. a, Ahmed, Y., Powell, A.K., Turnbull, J.E., Holt, C.E., Hohenester, E., 2006. A molecular mechanism for the heparan sulfate dependence of slit-robo signaling. J. Biol. Chem. 281, 39693–8.

Hutagalung, A.H., Novick, P.J., 2011. Role of Rab GTPases in Membrane Traffic and Cell Physiology. Physiol. Rev. 91, 119 –149.

Hynes, R.O., Naba, A., 2012. Overview of the matrisome--an inventory of extracellular matrix constituents and functions. Cold Spring Harb. Perspect. Biol. 4, a004903.

Ibraghimov-Beskrovnaya, O., Ervasti, J.M., Leveille, C.J., Slaughter, C.A., Sernett, S.W., Campbell, K.P., 1992. Primary structure of dystrophin-associated glycoproteins linking dystrophin to the extracellular matrix. Nature 355, 696–702. doi:10.1038/355696a0

Isabella, A.J., Horne-Badovinac, S., 2016. Rab10-Mediated Secretion Synergizes with Tissue Movement to Build a Polarized Basement Membrane Architecture for Organ Morphogenesis. Dev. Cell 38, 47–60.

Isabella, A.J., Horne-Badovinac, S., 2015a. Building from the Ground up: Basement Membranes in Drosophila Development, in: Miner, J. (Ed.), Current Topics in Membranes. Elsevier Ltd.

Isabella, A.J., Horne-Badovinac, S., 2015b. Dynamic regulation of basement membrane protein levels promotes egg chamber elongation in Drosophila. Dev. Biol. 406, 212–221.

Itoh, T., Satoh, M., Kanno, E., Fukuda, M., 2006. Screening for target Rabs of TBC (Tre-2/Bub2/Cdc16) domain-containing proteins based on their Rab-binding activity. Genes Cells 11, 1023–37. doi:10.1111/j.1365-2443.2006.00997.x

Johnson, K., Ghose, A., Epstein, E., Lincecum, J., O/Connor, M., Van Vactor, D., 2004. Axonal Heparan Sulfate Proteoglycans Regulate the Distribution and Efficiency of the Repellent Slit during Midline Axon Guidance. Curr. Biol. 14, 499–504.

Khoshnoodi, J., Pedchenko, V., Hudson, B.G., 2008. Mammalian collagen IV. Microsc. Res. Tech. 71, 357–70.

Kim, D.-H., Provenzano, P.P., Smith, C.L., Levchenko, A., 2012. Matrix nanotopography as a regulator of cell function. J. Cell Biol. 197, 351–60.

Kim, S.N., Jeibmann, A., Halama, K., Witte, H.T., Wälte, M., Matzat, T., Schillers, H., Faber, C., Senner, V., Paulus, W., Klämbt, C., 2014. ECM stiffness regulates glial migration in Drosophila and mammalian glioma models. Development 141, 3233–42.

Klagsbrun, M., 1990. The affinity of fibroblast growth factors (FGFs) for heparin; FGF-heparan sulfate interactions in cells and extracellular matrix. Curr. Opin. Cell Biol. 2, 857–863.

Knoblich, J. a, 2008. Mechanisms of asymmetric stem cell division. Cell 132, 583–97.

Kondylis, V., Pizette, S., Rabouille, C., 2009. The early secretory pathway in development: a tale of proteins and mRNAs. Semin. Cell Dev. Biol. 20, 817–27.

Kondylis, V., Rabouille, C., 2009. The Golgi apparatus: lessons from Drosophila. FEBS Lett. 583, 3827–38.

Koride, S., He, L., Xiong, L., Lan, G., Montell, D., Sun, S., 2014. Mechanochemical regulation of oscillatory follicle cell dynamics in the developing Drosophila egg chamber. Mol. Biol. Cell 25, 3709–3716.

Krammer, A., Craig, D., Thomas, W.E., Schulten, K., Vogel, V., 2002. A structural model for force regulated integrin binding to fibronectin's RGD-synergy site. Matrix Biol. 21, 139–147. doi:10.1016/S0945-053X(01)00197-4

Kraut, R., Menon, K., Zinn, K., 2001. A gain-of-function screen for genes controlling motor axon guidance and synaptogenesis in Drosophila. Curr. Biol. 11, 417–430.

Kusche-Gullberg, M., Garrison, K., MacKrell, A., Fessler, L., Fessler, J., 1992. Laminin A chain: expression during Drosophila development and genomic sequence. EMBO J. 11, 4519–4527.

Laflamme, C., Assaker, G., Ramel, D., Dorn, J.F., She, D., Maddox, P.S., Emery, G., 2012. Evi5 promotes collective cell migration through its Rab-GAP activity. J. Cell Biol. 198, 57–67. doi:10.1083/jcb.201112114

Le Parco, Y., Knibiehler, B., Cecchini, J., Mirre, C., 1986. Stage and Tissue-specific Expression of a Collagen Gene during Drosophila melanogaster Development. Exp. Cell Res. 163,

405–412.

Lerner, D.W., McCoy, D., Isabella, A.J., Mahowald, A.P., Gerlach, G.F., Chaudhry, T. a, Horne-Badovinac, S., 2013. A Rab10-dependent mechanism for polarized basement membrane secretion during organ morphogenesis. Dev. Cell 24, 159–68.

Lewellyn, L., Cetera, M., Horne-Badovinac, S., 2013. Misshapen decreases integrin levels to promote epithelial motility and planar polarity in Drosophila. J. Cell Biol. 200, 721–9.

Li, Z., Zhang, Y., Han, L., Shi, L., Lin, X., 2013. Trachea-derived dpp controls adult midgut homeostasis in Drosophila. Dev. Cell 24, 133–43.

Lin, X., Buff, E., Perrimon, N., Michelson, A., 1999. Heparan sulfate proteoglycans are essential for FGF receptor signaling during Drosophila embryonic development. Development 126, 3715–3723.

Lo, C.-M., Wang, H.-B., Dembo, M., Wang, Y.-L., 2000. Cell movement is guided by the rigidity of the substrate. Biophys. J. 79, 144–52.

López-Onieva, L., Fernández-Miñán, A., González-Reyes, A., 2008. Jak/Stat signalling in niche support cells regulates dpp transcription to control germline stem cell maintenance in the Drosophila ovary. Development 135, 533–40.

Losick, V.P., Morris, L.X., Fox, D.T., Spradling, A., 2011. Drosophila stem cell niches: a decade of discovery suggests a unified view of stem cell regulation. Dev. Cell 21, 159–71.

Lowenstein, P., Morrison, E., Bain, D., Shering, A., Banding, G., Douglas, P., Castro, M., 1994. Polarized Distribution of the Trans-Golai Network Marker TGN38 During the In Vitro Developmeh of Neocortical Neurons : Effects of Nocodazole and Brefeldin A. Eur. J. Neurosci. 6, 1453–1465.

Marat, A.L., Dokainish, H., McPherson, P.S., 2011. DENN domain proteins: regulators of Rab GTPases. J. Biol. Chem. 286, 13791–800.

Martin-Belmonte, F., Gassama, A., Datta, A., Yu, W., Rescher, U., Gerke, V., Mostov, K., 2007. PTEN-mediated apical segregation of phosphoinositides controls epithelial morphogenesis through Cdc42. Cell 128, 383–97.

Martin, D., Zusman, S., Li, X., Williams, E., Khare, N., DaRocha, S., Chiquet-Ehrismann, R., Baumgartner, S., 1999. wing blister , A New Drosophila Laminin a Chain Required for Cell Adhesion and Migration during Embryonic and Imaginal Dev. J. Cell Biol. 145, 191–201.

Martinek, N., Shahab, J., Saathoff, M., Ringuette, M., 2008. Haemocyte-derived SPARC is required for collagen-IV-dependent stability of basal laminae in Drosophila embryos. J. Cell Sci. 124, 670–670.

Martinek, N., Shahab, J., Saathoff, M., Ringuette, M., 2008. Haemocyte-derived SPARC is required for collagen-IV-dependent stability of basal laminae in Drosophila embryos. J. Cell Sci. 121, 1671–1680.

Martinek, N., Zou, R., Berg, M., Sodek, J., Ringuette, M., 2002. Evolutionary conservation and association of SPARC with the basal lamina in Drosophila. Dev. Genes Evol. 212, 124–33.

McCall, A.S., Cummings, C.F., Bhave, G., Vanacore, R., Page-McCaw, A., Hudson, B.G., 2014. Bromine Is an Essential Trace Element for Assembly of Collagen IV Scaffolds in Tissue Development and Architecture. Cell 157, 1380–1392.

Micchelli, C. a, Perrimon, N., 2006. Evidence that stem cells reside in the adult Drosophila midgut epithelium. Nature 439, 475–9.

Miner, J.H., Yurchenco, P.D., 2004. Laminin functions in tissue morphogenesis. Annu. Rev. Cell Dev. Biol. 20, 255–84.

Mirouse, V., Christoforou, C.P., Fritsch, C., St. Johnston, D., Ray, R.P., 2009. Dystroglycan and Perlecan Provide a Basal Cue Required for Epithelial Polarity during Energetic Stress. Dev. Cell 16, 83–92. doi:10.1016/j.devcel.2008.11.006

Mirre, C., Cecchini, J., Parco, Y. Le, Knibiehler, B., 1988. De novo expression of a type IV collagen gene in Drosophila embryos is restricted to mesodermal derivatives and occurs at germ band shortening. Development 102, 369–376.

Morin, X., Daneman, R., Zavortink, M., Chia, W., 2001. A protein trap strategy to detect GFP-tagged proteins expressed from their endogenous loci in Drosophila. Proc. Natl. Acad. Sci. U. S. A. 98, 15050–15055.

Morrissey, M.A., Jayadev, R., Miley, G.R., Blebea, C.A., Chi, Q., Ihara, S., Sherwood, D.R., 2016. SPARC Promotes Cell Invasion In Vivo by Decreasing Type IV Collagen Levels in the Basement Membrane. PLoS Genet. 12, 1–24. doi:10.1371/journal.pgen.1005905

Morrissey, M.A., Sherwood, D.R., 2015. An active role for basement membrane assembly and modification in tissue sculpting. J. Cell Sci. 128, 1–8.

Myllyharju, J., Kivirikko, K.I., 2004. Collagens, modifying enzymes and their mutations in humans, flies and worms. Trends Genet. 20, 33–43.

Nagaraju, G.P., Dontula, R., El-Rayes, B.F., Lakka, S.S., 2014. Molecular mechanisms underlying the divergent roles of SPARC in human carcinogenesis. Carcinogenesis 35, 967–73.

Natori, Y., O'Meara, Y., Manning, E., Minto, A., Levine, J., Weise, W., Salant, D., 1992. Production and polarized secretion of basement membrane components by glomerular epithelial cells. Am. J. Physiol. 262, 131–7.

Nüsslein-Volhard, C., Wieschaus, E., Kluding, H., 1984. Mutations affecting the pattern of the larval cuticle in Drosophila melanogaster I. Zygotic loci on the second chromosome. Roux's Arch. Dev. Biol. 193, 267–282.

Ohlstein, B., Spradling, A., 2006. The adult Drosophila posterior midgut is maintained by pluripotent stem cells. Nature 439, 470–4.

Ozbek, S., Balasubramanian, P.G., Chiquet-Ehrismann, R., Tucker, R.P., Adams, J.C., 2010. The evolution of extracellular matrix. Mol. Biol. Cell 21, 4300–5.

Paralkar, V.M., Vukicevic, S., Reddi, A.H., 1991. Transforming growth factor β type 1 binds to collagen IV of basement membrane matrix: Implications for development. Dev. Biol. 143, 303–308.

Park, Y., Rangel, C., Reynolds, M.M., Caldwell, M.C., Johns, M., Nayak, M., Welsh, C.J.R., McDermott, S., Datta, S., 2003. Drosophila Perlecan modulates FGF and Hedgehog signals to activate neural stem cell division. Dev. Biol. 253, 247–257.

Pastor-Pareja, J.C., Xu, T., 2011. Shaping Cells and Organs in Drosophila by Opposing Roles of Fat Body-Secreted Collagen IV and Perlecan. Dev. Cell 21, 245–256.

Perrimon, N., Bernfield, M., 2000. Specificities of heparan sulphate proteoglycans in developmental processes. Nature 404, 725–728.

Pierce, J.P., Mayer, T., McCarthy, J.B., 2001. Evidence for a satellite secretory pathway in neuronal dendritic spines. Curr. Biol. 11, 351–355.

Portela, M., Casas-Tinto, S., Rhiner, C., López-Gay, J.M., Domínguez, O., Soldini, D., Moreno, E., 2010. Drosophila SPARC is a self-protective signal expressed by loser cells during cell competition. Dev. Cell 19, 562–573.

Prasad, M., Jang, A.C.-C., Starz-Gaiano, M., Melani, M., Montell, D.J., 2007. A protocol for culturing Drosophila melanogaster stage 9 egg chambers for live imaging. Nat. Protoc. 2, 2467–2473.

Provenzano, P.P., Eliceiri, K.W., Campbell, J.M., Inman, D.R., White, J.G., Keely, P.J., 2006. Collagen reorganization at the tumor-stromal interface facilitates local invasion. BMC Med. 4, 38.

Provenzano, P.P., Inman, D.R., Eliceiri, K.W., Trier, S.M., Keely, P.J., 2008. Contact guidance mediated three-dimensional cell migration is regulated by Rho/ROCK-dependent matrix reorganization. Biophys. J. 95, 5374–84.

Qin, J., Liang, J., Ding, M., 2014. Perlecan antagonizes collagen IV and ADAMTS9/GON-1 in restricting the growth of presynaptic boutons. J. Neurosci. 34, 10311–24.

Ramírez, O. a, Couve, A., 2011. The endoplasmic reticulum and protein trafficking in dendrites and axons. Trends Cell Biol. 21, 219–27.

Reinhart-King, C. a, Dembo, M., Hammer, D. a, 2008. Cell-cell mechanical communication through compliant substrates. Biophys. J. 95, 6044–51.

Rezakhaniha, R., Agianniotis, A., Schrauwen, J.T.C., Griffa, A., Sage, D., Bouten, C.V.C., Van De Vosse, F.N., Unser, M., Stergiopulos, N., 2012. Experimental investigation of collagen waviness and orientation in the arterial adventitia using confocal laser scanning microscopy. Biomech. Model. Mechanobiol. 11, 461–473.

Roca-Cusachs, P., Sunyer, R., Trepat, X., 2013. Mechanical guidance of cell migration: lessons from chemotaxis. Curr. Opin. Cell Biol. 25, 543–9.

Rodriguez-Boulan, E., Kreitzer, G., Müsch, A., 2005. Organization of vesicular trafficking in epithelia. Nat. Rev. Mol. Cell Biol. 6, 233–247.

Rubin, J., Choi, Y., Segal, R., 2002. Cerebellar proteoglycans regulate sonic hedgehog responses during development. Development 129, 2223–2232.

Sage, H., Vernon, R.B., Funk, S.E., Everitt, E.A., Angello, J., 1989. SPARC, a secreted protein associated with cellular proliferation, inhibits cell spreading in vitro and exhibits Ca+2-dependent binding to the extracellular matrix. J. Cell Biol. 109, 341–56.

Saito, K., Chen, M., Bard, F., Chen, S., Zhou, H., Woodley, D., Polischuk, R., Schekman, R., Malhotra, V., 2009. TANGO1 facilitates cargo loading at endoplasmic reticulum exit sites. Cell 136, 891–902.

Sano, H., Peck, G.R., Blachon, S., Lienhard, G.E., 2015. A potential link between insulin signaling and GLUT4 translocation: Association of Rab10-GTP with the exocyst subunit Exoc6/6b. Biochem. Biophys. Res. Commun. 465, 6–10.

Santiago-Tirado, F.H., Bretscher, A., 2011. Membrane-trafficking sorting hubs: cooperation between PI4P and small GTPases at the trans-Golgi network. Trends Cell Biol. 21, 515–25.

Sarov, M., Barz, C., Jambor, H., Hein, M.Y., Schmied, C., Suchold, D., Stender, B., Janosch, S., KJ, V.V., Krishnan, R., Krishnamoorthy, A., Ferreira, I.R., Ejsmont, R.K., Finkl, K., Hasse, S., Kämpfer, P., Plewka, N., Vinis, E., Schloissnig, S., Knust, E., Hartenstein, V., Mann, M., Ramaswami, M., VijayRaghavan, K., Tomancak, P., Schnorrer, F., 2016. A genome-wide resource for the analysis of protein localisation in Drosophila. Elife 5, 1689–1699.

Sawala, A., Sutcliffe, C., Ashe, H.L., 2012. Multistep molecular mechanism for bone morphogenetic protein extracellular transport in the Drosophila embryo. Proc. Natl. Acad. Sci. U. S. A. 109, 11222–7.

Schiller, H.B., Fässler, R., 2013. Mechanosensitivity and compositional dynamics of cell–matrix adhesions. EMBO Rep. 14, 509–519. doi:10.1038/embor.2013.49

Schneider, M., Khalil, A. a, Poulton, J., Castillejo-Lopez, C., Egger-Adam, D., Wodarz, A., Deng, W.-M., Baumgartner, S., 2006. Perlecan and Dystroglycan act at the basal side of the Drosophila follicular epithelium to maintain epithelial organization. Development 133, 3805–15.

Schuck, S., Gerl, M.J., Ang, A., Manninen, A., Keller, P., Mellman, I., Simons, K., 2007. Rab10 is involved in basolateral transport in polarized Madin-Darby canine kidney cells. Traffic 8, 47–60. doi:10.1111/j.1600-0854.2006.00506.x

Seeger, M., Tear, G., Ferres-Marco, D., Goodman, C., 1993. Mutations Affecting Growth Cone Guidance in Drosophila : Genes Necessary for Guidance toward or away from the Midline. Neuron 10, 409–426.

Shahab, J., Baratta, C., Scuric, B., Godt, D., Venken, K.J.T., Ringuette, M.J., 2015. Loss of SPARC dysregulates basal lamina assembly to disrupt larval fat body homeostasis in Drosophila melanogaster. Dev. Dyn. 1–13.

Shahab, J., Baratta, C., Scuric, B., Godt, D., Venken, K.J.T., Ringuette, M.R., 2014. Loss of SPARC Dysregulates Basal Lamina Assembly to Disrupt Larval Fat Body Homeostasis in Drosophila melanogaster. Dev. Dyn.

Shi, A., Chen, C.C., Banerjee, R., Glodowski, D., Audhya, A., Rongo, C., Grant, B.D., 2010. EHBP-1 functions with RAB-10 during endocytic recycling in Caenorhabditis elegans. Mol. Biol. Cell 21, 2930–2943.

Smart, A.D., Course, M.M., Rawson, J., Selleck, S., Van Vactor, D., Johnson, K.G., 2011. Heparan sulfate proteoglycan specificity during axon pathway formation in the Drosophila embryo. Dev. Neurobiol. 71, 608–18.

Song, X., Zhu, C., Doan, C., Xie, T., 2002. Germline stem cells anchored by adherens junctions in the Drosophila ovary niches. Science (80-.). 296, 1855–1857.

Sorrosal, G., Pérez, L., Herranz, H., Milán, M., 2010. Scarface, a secreted serine protease-like protein, regulates polarized localization of laminin A at the basement membrane of the Drosophila embryo. EMBO Rep. 11, 3–9.

Srivastava, A., Pastor-Pareja, J.C., Igaki, T., Pagliarini, R., Xu, T., 2007. Basement membrane remodeling is essential for Drosophila disc eversion and tumor invasion. Proc. Natl. Acad. Sci. U. S. A. 104, 2721–6.

Steigemann, P., Molitor, A., Fellert, S., Jäckle, H., Vorbrüggen, G., 2004. Heparan sulfate proteoglycan syndecan promotes axonal and myotube guidance by slit/robo signaling. Curr. Biol. 14, 225–30.

Stevens, A., Jacobs, J., 2002. Integrins Regulate Responsiveness to Slit Repellent Signals. J. Neurosci. 22, 4448–4455.

Stoops, E.H., Caplan, M.J., 2014. Trafficking to the apical and basolateral membranes in polarized epithelial cells. J. Am. Soc. Nephrol. 25, 1375–86.

Svitkina, T., 2009. Imaging Cytoskeleton Components by Electron Microscopy. Methods Mol Biol. 586, 187–206.

Takagi, Y., Nomizu, M., Gullberg, D., MacKrell, a. J., Keene, D.R., Yamada, Y., Fessler, J.H., 1996. Conserved Neuron Promoting Activity in Drosophila and Vertebrate Laminin 1. J. Biol. Chem. 271, 18074–18081.

Tan, J., Saltzman, W.M., 2002. Topographical control of human neutrophil motility on micropatterned materials with various surface chemistry. Biomaterials 23, 3215–3225.

Tanner, K., Mori, H., Mroue, R., Bruni-cardoso, A., Bissell, M.J., 2011. Coherent angular motion in the establishment of multicellular architecture of glandular tissues 2011. doi:10.1073/pnas.1119578109

Taylor, C.A., Yan, J., Howell, A.S., Dong, X., Shen, K., 2015. RAB-10 Regulates Dendritic Branching by Balancing Dendritic Transport. PLOS Genet. 11, e1005695.

The, I., Bellaiche, Y., Perrimon, N., 1999. Hedgehog movement is regulated through tout velu – Dependent Synthesis of a Heparan Sulfate Proteoglycan. Mol. Cell 4, 633–639.

Tian, A., Jiang, J., 2014. Intestinal epithelium-derived BMP controls stem cell self-renewal in Drosophila adult midgut. Elife 3, e01857.

Umulis, D.M., Shimmi, O., O'Connor, M.B., Othmer, H.G., 2010. Organism-scale modeling of early Drosophila patterning via bone morphogenetic proteins. Dev. Cell 18, 260–74.

Varner, V.D., Nelson, C.M., 2014. Cellular and physical mechanisms of branching morphogenesis. Development 141, 2750–2759.

Venditti, R., Scanu, T., Santoro, M., Di Tullio, G., Spaar, A., Gaibisso, R., Beznoussenko, G., Mironov, A., Mironov Jr, A., Zelante, L., Piemontese, M., Notarangelo, A., Malhotra, V., Vertel, B., Wilson, C., De Matteis, M., 2012. Sedlin Controls the ER Export of Procollagen by Regulating the Sar1 Cycle. Science (80-.). 337, 1668–1672.

Venken, K.J.T., Schulze, K.L., Haelterman, N.A., Pan, H., He, Y., Evans-holm, M., Carlson, J.W., Levis, R.W., Spradling, A.C., Hoskins, R.A., Bellen, H.J., 2011. MiMIC : a highly versatile transposon insertion resource for engineering Drosophila melanogaster genes. Nat. Methods 8, 737–43.

Vertel, B., Velasco, A., LaFrance, S., Walters, L., Kaczman-Daniel, K., 1989. Precursors of Chondroitin Sulfate Proteoglycan Are Segregated within a Subcompartment of the Chondrocyte Endoplasmic Reticulum. J. Cell Biol. 109, 1827–1836.

Viktorinová, I., Dahmann, C., 2013. Microtubule Polarity Predicts Direction of Egg Chamber Rotation in Drosophila. Curr. Biol. 23, 1472–1477.

Viktorinová, I., König, T., Schlichting, K., Dahmann, C., 2009. The cadherin Fat2 is required for planar cell polarity in the Drosophila ovary. Development 136, 4123–32.

Voigt, A., Pflanz, R., Schäfer, U., Jäckle, H., 2002. Perlecan participates in proliferation activation of quiescent Drosophila neuroblasts. Dev. Dyn. 224, 403–12.

Wang, H., Lacoche, S., Huang, L., Xue, B., Muthuswamy, S.K., 2013. Rotational motion during three-dimensional morphogenesis of mammary epithelial acini relates to laminin matrix assembly 110, 163–168. doi:10.1073/pnas.1201141110

Wang, T., Liu, Y., Xu, X.-H., Deng, C.-Y., Wu, K.-Y., Zhu, J., Fu, X.-Q., He, M., Luo, Z.-G., 2011. Lgl1 activation of rab10 promotes axonal membrane trafficking underlying neuronal polarization. Dev. Cell 21, 431–44. doi:10.1016/j.devcel.2011.07.007

Wang, X., Harris, R.E., Bayston, L.J., Ashe, H.L., 2008. Type IV collagens regulate BMP signalling in Drosophila. Nature 455, 72–7.

Wilson, D.G., Phamluong, K., Li, L., Sun, M., Cao, T.C., Liu, P.S., Modrusan, Z., Sandoval, W.N., Rangell, L., Carano, R. a D., Peterson, A.S., Solloway, M.J., 2011. Global defects in collagen secretion in a Mia3/TANGO1 knockout mouse. J. Cell Biol. 193, 935–51.

Xie, T., Spradling, A.C., 1998. decapentaplegic is essential for the maintenance and division of germline stem cells in the Drosophila ovary. Cell 94, 251–60.

Xiong, B., Bayat, V., Jaiswal, M., Zhang, K., Sandoval, H., Charng, W.-L., Li, T., David, G., Duraine, L., Lin, Y.-Q., Neely, G.G., Yamamoto, S., Bellen, H.J., 2012. Crag Is a GEF for Rab11 Required for Rhodopsin Trafficking and Maintenance of Adult Photoreceptor Cells. PLoS Biol. 10, e1001438.

Yasothornsrikul, S., Davis, W.J., Cramer, G., Kimbrell, D. a, Dearolf, C.R., 1997. viking: identification and characterization of a second type IV collagen in Drosophila. Gene 198, 17–25.

Yoshimura, S., Gerondopoulos, A., Linford, A., Rigden, D.J., Barr, F.A., 2010. Family-wide characterization of the DENN domain Rab GDP-GTP exchange factors. J. Cell Biol. 191, 367–81.

Yurchenco, P.D., 2011. Basement membranes: cell scaffoldings and signaling platforms. Cold Spring Harb. Perspect. Biol. 3, a004911.

Zhang, J., Schulze, K.L., Hiesinger, P.R., Suyama, K., Wang, S., Fish, M., Acar, M., Hoskins, R.A., Bellen, H.J., Scott, M.P., 2006. Thirty-One Flavors of Drosophila Rab Proteins. Genetics 176, 1307–1322.

Zou, W., Yadav, S., DeVault, L., Nung Jan, Y., Sherwood, D.R., 2015. RAB-10-Dependent Membrane Transport Is Required for Dendrite Arborization. PLOS Genet. 11, e1005484.